TECHNISCHE UNIVERSITÄT WIEN

DISSERTATION

Investigation of the dynamic behavior of variable speed pumped storage hydropower plants for Frequency Containment Reserve provision

ausgeführt zum Zwecke der Erlangung des akademischen Grades eines Doktors der technischen Wissenschaften

unter der Leitung von
Univ.-Prof. Dr.-Ing. Wolfgang Gawlik
Institut für Energiesysteme und Elektrische Antriebe

eingereicht an der Technischen Universität Wien
Fakultät für Elektrotechnik und Informationstechnik

von
Dipl.-Ing. Christoph Maier, BSc
Matr.-Nr. 0425726

Wien, Februar 2023

Christoph Maier

Contents

Abstract

Pumped hydroelectric energy storage (PSH) is the most established large-scale electrical energy storage technology as of now. PSH covers a large share of regulation and balancing tasks in many power systems worldwide. New technologies for variable speed drive concepts have emerged in the last two decades. They are now being integrated in power systems as large and flexible sources of electrical energy storage. This thesis investigates two PSH concepts with variable speed power units, a doubly-fed induction motor-generator and a synchronous motor-generator with a full-size converter, for their dynamic behavior. Furthermore, transient simulations are conducted to investigate the possibility of providing frequency containment reserve provision (FCR) during pump and turbine operations based on ENTSO-E Continental Europe requirements.

Monitoring a correct FCR provision from the balancing service provider is becoming more and more advanced as data transfer to the TSO intensifies. Three methodologies are presented, which are still part of ongoing research and are more and more introduced in live operations at TSOs. These monitoring methods are applied to prove a correct FCR provision of both variable speed unit schemes in turbine and pump mode. All three methods determine a correct FCR provision by the variable speed PSH, and each method's advantages are discussed.

Finally, an analysis of the economics of FCR provided by variable speed pumped hydropower plants is given. Results show a high dependence on the ratio between FCR price and electricity price for an economic FCR provision of variable speed pump-turbine storage.

Kurzfassung

Pumpspeicherkraftwerke sind die derzeit am weitesten verbreitete Technologie zur Speicherung elektrischer Energie im großen Maßstab. Sie übernehmen einen großen Teil der Frequenzregelungs- und Ausgleichsaufgaben in vielen Energiesystemen auf der ganzen Welt. In den letzten zwei Jahrzehnten sind neue Technologien für drehzahlvariable Antriebskonzepte entstanden und werden nun als große und flexible elektrische Energiespeicher in Stromversorgungssysteme integriert. Zwei Pumpspeicherkonzepte mit drehzahlgeregelten Maschinen, eine doppeltgespeiste Asynchronmaschine und eine Synchronmaschine mit Vollumrichter, werden in dieser Arbeit auf ihr dynamisches Verhalten untersucht. Darüber hinaus werden transiente Simulationen durchgeführt, um die Möglichkeit der Bereitstellung von Primärregelenergie (Frequency Containment Reserve - FCR) während des Pump- und Turbinenbetriebs auf der Grundlage der ENTSO-E Continental Europe Anforderungen für FCR zu untersuchen.

Die Überwachung einer korrekten FCR-Bereitstellung durch den Regelenergieanbieter wird mit zunehmender Datenübertragung zum Übertragungsnetzbetreiber immer fortschrittlicher. Es werden drei Methoden, die sich noch im Forschungsstand befinden und zunehmend in den Live-Betrieb bei den Übertragungsnetzbetreibern eingeführt werden sollen, vorgestellt. Die Anwendung dieser Überwachungsmethoden zum Nachweis einer korrekten FCR-Bereitstellung beider drehzahlvariablen Konzepte im Turbinen- und Pumpenmodus wird ebenfalls demonstriert. Alle drei Methoden zeigen die Korrektheit der Primärenergiebereitstellung durch die drehzahlvariablen Pumpspeicherkraftwerke und Vorteile jeder Methode werden diskutiert.

Abschließend erfolgt eine Analyse der Wirtschaftlichkeit der FCR, die durch Pumpspeicherkraftwerke mit variabler Drehzahl bereitgestellt wird. Die Ergebnisse zeigen, dass eine hohe Abhängigkeit vom Verhältnis zwischen FCR-Preis und Strompreis für eine wirtschaftliche FCR-Bereitstellung von drehzahlvariablen Pumpturbinenspeichern vorherrscht.

Abbreviations

aFRR Automatic Frequency Restoration Reserve, page 13

BEL Best Efficiency Line, page 43

BEP Best Efficiency Point, page 44

BSP Balancing Service Provider, page 14

DFIM Doubly-Fed Induction Motor-Generator, page 11

DTE Distributed Technical Entity, page 17

EES Electrical Energy Storage, page 5

EST Energy Storage Technology, page 5

FCR Frequency Containment Reserve, page 13

FSPT Fixed Speed Pump-Turbine, page 10

FSTS Fixed Speed Ternary Set, page 11

GVO Guide Vane Opening, page 44

HS Hydraulic Short Circuit, page 11

LFC Load-Frequency-Control, page 13

MFP Maximum FCR Provision Operating Point, page 84

mFRR Manual Frequency Restoration Reserve, page 14

PHES Pumped Hydroelectric Energy Storage, page 6

PSH Pumped-Storage Hydropower, page 6

Abbreviations

RES Renewable Energy Sources, page 7

RGCE Regional Group Central Europe, page 17

RR Replacement Reserves, page 14

SAFA Synchronous Area Framework, page 13

SOGL System Operation Guideline, page 14

TE Technical Entity, page 17

TSO Transmission System Operator, page 13

VSDFG Variable Speed Doubly-Fed Induction Motor-Generator, page 11

VSFSC Variable Speed Full Size Converter, page 11

VSPT Variable Speed Pump-Turbine, page 50

1 Motivation

1.1 Problem Statement

Hydropower is the largest accessed global source of renewable energy today and has been playing an important role in electric power systems for decades. It is used as a stable and efficient power source and to regulate and balance power systems worldwide. The electricity sector's decarbonization efforts dominate today's global energy strategies. The net generating capacity of wind and solar plants in the ENTSO-E area has continuously risen in the last decade [1]. The massive integration of renewable generation causes increasing fluctuations in the electrical energy supply [2]. These fluctuations are compensated by rotating masses of synchronous generators, storage systems, and the utilization of flexible conventional power plants [3]. Large-scale electrical energy storage has been accomplished primarily by pumped-storage power plants (PSH) in the last decades, while more and more high-capacity battery storage systems are investigated (e.g. [4]) and entering the market. With less inertia in the system due to converter-based generation, conventional PSH do not have the capabilities to react and regulate occurring grid imbalances quickly enough [5]. To adapt to these new situations and grid codes, different technologies for PSH emerged in the past years, such as the hydraulic short circuit scheme and the variable speed machines, as they rise the operational flexibility to enable a more dynamic operation. The two leading technologies for variable-speed pump-turbines of recent years are the variable speed doubly-fed generator (VSDFG) and the variable-speed full-size converter (VSFSC). These technologies have the opportunity to participate in the restrictive energy balancing market in a wide operating range to generate additional revenues in an increasingly uneconomical environment for new pumped-storage projects [6]. For the profitability of pumped storage plants, participation in the control and balancing energy market is important as a complement to just peak/off-peak management. Within its synchronous area of ENTSO-E, the control actions and the active power

reserves are organized in a hierarchical structure. Measurements to provide a stable system frequency are initiated by the TSOs within the synchronous area. Control actions to counteract load and power generation imbalances are performed by different complementary processes, each relying on reserves with different characteristics and qualities (FCR, aFRR, mFRR, RR) [7]. Participation in the balancing energy market is usually limited to aFRR, mFRR, and RR provision for conventional PSH. Hence, an important question is whether the additional provision of FCR is technically feasible for variable speed pump-turbines and makes economic sense.

1.2 Research Questions

The thesis's main focus is to analyze the frequency containment reserve (FCR) capability of the variable speed doubly-fed generator and the variable-speed full-size converter based on ENTSO-E Continental Europe requirements. Therefore, a transient model of both concepts is developed and validated based on a real-life pumped hydro storage facility. This model differs from existing literature by implementing extensive hydraulic, electrical, and control elements for two variable speed pump-turbine schemes and allows long-term transient simulations of 4 hours (FCR bid resolution) or more. Furthermore, this thesis presents three comprehensive FCR monitoring methodologies, which are currently state of research. Modeling of these monitoring methods and improvements, especially to the channel methodology, are made to enable a practical application. The methods are further used to prove a correct FCR provision of the variable speed pump-turbine plants. Finally, an analysis of the economics of FCR provided by variable speed pumped hydropower plants is necessary to determine profitability from the FCR bidding participation and the optimal operation points for it.

Four research questions are defined which correspond to the goal definitions of this dissertation:

- What dynamic aspects and properties of variable speed pumped storage hydropower plants need to be considered for modeling FCR provision?
- What is the effective operating range of variable speed pumped storage hydropower plants for FCR provision?
- What are suitable methods for monitoring a correct FCR provision?
- What are economically feasible operating points for FCR provision by variable speed pumped storage hydropower plants?

1.3 Data Basis and Research Activities

The data basis for the dynamic models of the (variable speed) pump-turbines was collected during the research project "GSG-GreenStorageGrid". This K-Project was funded in the framework of COMET - Competence Centers for Excellent Technologies by the Federal Ministry of Transport, Innovation and Technology, the Federal Ministry of Science, Research and Economy, the Vienna Business Agency, the Federal Province of Lower Austria and by the Federal Province of Upper Austria. The program line COMET is administered by the the Austrian Research Promotion Agency (FFG). The project GreenStorageGrid (GSG) took an integral and holistic approach across all energy generation and distribution systems. The project was composed of individual projects in the fields of energy storage and distribution. The innovation potential of GSG was based on the interface and interaction between hydraulic storage, thermo-chemical storage and grids as the connecting element. The main task of GSG lay in modeling, simulation and optimization of technology towards a carbon-free energy economy. The project brought together some key players of the Austrian energy industry and research institutions.

The data basis for the presented monitoring methodologies were collected during multiple projects with ENTSO-E and Austrian Power Grid (APG).

Several publications are derived from the project mentioned above, which are reflected in the content of this thesis. Furthermore, several scientific papers (as primary and secondary author) were written in the course of research activities in the field of renewable energy integration and smart grid technologies. Additionally, diploma and bachelor theses were supervised and their results and findings were considered in this thesis. Table 1.1 gives an overview of selected publications.

Table 1.1: Overview of selected publications of the author

	Type of Publication	Title of Publication	Venue/Journal	Year
[8]	Diploma Thesis	*Zukünftige Speicherbewirtschaftung bei regenerativer Stromerzeugung am Beispiel Österreichs*	TU Wien	2012
[9]	Talk	*Speicherbewirtschaftung bei Vollversorgung Österreichs mit regenerativem Strom*	IEWT Wien	2013
[10]	Talk	*Eigenverbrauchssteigerung in Haushalten durch Demand-Side-Management*	13. Symposium Energieinnovation, Graz	2014
[11]	Talk	*Demand-Side-Management in einer Modellsiedlung - Endergebnisse des Projekts aDSM*	IEWT Wien	2015
[12]	Poster	*Modeling of flexible power plants in SIMSEN*	GSG - GreenStorageGrid Reviewing Day	2015
[13]	Talk	*SYMBIOSE-4-IUG - Verschränkung der Energienetze bei Industrie- und Gewerbekunden*	14. Symposium Energieinnovation, Graz	2016
[14]	Poster	*Symbiose-4-IuG - Systemübergreifende optimale dezentrale Verschränkung der Energienetze bei Industrie & Gewerbe*	Smart Grids Week 2016, Graz	2016
[15]	Talk	*Combined Electrical and Hydraulic Model for Dynamic Long-Term Operation of Pumped -Storage in SIMSEN*	19th International Seminar on Hydropower Plants, Laxenburg	2016
[16]	Journal	*Energieträgerübergreifende Planung und Analyse von Energiesystemen*	e&i Elektrotechnik und Informationstechnik	2016
[17]	Talk	*Vergleich von drehzahlvariablen Pumpspeichertechnologien in einem dynamischen Modell für Langzeitbetrachtungen*	IEWT Wien	2017
[3]	Talk and Poster	*Optimal allocation of energy storage and conversion technologies in an urban distributed energy system*	Congrès International des Réseaux Electriques de Distribution (CIRED), Madrid	2019

2 Introduction

This chapter gives an introduction to pumped hydroelectric energy storage technologies with a focus on variable speed pump-turbines. Furthermore, active power and frequency control is introduced. Finally, three monitoring methodologies for FCR provision are presented.

2.1 Pumped Hydroelectric Energy Storage

2.1.1 Introduction

Electrical energy storages (ESS) are an essential part of wide-area electric power systems to ensure a constant balance between electric power generation and consumption. Different energy storage technologies (EST) exist today for different storage applications in electric power grids. The most common storage processes (and their applications) are usually classified into five categories [18, 19]:

- **mechanical:** pumped-storage hydroelectricity, flywheels, dry gravitational, compressed air, thermo-mechanical
- **thermal:** sensible heat, latent heat, thermo-chemical
- **chemical:** power-to-gas (hydrogen, methane), alcohols, dimethyl ether, Fischer-Tropsch liquids
- **electrochemical:** batteries (Li-Ion, Pb-acid, Na, Ni), redox flow batteries (vanadium, zinc-bromine)
- **electrical systems:** super-capacitors, super-conducting magnets

The various storage systems differ in storage duration, charging and discharging times and power ratings. ESS are, therefore either more suitable for short-term, mid- and long-term applications depending on their underlying EST [18, 19]. Currently, the most

established electrical energy storage technology is pumped hydroelectric energy storage (PHES, also called pumped-storage hydropower or PSH), with a global installed capacity of around 130GW [20]. PHES are the main focus of this thesis and are described in more detail in the following chapters.

2.1.2 Basic Principle

Pumped hydroelectric energy storage operates by managing the gravitational potential energy of water. It consists of at least one upper water reservoir, possibly also fed by natural inflow, from which water is released via pressurized water pipe(s) (penstock) to produce electrical power when needed. Furthermore, it uses a lower reservoir to maintain the water to pump it back to the upper reservoir while consuming power from the grid. The amount of energy stored in the upper reservoir is proportional to its volume and the height difference between both reservoirs. The following equation expresses the stored energy E by using ρ as the density of the water, g as the acceleration of free fall, H as the difference in height, and V as the volume of water stored in the upper reservoir

$$E = \rho \cdot g \cdot H \cdot V \,. \tag{2.1}$$

By dividing both sides of the equation by time t the equation becomes

$$\frac{E}{t} = \frac{V}{t} \cdot \rho \cdot g \cdot H \,. \tag{2.2}$$

To get to the power equation, E/t is replaced by the power P and V/t by the volumetric flow of water Q

$$P = Q \cdot \rho \cdot g \cdot H \,. \tag{2.3}$$

However, there are losses in this conversion process based on the efficiency of the equipment. First, there are frictional losses due to the penstock pipe and in the turbine. Second, there are electrical losses in the generator, transformer and, depending on the PSH scheme, in the rectifier. So, an overall efficiency η represents these losses. Finally, the difference in height H has to be clarified. When the overall efficiency includes the penstock losses (sometimes also losses due to connection tunnels), the difference in height is called gross head H_{gross}, otherwise, it is called net head H_{net}. The effective difference in height also depends on the turbine technology. For Pelton turbines, it represents the difference between the water level behind the dam and the centerline of the turbine at the powerhouse. For Francis turbines, the downstream water level at the outlet of the draft tube, called “tail water level” need to

be used. The following equation includes the overall efficiency η (frictional and electrical losses included) and the gross head H_{gross}

$$P = \eta \cdot Q \cdot \rho \cdot g \cdot H_{gross} \,. \tag{2.4}$$

Figure 2.1 shows a diagram of the principle design of a PSH. Besides the reservoirs, it consists of a powerhouse that accommodates the hydraulic machine(s) and the motor-generator. A transformer establishes the power plants grid connection.

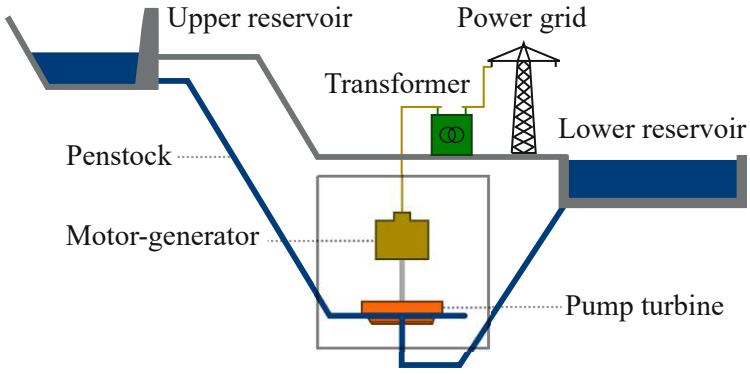

Figure 2.1: Pumped hydroelectric energy storage scheme with pump-turbine

PSH have a wide field of application. Traditionally, they are used to utilize surplus electricity from base load power plants by shifting electrical energy from off-peak to peak demand. Therefore, the operation of thermal or nuclear power plants could be optimized by extending their operating times at peak efficiency. The change from turbine to pump mode of the PSH was only necessary a small number of times during the day triggered by peak and off-peak energy pricing.

The energy transition to a renewable energy system expands and changes the application of PSH from a system viewpoint. The compensation of the non-influenceable meteorological and atmospheric conditions, which lead to fluctuating, non-consumption-compliant power production from (RES), becomes the focus of energy storage. PSH are tasked to increase the operational reliability in electricity grids (load-frequency control) by immediately balancing peak demand in a power supply network and rapid absorption of excess power in the event of a sudden load loss. Participating in the balancing markets triggered innovations to increase the speed and flexibility of new generation PSH.

2.1.3 Hydraulic Equipment Overview

The hydraulic machines for pumped storage hydropower plants can be classified into three main types:

- separate pump and turbine units
- reversible pump-turbine units
- ternary units

The selection of the hydraulic equipment for pumped-storage applications depend on the head (H) and the flow (Q). The main types of hydraulic machines used for pumped storage hydropower projects are impulse and reaction turbines. The Pelton turbine is the dominant impulse turbine today. Water under high pressure is released through one or more fine nozzles that produce high-speed jets of water. The jets are directed onto a bucket-shaped paddle on the turbine wheel. They operate in free air and are not submerged. They are mainly used where a high head of water of more than 450 m is present, and a low flow rate is available. The maximum head for a single Pelton turbine is normally around 1000 m. [21]

The most popular reaction turbine is the Francis turbine. The turbine responds to the pressure created by the weight of water at the base of the head. The turbine needs to be completely submerged. The water flow enters the turbine in a radial direction, and water must reach all blades equally. Water flow can be controlled by a set of gates around the turbine. Typically, Francis turbines are chosen for head heights between 100 m and 300 m. The limiting factor for a given head is the flow rate. Applications for higher heads lead to a smaller design size of the turbine and require a large flow to be successful. [21]

Reversible pump-turbine units usually include a Francis turbine that can also act as a pump depending on the direction of rotation. Ternary and separate units use either a Pelton turbine or Francis turbine and a separate pump (single or multi-stage). Figure 2.2 shows the range of application for various hydro turbines on a Q(H)-graph.

2.1.4 Generator Types for Pumped Hydro Power Plants

The generator in a hydropower plant is connected to the turbine through their common shaft. Many small plants employ asynchronous generators due to low costs and easier structure and rely on the grid to help them control their speed of operation. The efficiency of small asynchronous generators is much lower than that of large synchronous generators. Conventional large-scale synchronous speed hydropower plants have a turbine (reversible pump-turbine or separate turbine and pump) that uses a synchronous motor-generator and is directly connected to a grid (50 or 60 Hz). The rotating speed of both, turbine and motor-generator, is determined by the grid frequency and the number of poles of the generator. Francis turbines typically have rotational speeds between 100 and 1500 rpm, Pelton turbines between 400-1000 rpm [21]. The flexibility of the rotational speed is achieved by varying the number of poles.

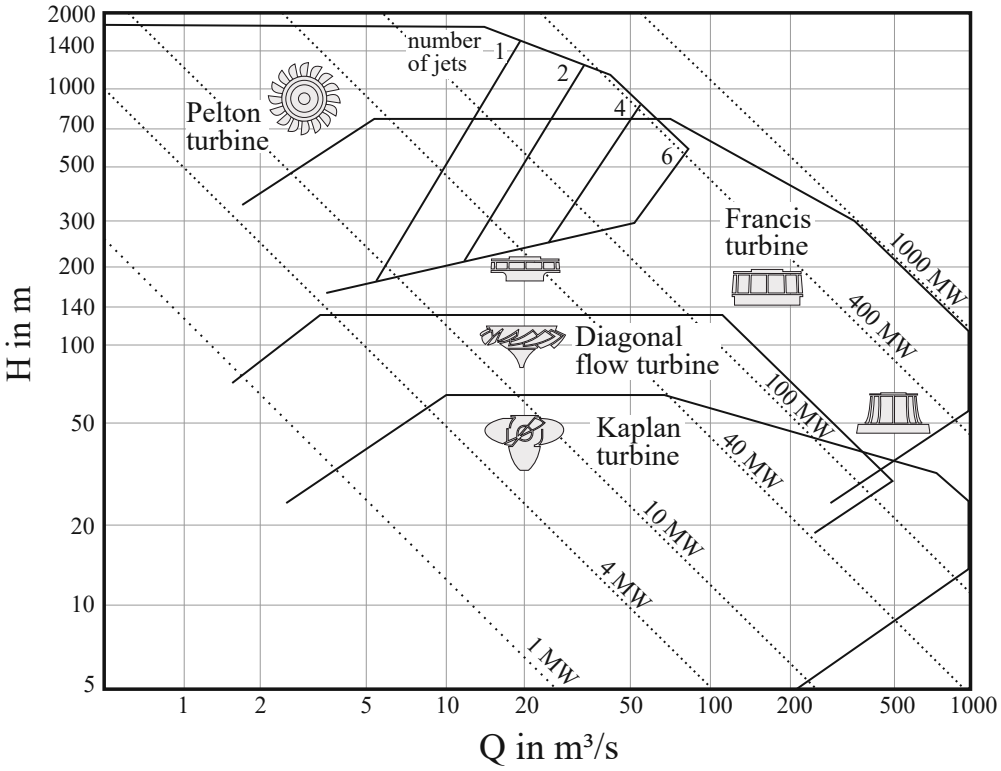

Figure 2.2: Range of application for various hydro turbines according to Sulzer Escher Wyss (based on [22])

For example, if the motor-generator is connected to a 50 Hz grid, a two-pole generator rotates at 3000 rpm and a four-pole one at 1500 rpm. In pump mode at a fixed speed, the absorbed power is only dependent on the head, and at a fixed head, there is no power regulation capability. Most large-scale hydropower plants still rely on directly connected synchronous generators. However, an increasing number of hydropower units are starting to install variable speed generators instead. These can operate at a wide range of speeds, which is especially useful to optimize their efficiency during operation and to enable control during pump operations. Two motor-generator technologies emerged for variable speed pump-turbines, the doubly-fed induction motor-generator and the synchronous motor-generator in combination with a full-size converter. The doubly-fed induction machine is an electric motor-generator where an adjustable frequency AC power converter feeds the field magnet windings. Therefore, the magnetic field can be made to rotate, allowing variation in motor or generator speed. The armature windings are still directly connected to a 50 Hz or 60 Hz grid. The converter needs to be designed to power only a percentage of the rated power of the motor-generator relative to the desired speed variation, typically around 10% of the rated power.

The second scheme uses a full-size power converter that connects the armature windings of a synchronous motor-generator to the grid. The converter provides the

conversion of the grid frequency to the operational frequency of the motor-generator. Therefore, the converter has to be designed to deal with the full power of the input or output of the motor-generator. However, restrictions on the solid-state component capacities and economic reasons limit the use of the design in power. The converter losses, in this case, are higher as a percent of the rated power of the motor-generator, but wider electrical speed variations can be achieved. Furthermore, no special equipment is needed to start up the pump in water, and a direct transition between pump and turbine operation is possible.

The efficiency advantages of variable speed pump-turbine units can be explained by using the *Hill Charts*. They describe the steady-state relationships of the turbine speed N, the flow rate Q, the guide vane opening y, the water head H, and the mechanical torque T. The hydraulic pump-turbine characteristic is further specified by unit speed n_{11}, unit flow q_{11} and unit torque t_{11} (see section 4.1). The industrial manufacturers usually provide these parameters through measurement from a scaled model of the pump-turbine [23]. Figure 2.3 shows the principle of variable speed operation with the help of the *Hill Charts*. The efficiency of the turbine η can be improved for lower unit flow rates q_{11} by reducing the unit speed n_{11} settings.

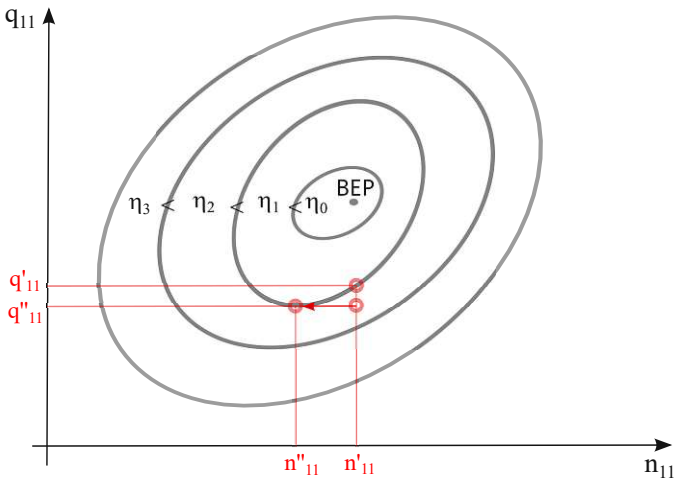

Figure 2.3: Explanation of the principle of variable speed operation with the aid of *Hill Charts* (turbine operation)

2.1.5 Concepts

Depending on the dimensions, parameters and desired flexibility of pumped storage project, four combinations of hydraulic and electrical equipment for pump-turbines are mentioned:

- FSPT (fixed speed pump-turbine): PSH plant with a fixed speed pump–turbine. A synchronous motor-generator and transformer connected the hydraulic machine

to the power grid.

- FSTS (fixed speed ternary set): PSH plant with a fixed speed pump and a separate fixed speed turbine. The hydraulic turbine can either be a Pelton or a Francis turbine. If both hydraulic units are allowed to operate simultaneously, a so-called hydraulic short circuit (HS) is possible. In this mode, the power input from the power grid during pump operations can the regulated by varying the power output of the turbine. A notable implementation of this principle in Austria is the power plant Kops 2.

- VSDFG (variable speed doubly-fed induction motor-generator): PSH plant with a pump-turbine and a grid connection by a (DFIM). This setup enables the pump-turbine to operate with variable speed. In Germany, the PSH plant in Goldisthal uses this scheme to power a 265 MW Francis pump-turbine.

- VSFSC (variable speed full size converter): a full size converter connects a synchronous motor-generator powered by a pump-turbine with the power grid. This scheme offers the highest flexibility for pump-turbines. A notable implementations is the pumped hydro storage plant Grimsel 2 in Switzerland with a 100 MW full size converter. However, in this case, the pump and turbine are separate machines and converter-based operations in turbine mode is not considered [24].

Figure 2.4 illustrates the four typical pumped hydro power plant schemes.

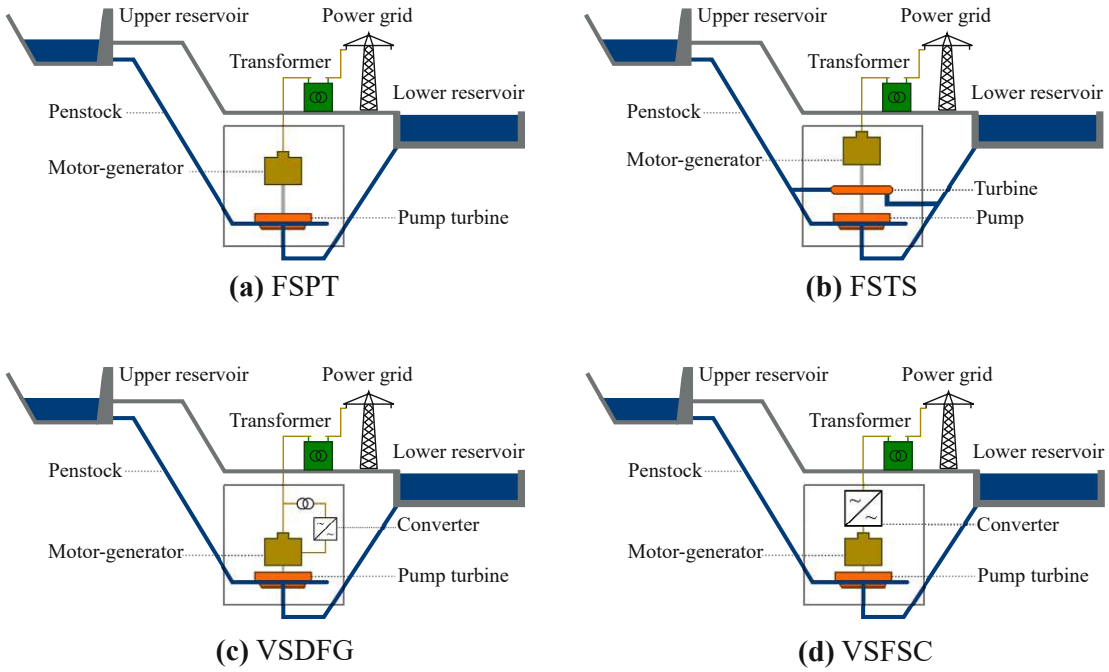

Figure 2.4: PSH schemes

A characterization based on the equipment used in Pumped hydro storage plants can also be made considering their ability to respond to grid support. The design of the waterways, penstocks, surge chambers and discharge tunnels need to done according to speed requirements for regulating the power input or output. Figure 2.5 shows the plant regulation range considering the electrical power output/input using Francis turbines. The lowest and less flexible option is conventional reversible units with no regulatory option in pump mode. Variable speed pump turbines can operate at lower power input or output. Ternary pump turbines are also very flexible and have the fastest response range.

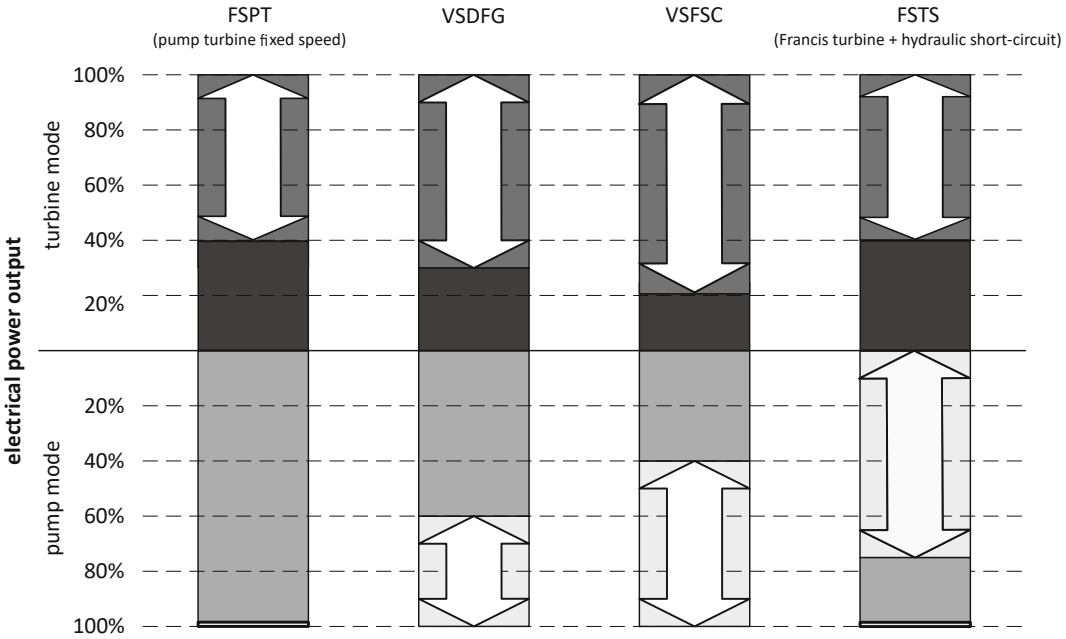

Figure 2.5: Plant regulation range of pumped storage hydro plants

There are different mode change times for the various unit concepts. A change of mode of operation for pump–turbines from pump to turbine operation and vice versa typically require a standstill. Hence, mode change times are longer. Fixed speed and variable speed drives with DFIM need to allow the dewatering of the pump for the transition from turbine to pump mode, with lasts at least 240 s [25]. FSTS with hydraulic short circuit are faster since both machines can operate simultaneously, and no standstill is required to change the rotational direction. The VSFSC enables fast start-up time and, therefore fast transition times from pump to turbine and the other way around. A direct pump start-up in water is possible since no synchronization time is required, and almost nominal torque is available from standstill [26].

Table 2.1 lists the mode change times for typical examples of the mentioned unit concepts.

Table 2.1: Mode change times for various unit concepts [26–28]

Mode Change	Pump Turbine			
	FSPT	FSTS+HS	VSDFG	VSFSC
Standstill → Turbine mode	75-90 s	65-90 s	90 s	n.a. [1]
Standstill → Pump mode	160-340 s	80-85 s	230 s	60 s [2]
Turbine mode →Pump mode	420 s	25-45 s	470 s	>32 s [3]
Pump mode →Turbine mode	90-190 s	25-60 s	280 s	>16 s [3]

2.2 Active Power and Frequency Control

Wide area electric power systems are operated at a synchronized frequency and link alternative current generators together by a transmission grid to provide power to the connected load at the same frequency. At every instant in time, a balance between load, generation, and losses is required to avoid a deviation from the system frequency of the interconnected power grid. Inevitable deviations from this balance are considered small, for example, during random load variations or large during a loss of generation or a significant load. A load-frequency-control (LFC) scheme is necessary in wide area synchronous grids to restore the system frequency after imbalances. Considering connected power, the synchronous grid of Continental Europe (managed by the ENTSO-E) is the largest synchronous electrical grid in the world as of now and operates at a utility frequency of 50 Hz. The Commission Regulation (EU) 2017/1485 of 2 August 2017 established a guideline on electricity transmission system operation, called "System Operation Guideline" (SOGL), including LFC requirements in the EU. Since April 2019, the Synchronous Area Framework (SAFA)[7] defines an updated collection of principles and rules for load-frequency control and reserves for the ENTSO-E Regional Group Continental Europe. SAFA and SOGL are slightly different in the dynamic requirements for FCR, as described in detail in subsection 2.2.1.

Within its synchronous area, the control actions and the active power reserves are organized in a hierarchical structure. Measurements to provide a stable system frequency are initiated by the TSOs within the synchronous area. Control actions to counteract load and power generation imbalances are performed by different complementary processes, each relying on reserves with different characteristics and qualities [7]:

a) Frequency Containment Reserves (FCR) - also previously referred to as Primary Control Reserves

b) Automatic Frequency Restoration Reserves (aFRR) - also previously referred to

[1] Currently, no VSFSC scheme with a pump-turbine exists
[2] Based on Grimsel 2
[3] Based on a reduced scale model test

as Secondary Control Reserves

c) Manual Frequency Restoration Reserves (mFRR) - previous Tertiary Control Reserves with an activation time independent of the time of activation of at most 15 minutes

d) Replacement Reserves (RR) - previous Tertiary Control Reserves which correspond to various types of reserves

FCR is a part of LFC that immediately responds to frequency deviations. The aim of FCR is to contain the system frequency deviation after an incident within a pre-defined range. FCR is replaced by the aFRR to free up the FCR active power reserves for new imbalances. The aFRR active power reserves are activated automatically within the imbalanced LFC Area to restore system frequency to the nominal frequency. Moreover, TSOs can activate the mFRR and the RR to restore or complement the aFRR.

Figure 2.6 shows the schedule of the different LFC processes for the ENTSO-E Regional Group Continental Europe.

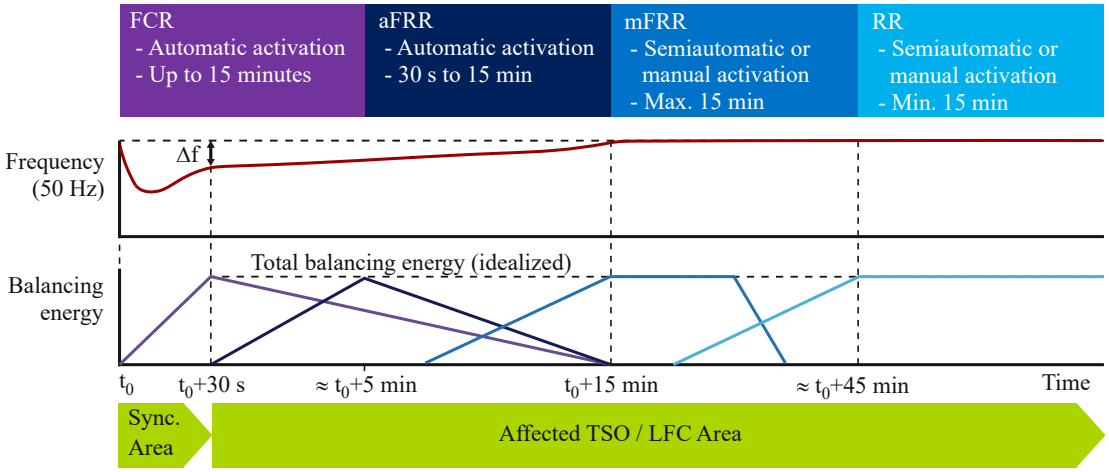

Figure 2.6: Load-Frequency-Control process following the Network Code of ENTSO-E Regional Group Continental Europe (Source: [29], modified)

The following section gives an introduction of the LFC processes FCR of ENTSO-E Regional Group Continental Europe as it is the process with the highest technical requirements concerning ramp rates and response time.

2.2.1 Frequency Containment Reserve

The balancing service provider (BSP) is a market participant with reserve-providing units or reserve-providing groups able to provide balancing services to TSOs [30]. Balancing service providers delivering FCR are subject to the following activation limits according to the current SOGL Article 154-7 interpretation:

a) *the activation of FCR shall not be artificially delayed and begin as soon as possible after a frequency deviation;*

b) *in case of a frequency deviation equal to or larger than 200 mHz, at least 50 % of the full FCR capacity shall be delivered at the latest after 15 seconds;*

c) *in case of a frequency deviation equal to or larger than 200 mHz, 100 % of the full FCR capacity shall be delivered at the latest after 30 seconds;*

d) *in case of a frequency deviation equal to or larger than 200 mHz, the activation of the full FCR capacity shall rise at least linearly from 15 to 30 seconds; and*

e) *in case of a frequency deviation smaller than 200 mHz the related activated FCR capacity shall be at least proportional with the same time behaviour referred to in points (a) to (d).*

Recently, the new proposal for the activation limits of FCR delivery has been discussed, but not ratified yet. The "All CE TSOs' proposal for additional properties of FCR as a part of the Synchronous Area Framework Agreement in accordance with Article 154(2) of the Commission Regulation (EU) 2017/1485 of 2 August 2017 establishing a guideline on electricity transmission system operation" (SAFA) defines new requirements for the provision of FCR. According to article 2 (version 28.12.2020):

> *Each TSO shall ensure that the activation of FCR providing units and FCR providing groups:*
>
> a) *is not artificially delayed and begins as soon as possible but no later than 2 seconds after a frequency deviation and;*
>
> b) *rises at least linearly.*
>
> *When one of the requirements a) or b) cannot be met, the FCR providing group or FCR providing unit shall provide technical evidence to the connecting TSO. The TSO assesses these justifications and decides whether or not the unit or group can be qualified to provide FCR. A refusal to be qualified shall be duly motivated by the reserve connecting TSO. The motivated decision shall be communicated to the FCR provider and relevant regulatory authority.*

A strict implementation of both FCR activation requirements are investigated in figure 2.7 (SOGL) and figure 2.8 (SAFA) for a frequency step of -200 mHz and a 1 MW awarded bid. Also displayed are the corresponding power signals for a first-order delay (T = 6 s) FCR providing unit. The tolerance channel is the area between the lower and upper boundary. For practical implementation, the basic limits need to be slightly improved (see subsection 2.2.2.2).

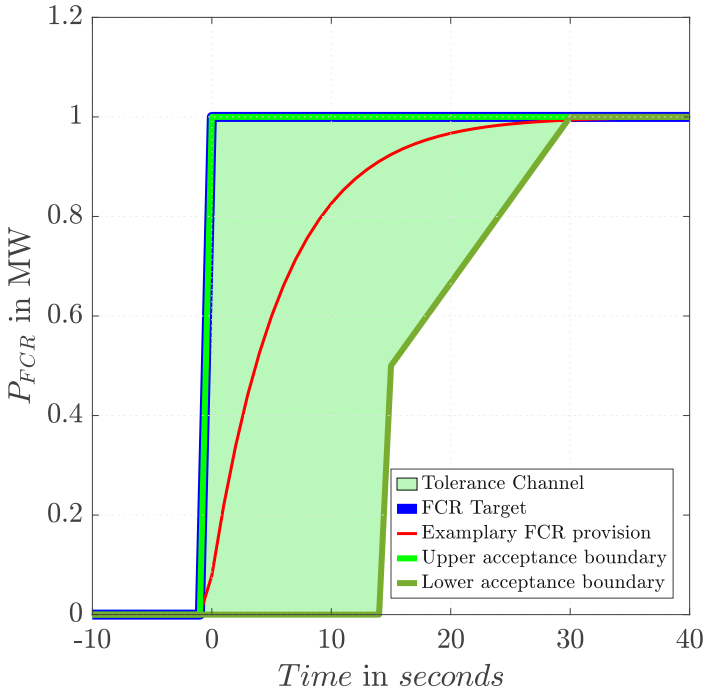

Figure 2.7: Tolerance channel based on a FCR target step at 0 s to 1 MW and the power output of a first-order delay (T = 6 s) BSP, considering the SOGL requirements for FCR provision

The FCR procurement takes currently place in a common market for TSOs from Austria, Belgium, Netherlands, France, Germany, Slovenia, Switzerland and West Denmark. The FCR cooperation's product characteristics are defined as follows [31]:

- Symmetric product (meaning that upward and downward FCR are procured together)
- Duration of product delivery: usually 4 hours, subject to daylight saving time shift.
- TSOs allow divisible and indivisible bids. Indivisible bids can have a maximum bid size of 25 MW in all the participating countries.
- Minimum bid size is 1 MW and resolution is 1 MW as well.
- In accordance with SO Reg. (Annex VI "Limits and requirements for the exchange of FCR"): Core shares and maximum transfer capacities (export limits) exist as limitations in the FCR market.

2.2.2 Monitoring of FCR Provision

The question of monitoring the availability and activation of FCR has become increasingly important. New reserve markets are discussed, or existing markets are opening up for new providers. Furthermore, changes in the behavior of market

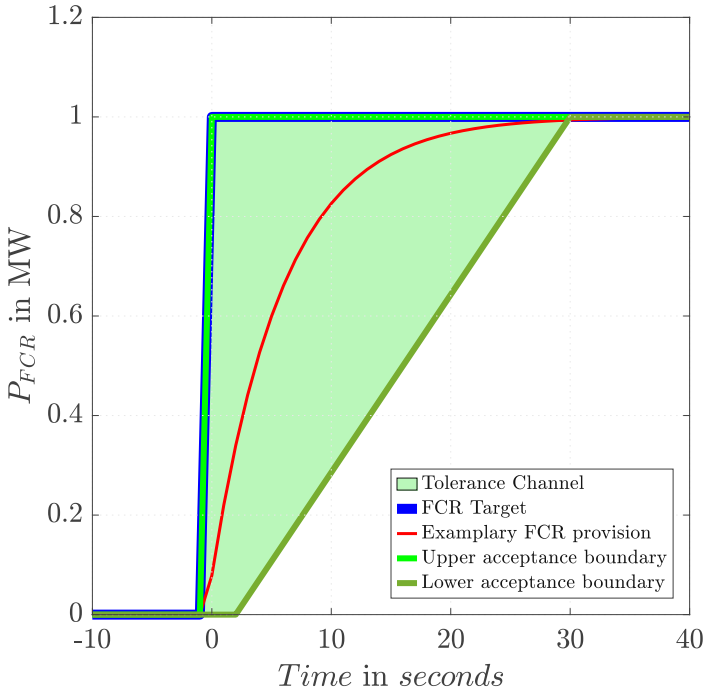

Figure 2.8: Tolerance channel based on a FCR target step at 0 s to 1 MW and the power output of a first-order delay (T = 6 s) BSP, considering the new SAFA requirements for FCR provision

participants (balancing service providers or BSP) make it harder to predict and monitor their participation in these markets. Up to now, no harmonized concept for FCR monitoring in RGCE exists. Thus, the respective approaches of TSOs are entirely different. Experience of TSOs who have tried to set up more complex monitoring approaches shows that there are remarkable challenges, not only for conventional Technical Entities (TEs) but also for the growing number of distributed technical entities (DTEs) partly using new technologies and participating in the provision of frequency control support. Monitoring the FCR provision generally consists of two tasks. The first task is to verify that the steady-state change in power output or input is in line with the steady-state frequency deviation and the required droop characteristic. The second task is to prove that the dynamics of the power output or input change are in line with the dynamics of the frequency deviation, the required droop characteristic, and the requirements of SAFA and SOGL.

There are currently five methods that are in use or discussed to monitor FCR provision:

- **Correlation methodology:** a statistical approach that calculates the linear correlation between the grid frequency and the activated FCR of the balancing service providers to determine the correct FCR provision.
- **Channel methodology:** a dynamic approach that determines a correct FCR provision by calculating a tolerance channel based on an upper and lower

acceptance boundary.

- **dp/df method**: a discontinuous, manual method that focuses on larger frequency deviations, which are more relevant for system security. In general, it could be applied on any frequency deviation. Inputs for this method are the measured power output, nominated FCR, and frequency measurements.
- **Dynamic normalization method:** a dynamic approach that combines a channel-based method with a dynamic model of the slowest admissible response. In addition, a graphic evaluation in the form of a normalization related to the correlation method is possible.
- **Performance scoring:** in this statistical method, regulating reserves are compensated based on performance using a performance score. The performance score consists of three different evaluation criteria named *Accuracy*, *Delay* and *Precision*. For the calculation every component is rated equally.

Out of these five methods, three methods for monitoring FCR provision are selected that are suited for automation and graphical evaluation (Correlation methodology, channel methodology and dynamic normalization method). These methods that are still part of ongoing research are implemented (with enhancements) and used in chapter 6 for monitoring purposes. The dp/df method as a manual evaluation is not suited for automation and is especially sensitive to noise. Therefore, it lacks comparability. The Performance scoring does not offer a graphical evaluation. Hence, no statements about under- or overfulfillment in case of a poor performance can be made. Moreover, it is not possible to consider upper and lower limits for FCR activation.

2.2.2.1 Correlation Methodology

This methodology uses a statistical approach to determine the activated FCR (see e.g. [32]). The basic idea is to calculate the linear correlation between the grid frequency f and the activated FCR of the balancing service providers (BSP). The expected result has an indirect proportionality between both values. Therefore, an increasing frequency initiates a reduction in power output of FCR delivering units, and a decreasing frequency leads to increased power output. Moreover, the Pearson's correlation index r can be calculated to quantify the rate of linear correlation between the grid frequency and activated FCR. For r only values between -1 and 1 are possible, while the desired outcome is a value close to -1:

$$r = \frac{\sum_{i=1}^{n}(f_i - \bar{f}) \cdot (p_i - \bar{p})}{\sqrt{\sum_{i=1}^{n}(f_i - \bar{f})^2 \cdot \sqrt{(p_i - \bar{p})^2}}} \tag{2.5}$$

In the equation, f represent the frequency and p the rated power of the FCR provision. For

- $r = -1$ a maximum reciprocal correlation is determined.
- $r = 0$ no correlation is determined.
- $r = +1$ a maximum proportional correlation is determined.

Linear regression is used to find a relationship between the frequency and the activated FCR from the BSP. The desired FCR provision from the BSP is called the FCR target ($P_{FCR,target}$). The FCR target is calculated using the droop K_{BSP} (in MW/Hz) multiplied by the frequency deviation from the set-point $\triangle f$ (see equation 2.6). The set-point frequency f_{set} in ENTSO-CE power system is 50 Hz. The FCR target $P_{FCR,target}$ is calculated for frequency deviations smaller than $\triangle f_{FCR,max}$, which is ±200 mHz, and the awarded FCR bid $P_{FCR,bid}$ (e.g. ±1 MW) by the following formula

$$P_{FCR,target}(f) = -K_{BSP} \cdot \triangle f = -\frac{P_{FCR,bid}}{\triangle f_{FCR,max}} \cdot (f - f_{set}) \tag{2.6}$$

Typically, the actual FCR provision of the BSP ($P_{FCR,BSP}$) follows the FCR target value ($P_{FCR,target}$), which is constantly changing because of constantly changing frequency deviations, within its dynamic capabilities. For every current frequency value (and accordingly for every actual frequency deviation and corresponding FCR target value), an actual $P_{FCR,BSP}$ value can be measured. The measurement resolution is typically 1 or 2 seconds. These data points are used in the correlation diagram. An example of the methods' graphic representation is shown in figure 2.9. In this diagram, the per unit base is used for $P_{FCR,BSP}$. The per unit base value is equal to the awarded FCR bid $P_{FCR,bid}$. The FCR provision of the BSP in per unit is calculated by

$$p_{FCR,BSP} = \frac{P_{FCR,BSP}}{P_{FCR,bid}}. \tag{2.7}$$

Since deviations from the target value (solid green line in figure 2.9) are expected, an additional tolerance is granted. The green dashed lines mark a ±10% tolerance (or ±0.1 per unit based on the awarded FCR bid) band around the target value based on the awarded FCR bid. The droop of the linear regression line K_{linReg} indicates the actual FCR provision of the BSP in MW per Hz and k_{linReg} in per unit per Hz. Since full activation of FCR occurs at 200 mHz, the droop of the linear regression line multiplied by 200 mHz delivers the indicator $P_{FCR,BSP,monitored}$ (in MW), respectively, $p_{FCR,BSP,monitored}$ (in p.u.) for the actual FCR provision of the BSP at full activation. Ideally, this value should be identically with the awarded FCR bid (or 1 per unit based

on the awarded FCR bid), which is a symmetrical product. Therefore, the monitored FCR provision $P_{FCR,BSP,monitored}$ of the BSP in MW is

$$P_{FCR,BSP,monitored} = -K_{linReg} \cdot \triangle f_{FCR,max} \tag{2.8}$$

and $p_{FCR,BSP,monitored}$ in per unit is found by

$$p_{FCR,BSP,monitored} = -\frac{K_{linReg}}{P_{FCR,bid}} \cdot \triangle f_{FCR,max}. \tag{2.9}$$

The monitored FCR provision $p_{FCR,BSP,monitored}$, in this case $\mp$0.91 p.u., can also be found in figure 2.9 as the values at the intersections with the 49.8 Hz, respectively 50.2 Hz plane. The FCR provision is considered correct, as the Pearson's correlation index $r$is close to -1, the data points are within the defined threshold and the monitored FCR provision is within 10 % of the requested value.

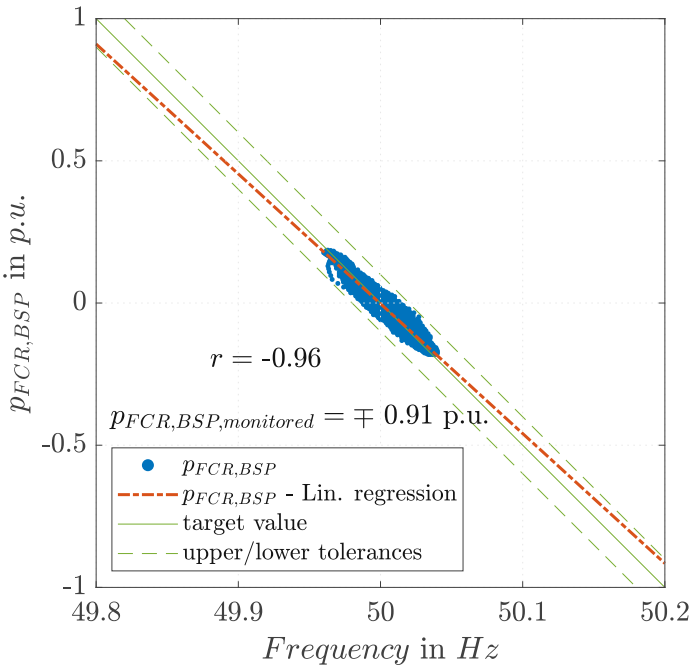

Figure 2.9: Correlation diagram of a 4 hour frequency measurement (with 1 s resolution) and activated FCR from a fictional BSP with the target droop and the regression line as well as the accepted threshold.

The behavior of the correlation methodology is demonstrated for different input signals to highlight its results for steady state and dynamic performance. First, the design hypothesis frequency deviation (see section 4.4) is used, and FCR provision is calculated for a BSP with a first-order delay behavior with a time constant of 6 seconds. This dynamic behavior of the BSP is considered fast enough to deliver a correct FCR provision according SOGL requirements. Figure 2.10 depicts the outcome for a BSP with 1 p.u. FCR bid when the correlation methodology is applied.

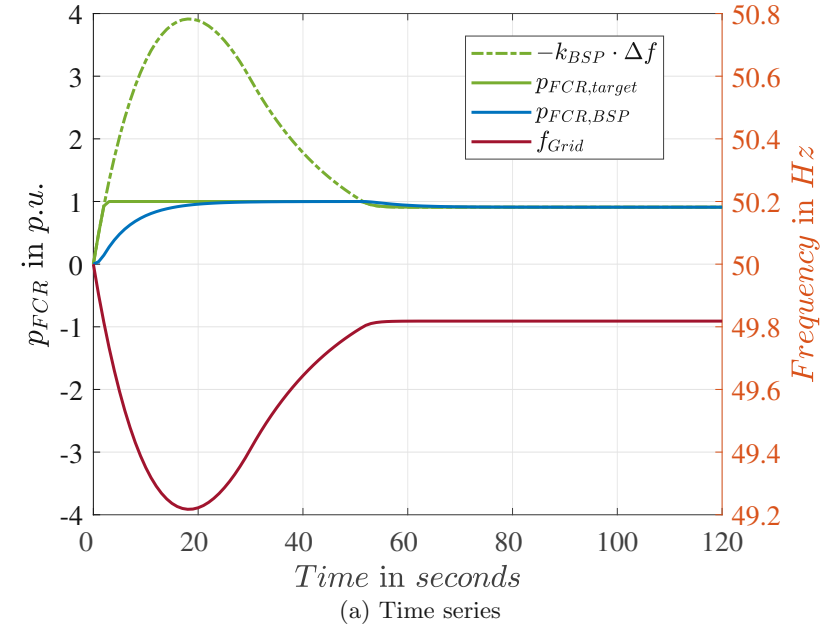

(a) Time series

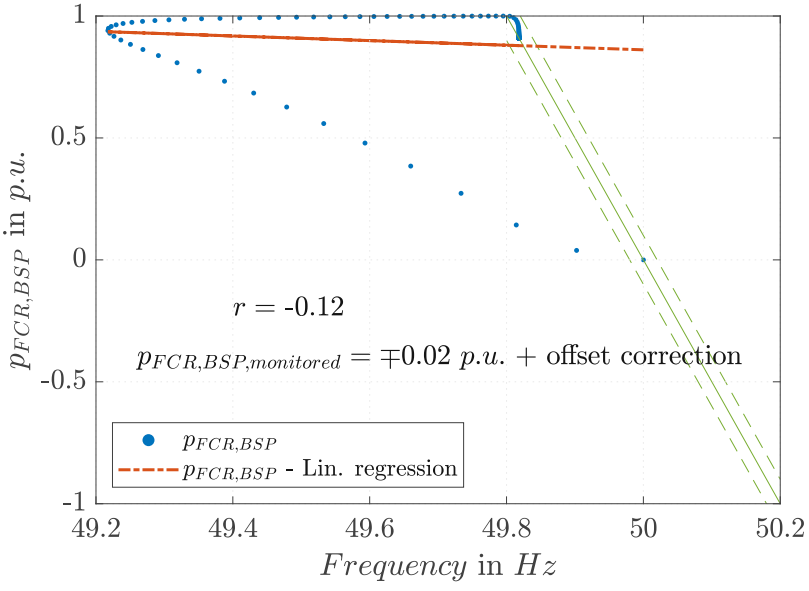

(b) Correlation diagram

Figure 2.10: Results for a frequency signal according to the design hypothesis (power gradient 100 MW/s) and a first-order delay block with $T = 6\,s$ as the FCR providing unit

The dynamic of the frequency signal is high, but full activation is reached after 25 s by the BSP. Hence, the FCR provision of the BSP is correct. However, the correlation diagram indicates a large deviation from its 10 % tolerance band. In this highly dynamic case, the correlation methodology is not performing well in monitoring a correct FCR provision, and other methods are better suited. Concerning quasi steady-state deviations, the correlation methodology works well in detecting non-compliance in FCR provision by a BSP. Figure 2.11 highlights two scenarios of non-compliant FCR delivery. In sub-figure 2.11a, the activation from the BSP is too small (only 80 % of FCR bid), which is detected as a wrong droop. Sub-figure 2.11b shows a limitation (with a maximum of 10 % of FCR bid) in the FCR provision by the BSP, which also leads to a smaller activation than required.

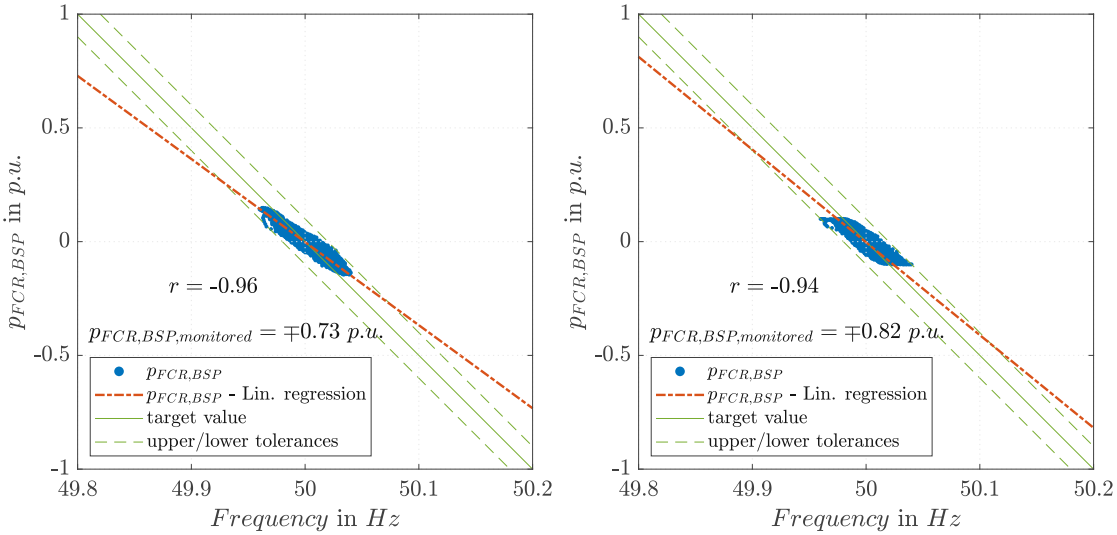

(a) Wrong droop (80 % of FCR bid)

(b) Limited provision (limited to 0.1 p.u.)

Figure 2.11: Correlation diagrams demonstrating and a first-order delay block with $T = 6\,s$ as the FCR providing unit

2.2.2.2 Channel Methodology

The Channel Methodology determines a correct FCR provision by calculating a tolerance channel based on an upper and lower acceptance boundary. Every frequency deviation, together with the awarded FCR bid for the delivery period, results in a new FCR target value and new channel boundaries for the next 30 seconds. For a positive FCR provision, the lower limit of the channel is built on the basis of Article 154-7 of the "System Operation Guideline" (SOGL) (see figure 2.7). Of course, the "Synchronous Area Framework" (SAFA) requirements (see figure 2.8) can also be used to determine the lower acceptance boundary. The upper limit is based on the FCR target. Furthermore, an additional tolerance of e.g. 5 % is considered on top of the

boundaries. An overshoot margin after an FCR target step of another 5 % for 6 seconds can also be granted on the upper boundary for a correct FCR delivery. Figure 2.12 shows the principle idea of the determination of the lower boundary of a tolerance channel according to Article 154-7 of the SOGL.

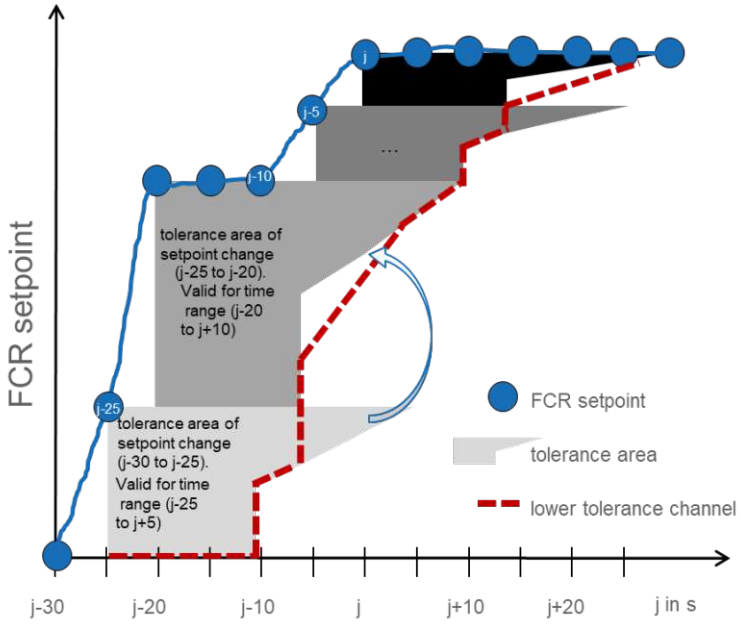

Figure 2.12: Example for the calculation of the lower boundary of the tolerance channel according to article 154-7 of the SOGL (source: RTE)

The simulation tool MATLAB®Simulink is utilized to calculate the tolerance channel based on SOGL and SAFA. In the model, the FCR channel lower acceptance boundary $P_{FCR,lab}$ and upper acceptance boundary $P_{FCR,uab}$ are calculated. Furthermore, a 5 % tolerance is added to the boundaries as well as a 6 s and 5 % additional tolerance for overshooting reactions to a target step. If the FCR target is zero, the channel's upper and lower boundary could be identical, and the channel would result in a single line. Any deviation from it from the FCR provider would be considered a breach of the tolerance channel. Therefore, a fixed band of 50 kW around the zero line is added. This additional tolerance can be quite significant for small FCR provisions and looses its influence for larger FCR deliveries.

Figure 2.13 shows the creation of an enhanced FCR channel according to the SOGL. First, the step response from 0 MW FCR provision to 1 MW and -1 MW is shown. Then the process is depicted for multiple steps of the same sign based on figure 2.12.

Figure 2.14 indicates the results for an enhanced tolerance channel according to the SAFA guidelines.

In both figures, the response of a BSP ($P_{FCR,BSP}$) with a first-order delay with a 6 s time constant is also represented. It can be seen that the output of the BSP is

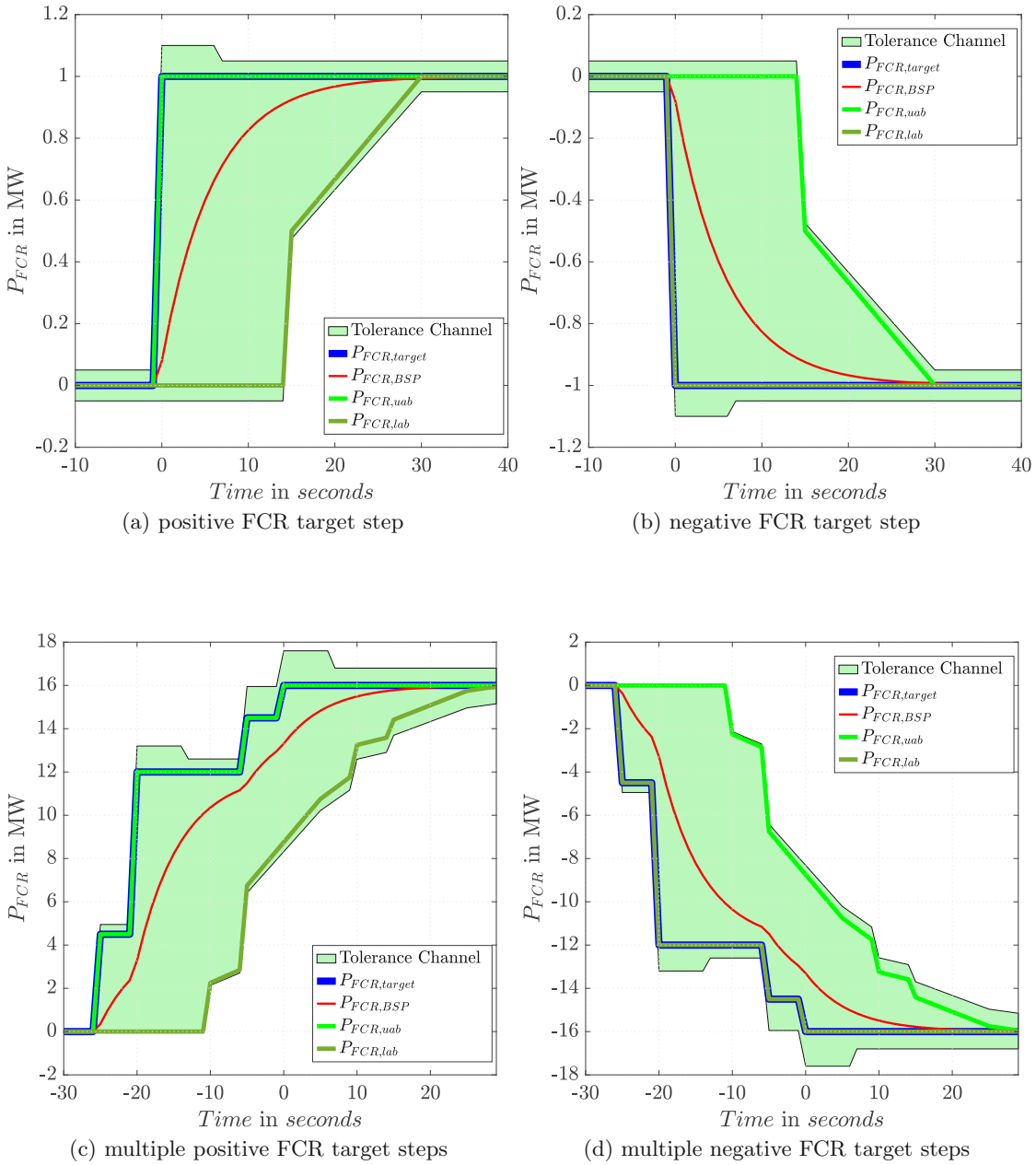

(a) positive FCR target step

(b) negative FCR target step

(c) multiple positive FCR target steps

(d) multiple negative FCR target steps

Figure 2.13: Creation of FCR channel according to SOGL

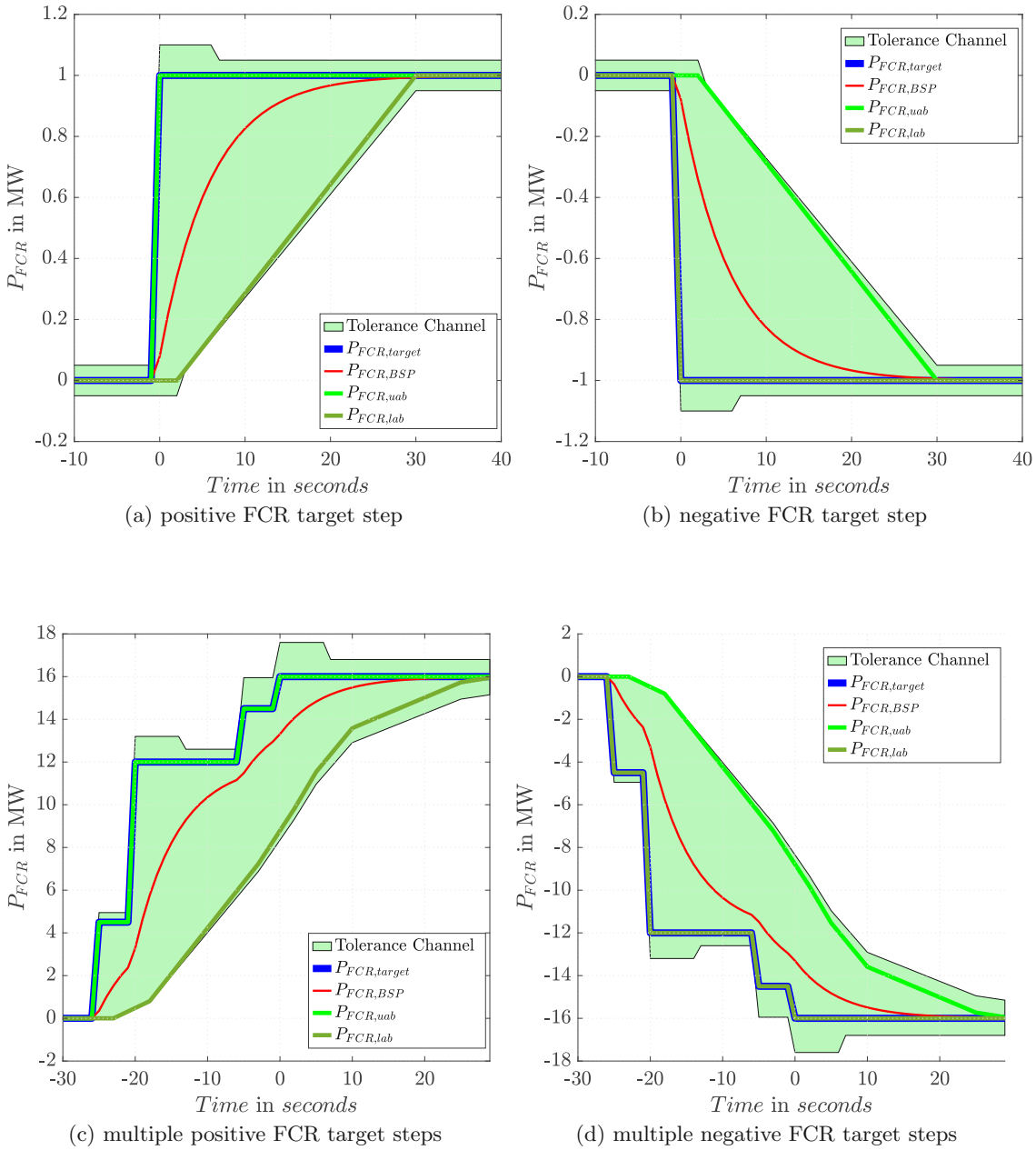

(a) positive FCR target step

(b) negative FCR target step

(c) multiple positive FCR target steps

(d) multiple negative FCR target steps

Figure 2.14: Creation of FCR channel according to SAFA

well within the boundaries for the FCR target step. However, an analysis of an FCR target signal with high fluctuations is also necessary to determine if the assumed BSP is dynamically fast enough for a correct provision at all times. Therefore, a 4 hour FCR provision of a BSP with a hypothetical first-order delay behavior (6 s time constant) is investigated with the improved channel methodology. Two cases are shown, one with a correct droop and one with a lower droop. Figure 2.15 depicts the results for these two scenarios for the SOGL requirements, as well the lower ($p_{FCR,ltb}$) and upper ($p_{FCR,utb}$) tolerance boundaries. All values are presented in per unit based on the positive FCR bid size. The FCR target value $P_{FCR,target}$ is calculated by equation 2.6 and transformed to per unit based on the FCR bis size. An error signal is also present, which is non-zero, when the FCR provision is outside of the tolerance channel. The error signal $P_{FCR,Error}$ (in MW) is calculated by

$$P_{FCR,Error}(P_{FCR,BSP}) = \begin{cases} 0 & , P_{FCR,ltb} \leq P_{FCR,BSP} \leq P_{FCR,utb} \\ P_{FCR,BSP} - P_{FCR,utb} & , P_{FCR,BSP} > P_{FCR,utb} \\ P_{FCR,BSP} - P_{FCR,ltb} & , P_{FCR,BSP} < P_{FCR,ltb} \end{cases} \tag{2.10}$$

The error signal $p_{FCR,Error}$ in p.u. can be obtained by dividing $P_{FCR,Error}$ by the positive FCR bid size.

Considering a correct droop setting, the error signal is zero during the observed 4 hour period. To demonstrate the ability to detect a incorrect FCR delivery, the droop of the BSP is reduced to 80 %. Especially in highly dynamic sections, the FCR provision of the BSP is outside of the channel, and the error signal is non-zero.

The same two scenarios calculated with the SAFA channel requirements are shown in figure 2.16. The channel based on SAFA is more restrictive, and a BSP with first-order delay ($T = 6\,s$) is already outside of the channel at times. A lower droop increases these instances and duration further. Therefore, the assumption that a BSP with a first-order delay behavior ($T = 6\,s$) stays within the tolerance channel based on SAFA is incorrect. One way to correct this is to increase the tolerance band of the SAFA-based channel.

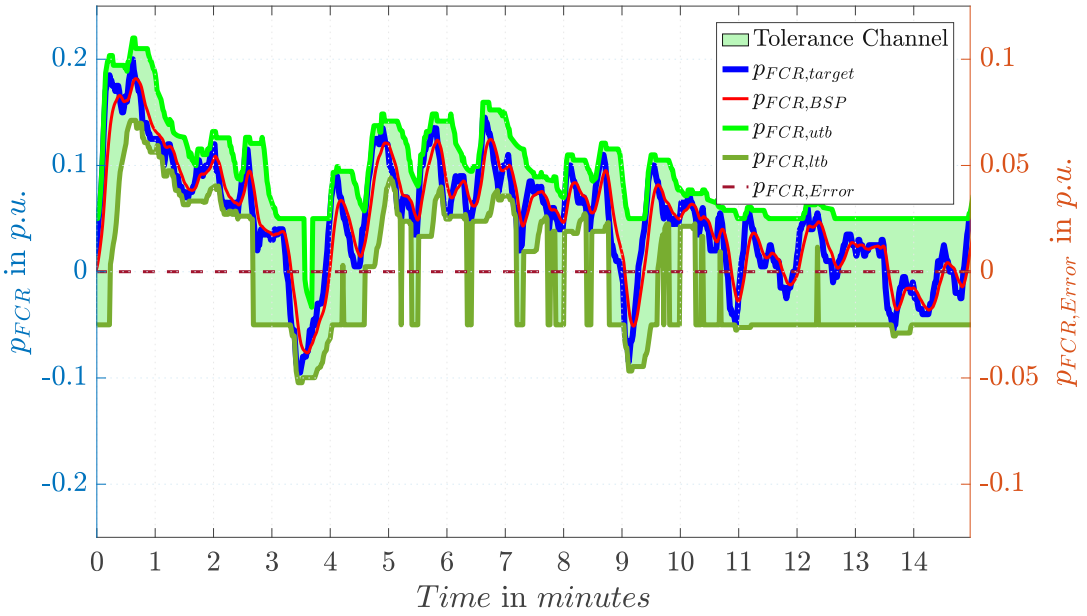

(a) Correct provision

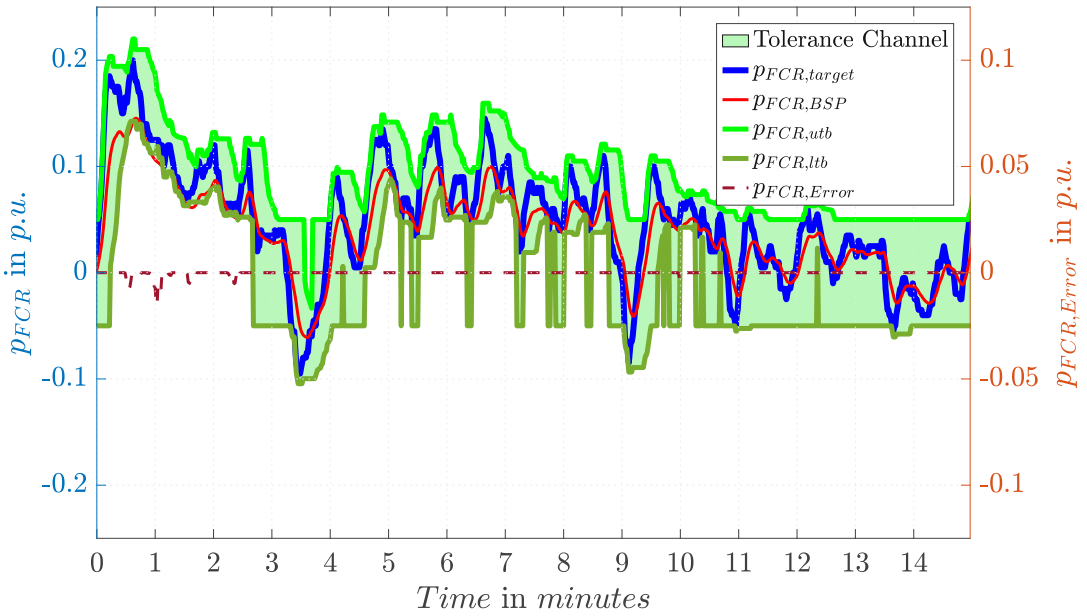

(b) Provision with a droop of 80 % of the original

Figure 2.15: Creation of FCR channel according to SOGL demonstrated with a first-order delay block with $T = 6\,s$ as the FCR providing unit

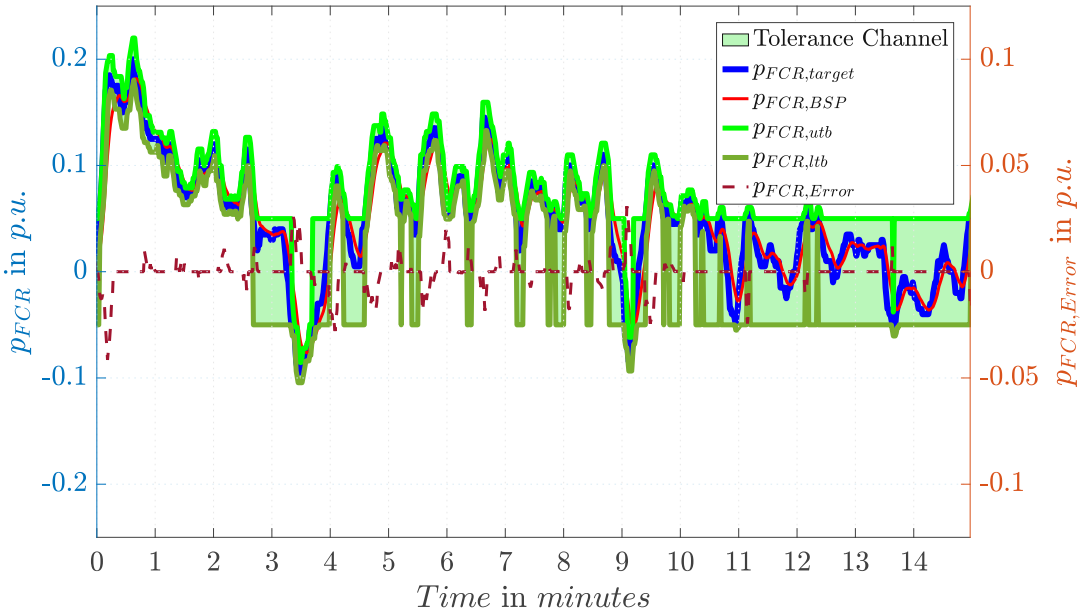

(a) Correct provision

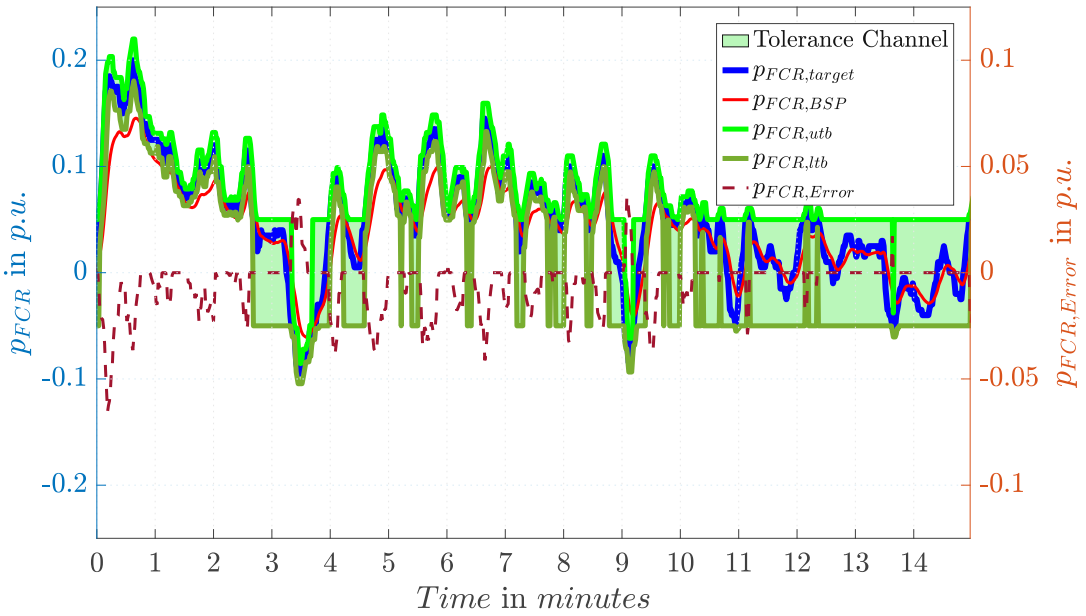

(b) Provision with a droop of 80 % of the original

Figure 2.16: Creation of FCR channel according to SAFA demonstrated with a first-order delay block with $T = 6\,s$ as the FCR providing unit

2.2.2.3 Dynamic Normalization Methodology

The dynamic normalization methodology approach combines a channel-based method with a dynamic model of the slowest admissible response. Furthermore, a graphic evaluation in the form of a normalization related to the correlation method is possible. The dynamic normalization methodology extends the correlation methodology to the requirements of SOGL. The methodology was created by the University of Stuttgart and has been documented e.g. in [33].

The creation of the tolerance channel is based on the transfer function $G_1(s)$, which according to [33], can be seen as the dynamic response to a frequency step of the slowest FCR providing unit that still complies with the FCR requirements specified in the SOGL. The transfer function $G_1(s)$ approximates the slower boundary specified in the SOGL for a step change of the frequency by 200 mHz [33]:

$$G_1(s) = \frac{0.0404}{s^3 + 0.745 \cdot s^2 + 0.4009 \cdot s + 0.0404} \cdot e^{-\tau_d \cdot s} \tag{2.11}$$

The time delay T_d is defined as 10 seconds and τ_d as $\frac{T_d}{1\,second}$. The input of the transfer function is the FCR target signal. For a positive FCR target change the slower boundary is the lower boundary, and for a negative FCR target change, the upper boundary. Sub-figure 2.17a shows an example of the FCR channel based on the methodology. Sub-figure 2.17b depicts a comparison between the response of the transfer function $G_1(s)$ for a set-point step from 0 to 1 p.u. and SOGL requirements. It is noticed by [33], that the response of the transfer function is intentionally less strict compared to SOGL to avoid unjustified identification of non-compliance.

The idea to use a transfer function instead of the explicit SOGL specifications is based on the fact, that the SOGL only specifies the required response to a step change in frequency. Requirements with respect to the response to arbitrary frequency signals are not specified. Applying the SOGL step response specifications for every frequency measurement data point assumes that both frequency and FCR activation have been at a steady state before. The use of the transfer function, however, approximates the non-linear SOGL step response and makes it possible to generalize the SOGL minimum requirements to arbitrary inputs. The minimum requirements specified in SOGL (see sub-figure 2.17b) cannot be represented as the response of a linear dynamical system due to its discontinuity. The SOGL requirements are interpreted in the dynamic normalization methodology as the boundaries of the set of admissible step responses and not as actual step responses.[33]

The evaluation of the FCR provision for a certain time span (e.g. 4 hours) is done by using normalization of the tolerance channel output data. With it, the deviations of the FCR activation at different times and for different tolerance channel widths are

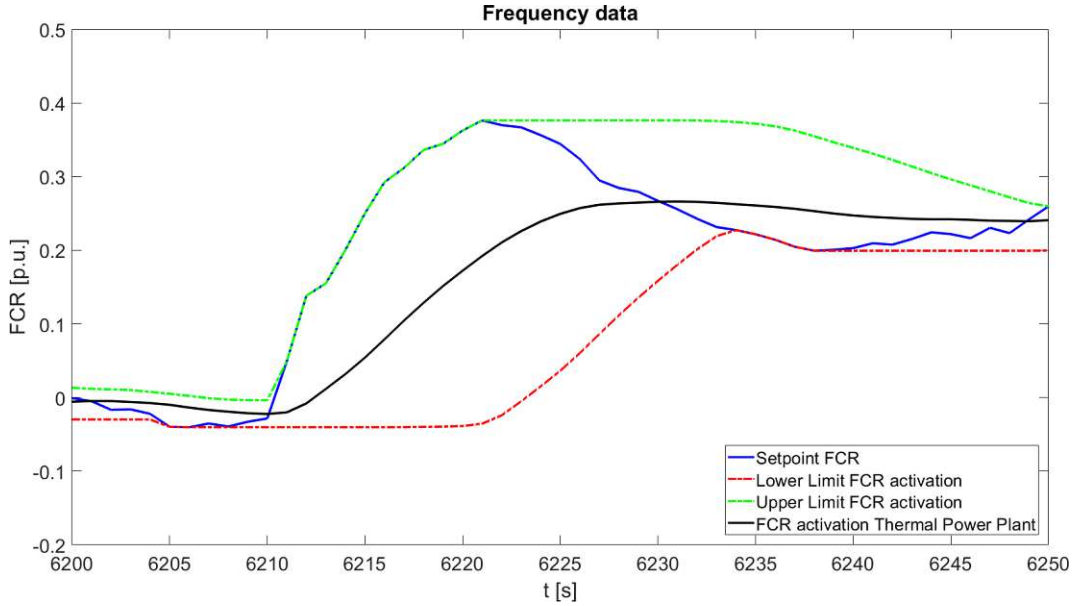

(a) Example of FCR channel to a specific frequency data

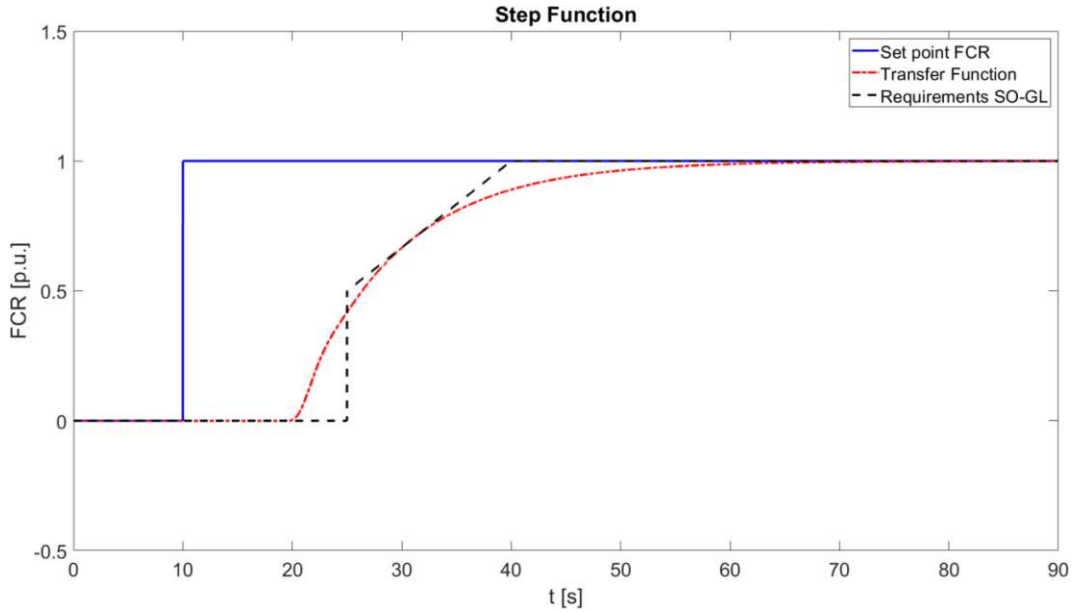

(b) Transfer function for a positive FCR set point step and SOGL requirements

Figure 2.17: Dynamic Normalization Methodology (source:[33])

possible. It can also be used for the definition of a condensed non-compliance indicator. The normalized deviation d_{norm} is determined according to [33] by the activated FCR of the providing unit (FCR_{act}), the lower bound (LB), and the mean value of the FCR channel (MV).

$$d_{norm} = \frac{FCR_{act} - MV}{MV - LB} \tag{2.12}$$

The FCR activation of the monitored unit can by categorized by the normalized deviation as following:

- $>$ 1: bigger than Upper Limit FCR activation
- $=$ 1: equal to Upper Limit FCR activation
- $<$ 1 and $>$ - 1: Within the tolerance channel (0: equal to the Mean value of FCR-Channel)
- $=$ -1: equal to Lower Limit FCR activation
- $<$ -1: smaller than Lower Limit FCR activation

Furthermore, a graphical analysis can be done for a chosen time period by plotting all values for d_{norm} over the corresponding MV. Figure 2.18 shows an example of the correlation of specific deviations, mean value of FCR-channel, and the respective boundaries. Moreover, different cases of non-compliance can be identified by the graphic evaluation. As [33] states, the normalization allows for a comparison of the deviations of the FCR activation at different times and for different tolerance channel widths and is, therefore, a prerequisite for the definition of a condensed non-compliance indicator. In the plot, all values for d_{norm} are plotted over the corresponding mean value of the FCR channel. The green line is the indicator for the mean value, where the specific deviation is zero. The red lines are the tolerance boundaries.

For this thesis, the dynamic normalization methodology is implemented in MATLAB®Simulink. For this thesis, the dynamic normalization methodology is implemented in MATLAB Simulink. To test the methodology implementation, the response of a BSP with a first-order delay with 6 s time constant to the 4 hour frequency signal previously used is calculated. Figure 2.19 shows the time series and the normalized deviation diagram for this scenario in per unit based on the awarded FCR bid. The FCR target value in p.u. is $p_{FCR,target}$, and $p_{FCR,BSP}$ is the response of a BSP with a first-order delay with a 6 s time constant. The presented error signal $p_{FCR,Error}$ in p.u. can be obtained by dividing $P_{FCR,Error}$ (see equation 2.10) by the positive FCR bid size. The lower ($p_{FCR,ltb}$) and upper ($p_{FCR,utb}$) tolerance boundaries are also shown. The tolerance channel is defined as the area between the upper and

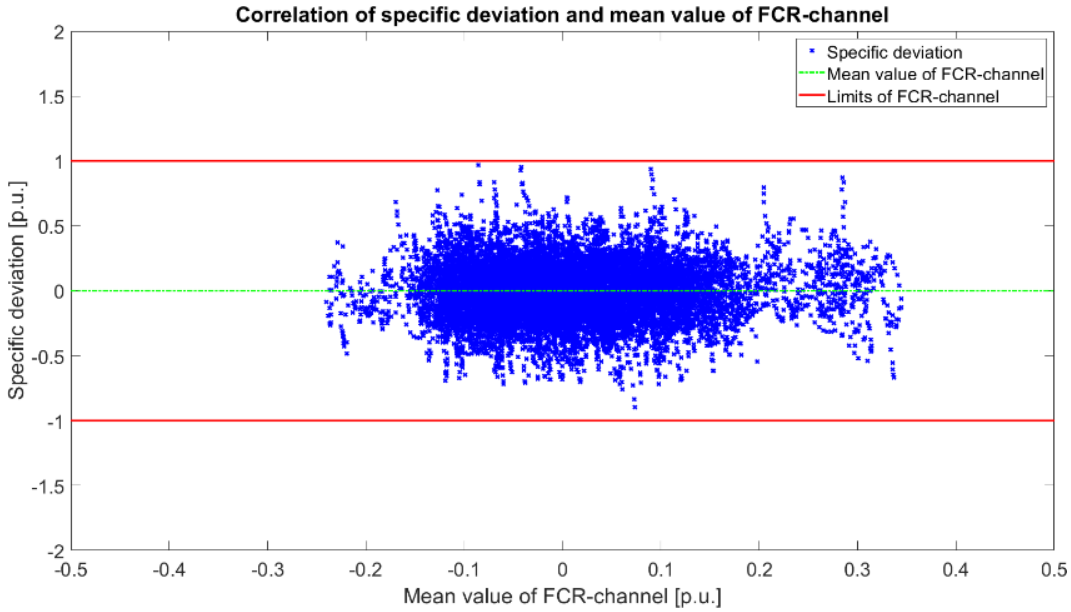

Figure 2.18: Correlation of specific deviation and mean value of FCR-channel (source:[33])

lower tolerance boundary. Compared to the channel methodology, the tolerance channel is considerably wider for small FCR provisions (compared to the FCR bid size).

The reason for this is the fact that the upper tolerance boundary *utb* and the lower tolerance boundary *ltb* consider a 5 % tolerance of the total FCR bid $P_{FCR,bid}$ on top of the mean value of the FCR channel MV_0 or the FCR target FCR_{set} [33].

$$P_{FCR,utb} = max\left\{ub_0; MV_0 + 0.05 \cdot P_{FCR,bid}; FCR_{set} + 0.05 \cdot P_{FCR,bid}\right\} \tag{2.13}$$

$$P_{FCR,ltb} = max\left\{lb_0; MV_0 - 0.05 \cdot P_{FCR,bid}; FCR_{set} - 0.05 \cdot P_{FCR,bid}\right\} \tag{2.14}$$

However, the additional 5 % tolerance for the FCR channel on top of the FCR target FCR_{set} can be omitted according to [33], as this addition can be considered optional. Figure 2.20 depicts the results for the tighter FCR channel for a correct droop (k-factor) and figure 2.21 the outcome for a droop of only 80 % of the original droop.

The error signal of the correct FCR provision of the BSP is zero for the whole period. This is also highlighted in the normalized deviation diagram since the result stays within the bounds of the FCR channel. The scenario with the 80 % droop delivers a non-zero error signal, but only for a few incidents. However, the normalized deviation is also visibly tilted to the left, which indicates an under-fulfillment.

The results of this method concerning the monitoring of FCR provisions by variable speed pump-turbines are shown in subsection 2.2.2.2.

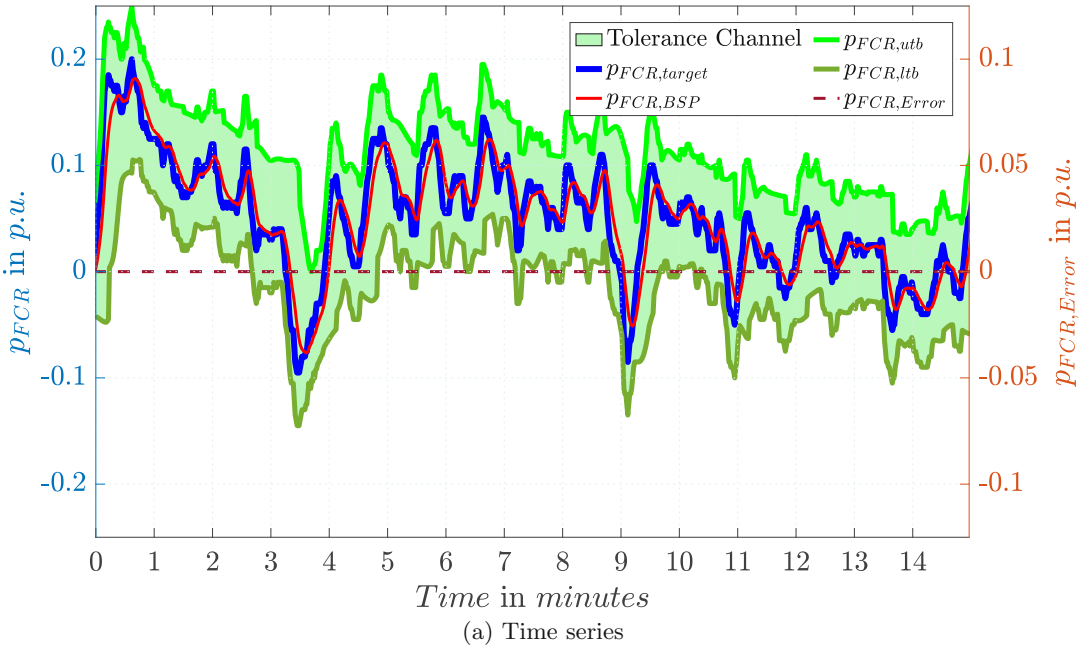

(a) Time series

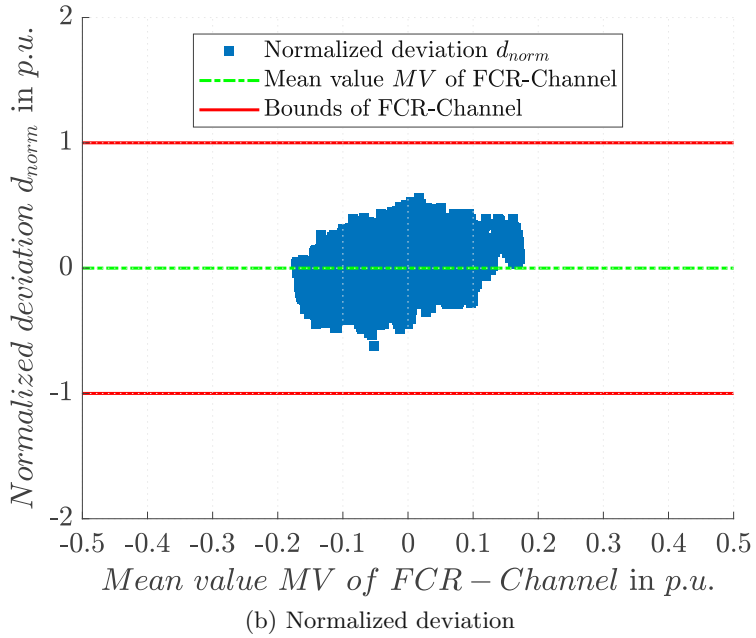

(b) Normalized deviation

Figure 2.19: Creation of FCR channel according to the dynamic normalization methodology demonstrated with a first-order delay block with $T = 6\,s$ as the FCR providing unit and an additional tolerance of 5 % of $P_{FCR,bid}$

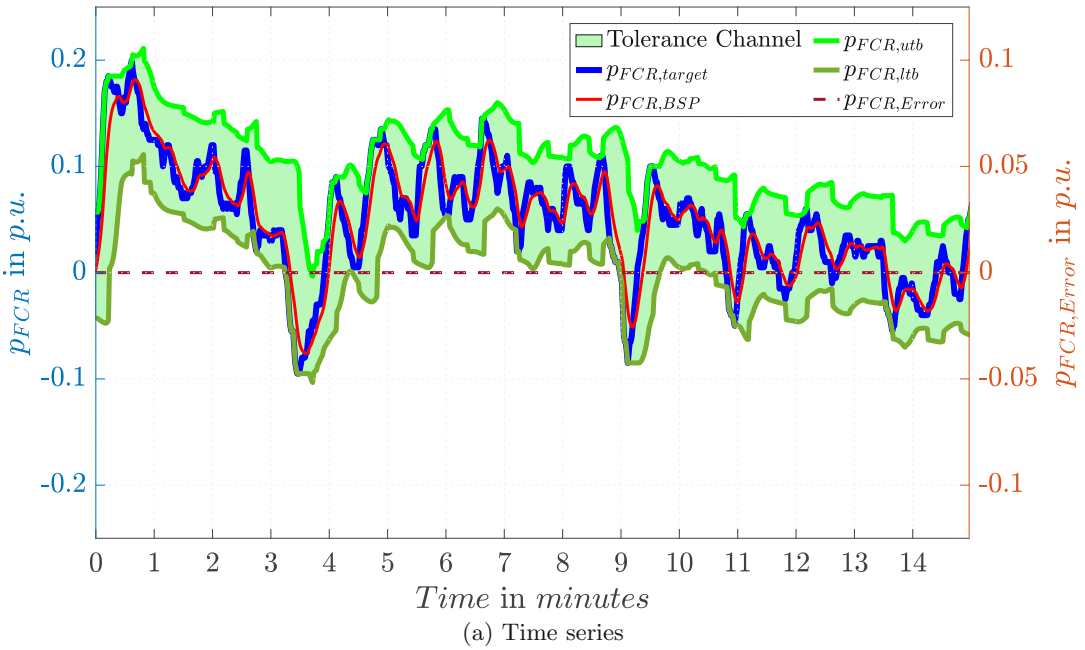

(a) Time series

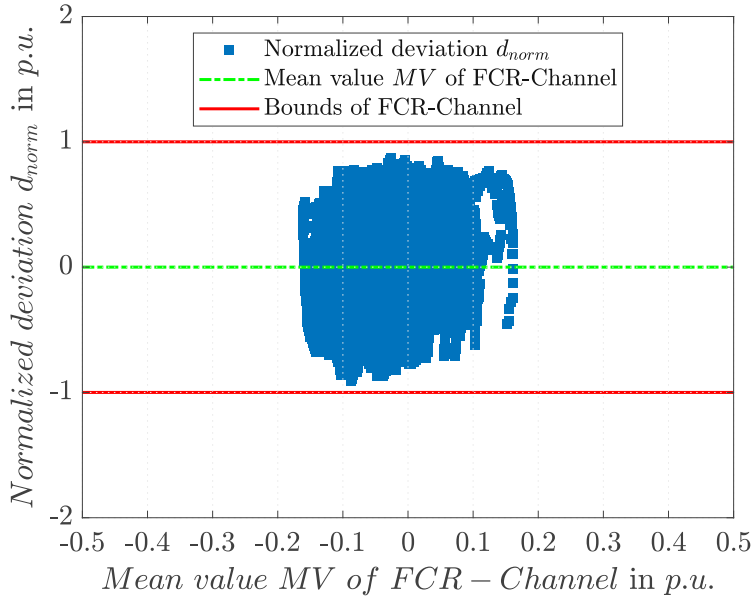

(b) Normalized deviation diagram

Figure 2.20: Creation of FCR channel according to the dynamic normalization methodology demonstrated with a first-order delay block with $T = 6\,s$ as the FCR providing unit without an additional tolerance of 5 % of $P_{FCR,bid}$

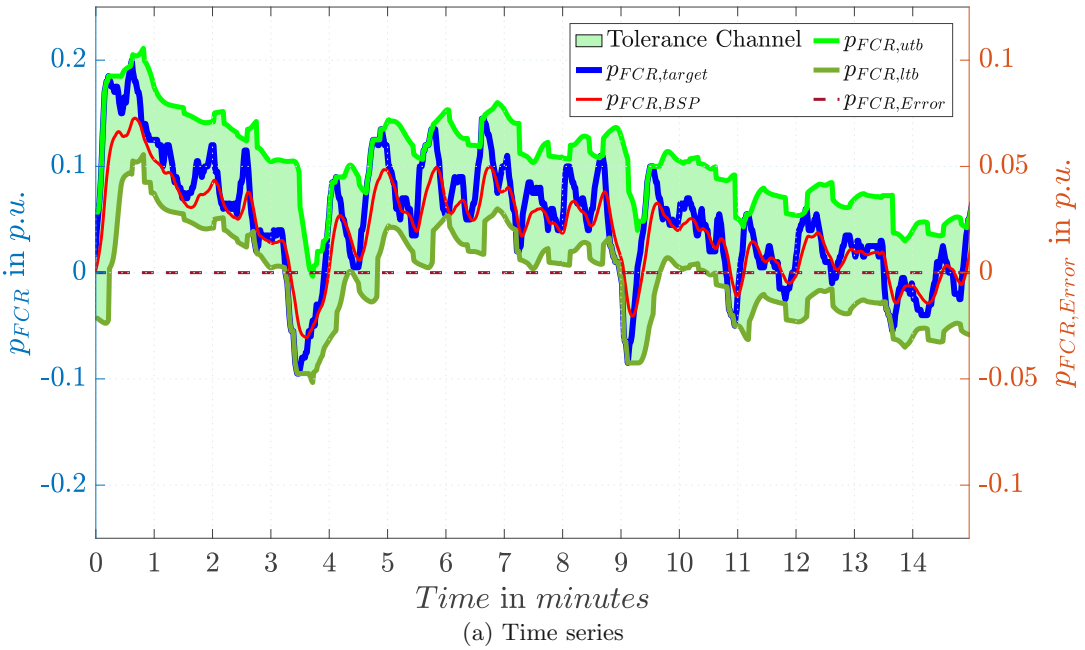

(a) Time series

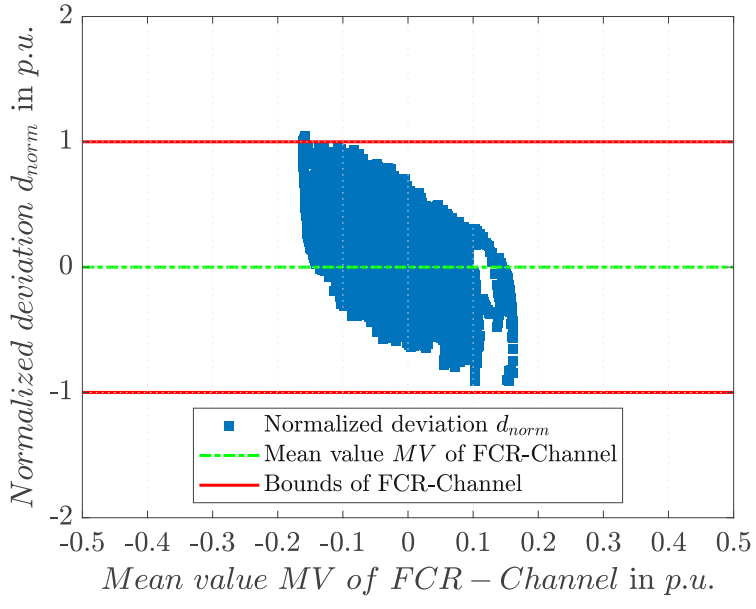

(b) Normalized deviation diagram

Figure 2.21: Creation of FCR channel according to the dynamic normalization methodology demonstrated with a first-order delay block with $T = 6\,s$ as the FCR providing unit, and a droop of 80 % of the original droop

3 State of the Art

3.1 Power Systems Simulators

There is a multitude of hydro unit models in the commercially available software packages. Market-leading solutions are provided by two companies, Siemens with PTI's PSS®E and General Electric with PSLF. According to [34] nearly all major U.S. utilities and system operators use one of these programs. An extensive review of existing hydroelectric turbine-governor simulation models is given by [34]. Appendix 10.1 lists the investigated models and a short description of them by [34]. The most commonly used models in the present North American system databases are HYGOV, WEHGOV, and WPIDHY10 models [35]. These models are not made explicitly for modeling pumped storage hydro plants since the bidirectional flow of power needs to be taken into account. When a reversible pump-turbine is investigated for dynamic simulations, a common excitation system model for the motor-generator can be utilized. The turbine-governor model, however, needs to be different for turbine and pump mode. An example is given by [35] for a conventional pumped storage hydro plant in pump mode.

Advanced PSH with variable speed drives employing a doubly fed induction machine have modeled and tested by [36, 37] for PSS®E. The tests conducted by [37] conclude that the model performed well for typical dynamic simulation analyses required by planning and interconnection studies. Furthermore, [37] states that new capabilities available in the model, for example, the provision of regulation services by an adjustable speed pumped storage plant in the pump mode could be demonstrated.

The software SIMSEN (modular SIMulation software for analysis of ENergy conversion Systems) is a simulation software for analyzing electrical power networks, adjustable speed drives and hydraulic systems [38, 39]. SIMSEN has been developed at the Swiss Federal Institute of Technology in Lausanne in cooperation with industrial partners since 1992. Originally developed for the simulation of electric systems, the

hydraulic components are also described by equivalent electric models. The current version can simulate stationary and transient processes in electrical and hydraulic systems and is therefore well suited for simulating pumped storage power plants. Consequentially, SIMSEN is used as the main simulation platform for the transient model of variable speed pump-turbines present in this thesis.

3.2 Compared Literature

Hydroelectric power plants with variable speed drives and their dynamic behavior have been studied e.g. [26, 36, 40–49] in recent years, highlighting their advantages in comparison to conventional fixed-speed PSH.

A detailed transient model of a VSDFG scheme using SIMSEN is described in [40]. It presents a model of a doubly-fed induction generator with voltage source inverter cascade on the rotor side. The modeling of the hydraulic system takes into consideration water-hammer, mass oscillations, and turbine characteristics effects. The thesis [46] describes a model for static operation in MATLAB. It provides information on active and reactive power capability for different rotational speeds. In [43] an overview of different configurations of variable speed units is given and the advantages and disadvantages of the different converter schemes are pointed out. A comprehensive mathematical model of a VSDFG is developed in [50]. An accurate description of important dynamic effects and the system's energy losses is given.

In [42] and [45] a pseudo-continuous approximation of a VSDFG is used and compared to a complete SIMSEN model. The voltage source inverter on the rotor side is replaced by three controlled voltage sources and the inverter on the transformer side is omitted. The simplifications lead to a computation time reduction of factor 60. The thesis [51] investigates the control and behavior of doubly-fed induction machines focused on low voltage ride through. The voltage source inverter is simplified to a pseudo-continuous model in SIMSEN based on space vector modulation to reduce simulation time. Still, the DC-link behavior could be observed. The thesis [52] introduces a simplified model of a VSFSC in SIMSEN and compares it to a complete model. A significant improvement concerning computational time could be achieved.

However, there is still room to explore the long-term dynamic electrical and hydraulic effects of different pumped storage power plants for FCR provision. Therefore, a new combined electrical and hydraulic model is introduced in this thesis using the simulation tool SIMSEN.The main focus of the thesis is set on analyzing frequency containment reserve (FCR) capability of these schemes based on ENTSO-E Continental Europe requirements. A transient model of both concepts is developed and validated based on a real-life pumped hydro storage facility. This model differs from

existing literature by implementing extensive hydraulic, electrical, and control elements for two variable speed pump-turbine schemes and allows long-term transient simulations of 4 hours (FCR bid resolution) or more.

4 Modeling

For power system stability studies choosing the suitable model and simulation tool is very important. Stability problems in power systems can be divided into three categories according to [53]: rotor angle stability, voltage stability, and frequency stability. An adequate model for the investigation of one stability problem also has to take the primary system variable in which instability can be observed, the size of the disturbance and the devices, processes, and the time span for assessing stability [53]. However, as [34] states, in practice, it is impossible to completely decouple these various stability problems from one another. A single event, especially in small systems, can produce associated frequency, voltage, and angular stability problems as [34] further mentions. Therefore, the level of detail of the used model is of particularly importance. The main focus of the thesis is the investigation of the dynamic behavior of variable speed hydropower plants for FCR provision. The provision FCR is needed due to frequency stability problems and investigated in the range of a few seconds up to four hours. Hence, the decision of the degree of detail of the combined hydraulic and electrical model strongly depends on the observed time span and the main system time constant. The model is based on a real-life pumped hydro storage facility with two identically pump-turbines, one connected to a fixed-speed synchronous motor-generator and the other to a variable speed motor-generator. The simulation tool SIMSEN is used to model the PSH's transient behavior during FCR provision. It offers a variety of dynamic models and makes it possible to model hydraulic, mechanical, electrical, and control elements in one simulation environment. To enable combined electrical and hydraulic long-term investigations of the dynamic behavior of PSHs some simplifications are necessary, however. Especially the investigation of variable speed PSH is connected with short time constraints due to switching frequencies above 1 kHz. This can lead to long simulation duration and large memory requirements. Therefore, the introduced model implements variable speed machines (doubly-fed induction generators and full-size converter scheme) as controlled voltage sources

without inverter switches to reduce simulation time and to enable long term investigations. Still, the models consider the hydraulic waterways, the turbine and pump operation as well as the synchronization of the machines to the network.

It has to be mentioned, that the hydraulic part of the overall model was developed within the research program "Green Energy Grid" by a project at the Institute of Energy Systems and Thermodynamics ([12, 15, 17, 54, 55]). Therefore, the focus of the description of the model centers around the electrical and control components.

4.1 Hydraulic and Mechanical Components

The mechanical components consist of the mass representation connected to the impeller and the mass element representing the mass of the motor-generator armature. One part of the hydraulic components of the PSH model is the headwater reservoir and the tailwater reservoir. They are connected by the waterway. The waterway splits two ways in the model, and each part consists of a pump-turbine (FSPT and VSDFG/VSFSC) of the same specifications. The pump-turbine characteristic is specified by unit speed n_{11}, unit flow q_{11}, and unit torque t_{11} measurements, which are represented by

$$n_{11} = n \cdot \frac{D}{\sqrt{H_{net}}} \tag{4.15}$$

$$q_{11} = \frac{Q}{D^2 \cdot \sqrt{H_{net}}} \tag{4.16}$$

$$t_{11} = \frac{T}{D^3 \cdot H_{net}} \tag{4.17}$$

where D is the impeller diameter, H_{net} the net head, Q the flow, T the mechanical torque and n the speed. The unit speed n_{11} thereby is the speed of a turbine with a diameter of 1 meter and a head value of 1 meter. The unit flow q_{11} represents the flow through a turbine with a diameter of 1 meter, and a head value of 1 meter, and the unit torque t_{11} is the torque of a turbine with a diameter of 1 meter and a head value of 1 meter. By using the unitary variables, unit speed, unit flow, and unit torque characteristics become valid for all turbines for all diameters of the same impeller design.

Hydraulic machines conventionally use the "Hill Charts" to describe the steady-state relationships of the turbine speed n, the guide vane opening y , the water flow rate Q , the mechanical torque T and the efficiency η. The turbine efficiency η_T is the ratio between mechanical power $P_{M,T}$ and hydraulic power $P_{H,T}$

$$\eta_T = \frac{P_{M,T}}{P_H} = \frac{P_{M,T}}{\rho \cdot g \cdot H_{net} \cdot Q} \,. \tag{4.18}$$

The pump efficiency η_P is defined as

$$\eta_P = \frac{P_H}{P_{M,P}} = \frac{\rho \cdot g \cdot H_{net} \cdot Q}{P_{M,P}} \,. \tag{4.19}$$

The hydraulic efficiency hill chart of both hydraulic machines in the model is depicted in figure 4.1 for turbine and pump mode. Furthermore, the normalized guide vane opening y from zero to one (maximum degree of opening) is shown. For closed gates, the unit flow is zero. The maximum degree of opening limits the operating area upwards. Finally, the lines of constant mechanical power are shown. The efficiencies for operating points beneath the zero mechanical power output line are not colored, since the discharge in these cases is too low to power the turbine. Power from the electrical grid would be necessary to operate the turbine in this area. In pump mode, the maximum power output of the motor-generator limits the pump power input.

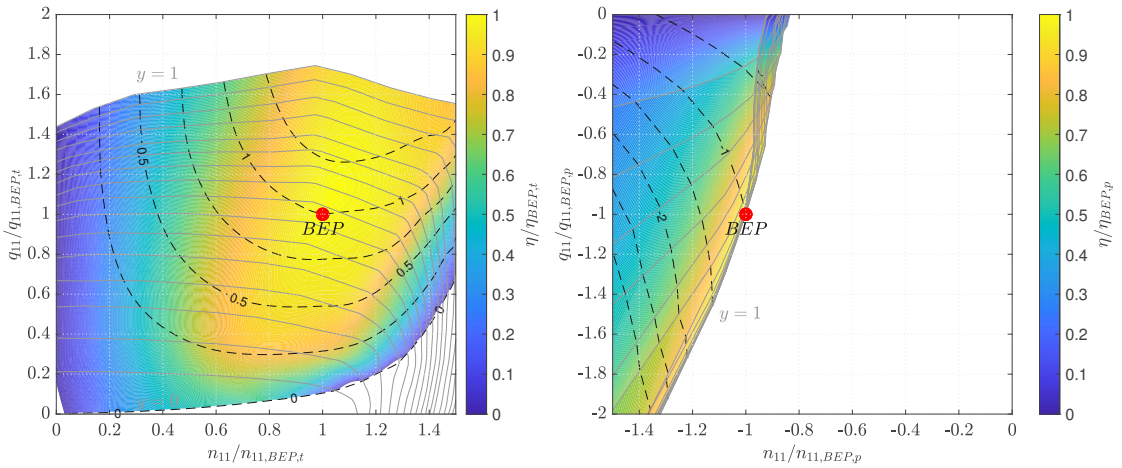

(a) Turbine mode (b) Pump mode

Figure 4.1: Hydraulic efficiency of the investigated pump-turbine in pump and turbine mode as well as corresponding guide vane openings y (gray) and constant mechanical power lines (dashed black line). n_{11} and q_{11} values are related to their best efficiency point, guide vane opening y to the maximum opening.

The operating area is further limited downwards by unfavorable flow conditions, which vary with design and plant structure and can lead to cavitation or the formation of vortices [56, 57]. Therefore, two scenarios for the general minimum of the hydraulic efficiency (65 % and 80 %) are introduced [55]. Considering this restriction, the best efficiency lines (BEL), based on the calculations of [55] are shown in figure 4.2 for the VSFSC, the VSDFG and the FSPT. In turbine mode, the different BELs originate from different speed constraints. The best efficiency line of the FSPT is a slightly bent curve due to changes in the net head because of other waterway losses. However, these net head variations are minimal; therefore, the BEL appears to be an almost exact vertical

line. Due to higher cavitation risk in pump mode, the pump-turbines design focuses on the pump mode and, therefore, operates in the sub-optimal area on the right side of the best efficiency point during turbine operations. The speed range of the VSFSC in turbine mode is highly flexible and can be reduced to low values to operate the power plant at the highest possible efficiency for the given power output. The VSDFG is limited to specific speed restrictions and, hence, cannot reach the BEP. However, the VSFSC's and VSDFG's best efficiency lines are congruent for higher power output levels..

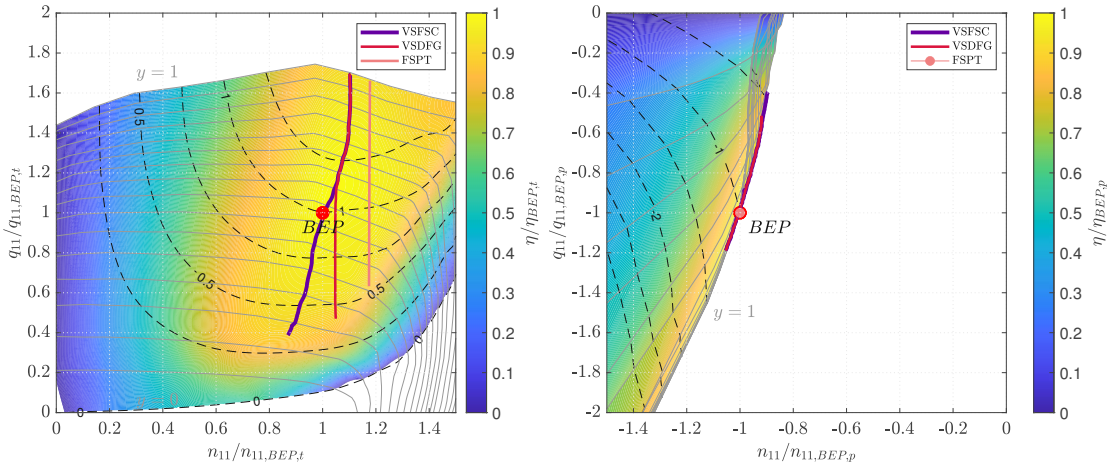

(a) Turbine mode (b) Pump mode

Figure 4.2: Hydraulic efficiency of the investigated pump-turbine in pump and turbine mode as well as corresponding guide vane openings y (gray) and constant mechanical power lines (dashed black line). All values are related to their best efficiency point.

In pump mode, gate vane regulation is impossible since the flow conditions are highly susceptible to cavitation [22]. Changing the speed is the only possibility to regulate the pump power input. Hence, the BEL of the FSTP is reduced to one operating point. The VSFSC and the VSDFG can regulate their power input by changing the speed settings. Again, the VSDFG is limited to smaller speed variations than the VSFSC. Within the speed restrictions of the VSDFG, the best efficiency lines of the VSDFG and VSFSC are congruent. The lower speed operating limit of the VSFSC is naturally given by pump instabilities at low flow rates when more than one operating point could occur for one speed and one GVO setting.

The previous deliberations are assuming a constant gross head. However, the gross head of PSH varies between the minimum and maximum values. The hydraulic efficiency depends on the power output and the gross head. The results of these dependencies are calculated by [55], and results are shown and analyzed in Appendix 10.2.

4.2 Electrical Components

The electrical components include the motor-generator, the transformer, the power system and it's connection to the power grid. As mentioned before, the motor-generator for the variable speed drive is simplified by using a controlled voltage source. Therefore, simulation time is reduced drastically as the step time of the model can be increased to 1 ms. For the simulation of one day, around one day of simulation time is needed, which enables long term simulations. Another benefit arises as the same electrical model can be utilized for the doubly-fed induction motor-generator and a synchronous motor-generator with full-size converter to investigate FCR provision. The PSH model can be adapted to represent a doubly-fed induction machine with a single hydraulic machine that can be operated as either pump or turbine. The investigated pump-turbine has a variable speed range from 0.9 p.u. to 1.04 p.u. in turbine and pump mode. The synchronous motor-generator is modeled without speed restrictions and can, therefore, operate in a wider operating area than the representation of the doubly-fed induction motor-generator. The additional electrical losses of the simplified motor-generator include the generator and the converter and are estimated with 2 % of the total power output or intake[55].

4.3 Control Components

Variable speed hydropower plants have an additional degree of freedom compared to FSTP. Controlling the power input/output of the motor-generator and turbine speed of the pump-turbine for optimal operations and/or faster transitions between operating points is the central character of the control strategy for VSPT.

4.3.1 Variable Speed Pump-Turbines

In turbine mode, power output is determined by a power set-point. The power set-point p can be provided manually for investigations of e.g. reaction to ramp signals. In this case, p is given as an external signal. The power set-point p can also be determined by the FCR controller. The FCR controller delivers the power output target depending on the bid size, the current power output, and the frequency. Furthermore, a reactive power set-point can be an additional input. The control strategy of the voltage source model part utilizes a multi-variable controller based on [58], and is modified and extended to obtain a correct angle of the voltage phasor. The input parameters for the control voltage source are the root mean square value of the line voltage ($U_{L,RMS}$) and the voltage phasor (THS). The system frequency can be set to 50 Hz or any given frequency characteristic.

The reference speed n_{set} for the best efficiency point, and the GVO depends on the

desired active power provision and the gross head. The voltage source is set to the reference power signal for fast power control, while the GVO controls the rotational speed of the pump-turbine. The speed controller comprises a modified PI-controller. Since actuator limits for the GVO (from 0 to 1 p.u) are inherent, a back-calculation as an anti-windup scheme is used in the PI controller [59]. Furthermore, a feed-forward of the reference GVO (y_{set}) is implemented to enhance controller performance [60]. Figure 4.3 shows the block diagram of the basic control components for variable speed drives (VSDFG and VSFSC) in turbine mode.

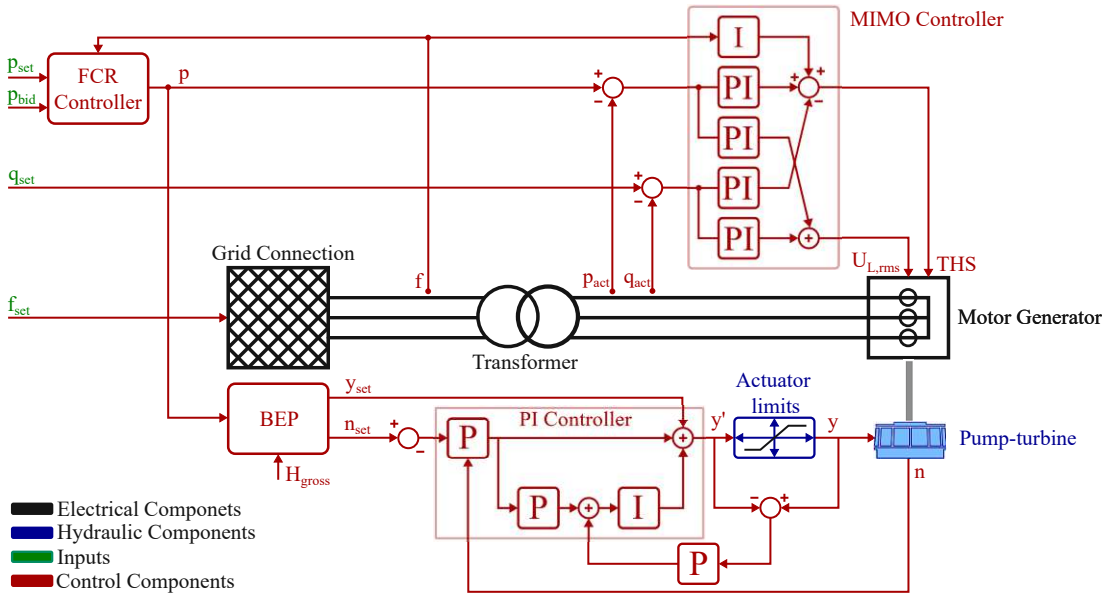

Figure 4.3: Block diagram of control components for VSDFG/VSFSC in turbine mode

During pump operations, control via gate vane opening is not possible. The GVO is set to maximum efficiency settings. Hence, there is no control loop for speed. Figure 4.4 shows the block diagram of the control components in pump mode. However, the electrical power input is still controlled by the MIMO controller. The rotational speed of the pump-turbine results from the operating point, where electrical and hydraulic power input is in equilibrium. When electrical power input is increased, for example, the pump-turbine accelerates and increases the speed, leading to more hydraulic power intake. The acceleration stops when a new steady operating point is reached.

4.3.2 Fixed-Speed Pump-Turbine

The control scheme of the FSPT, in comparison, is shown in figure 4.5 for turbine mode and in figure 4.6 for pump mode. The power output in turbine mode is based on the power reference signal p_{set} as input for the PI controller and y_{set} for the GVO for feed-forward control. The synchronous machine excitation is controlled by a standard

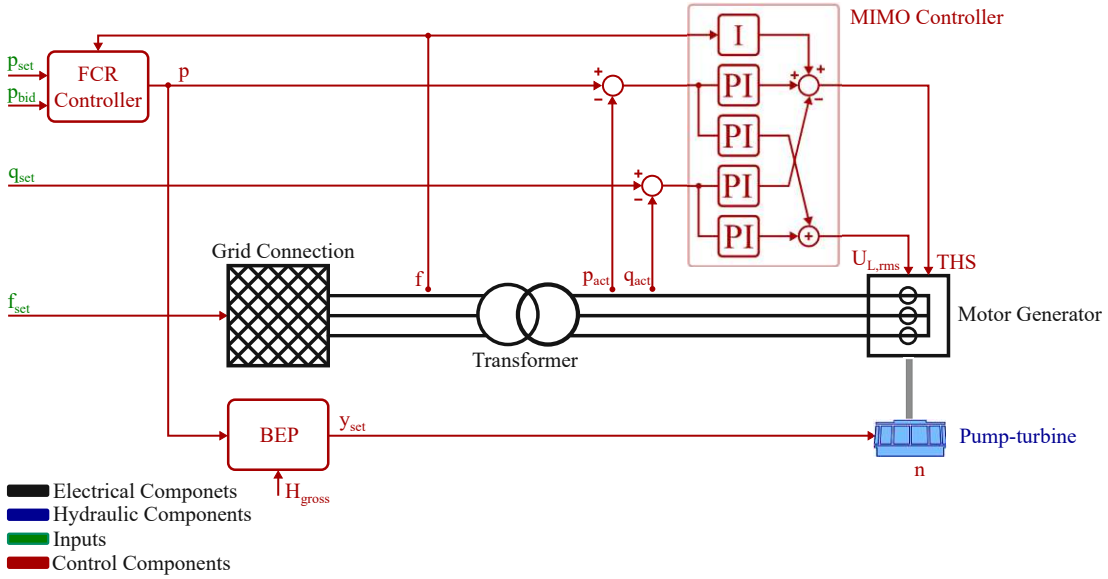

Figure 4.4: Block diagram of control components for VSDFG/VSFSC in pump mode

PID voltage controller. The reactive power set-point is controlled by an additional PI controller. A FCR controller is not implemented, as FCR provision is only investigated for the variable speed unit.

In pump mode, the electrical power intake of the pump-turbine from the grid is based on the system frequency. The GVO is set to the maximum efficiency position to minimize cavitation and no further control ability is possible.

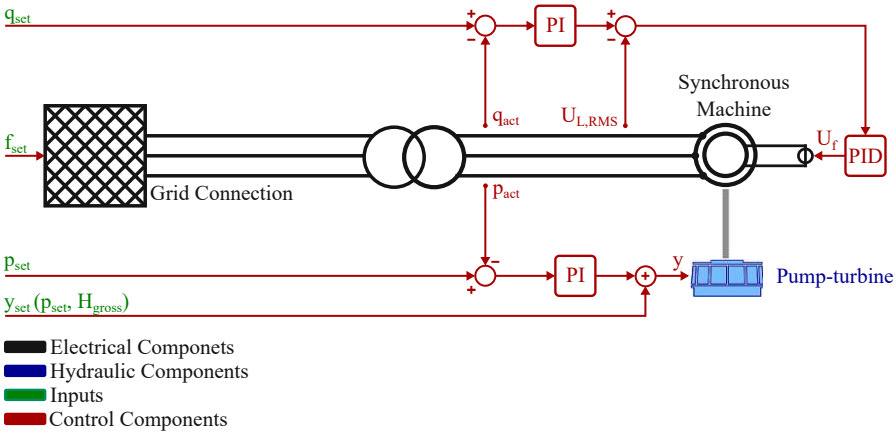

Figure 4.5: Block diagram of control components for FSPT in turbine mode

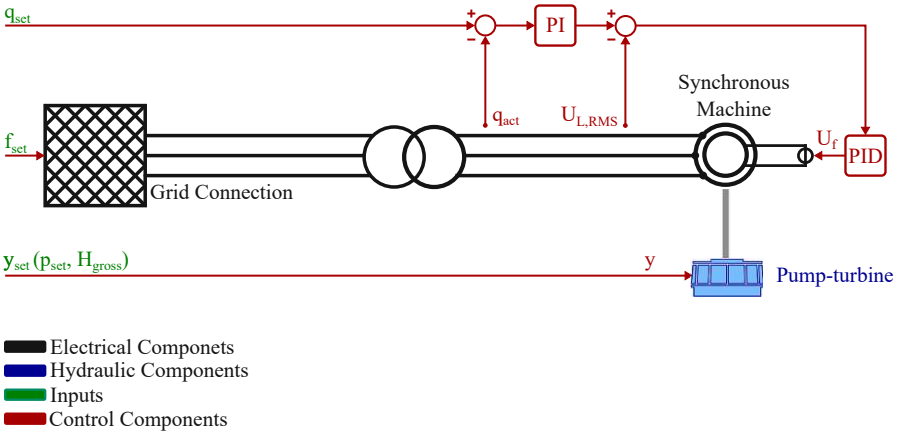

Figure 4.6: Block diagram of control components for FSPT in pump mode

4.4 Grid Model

As part of the overall model, the electrical grid model has the task of reflecting the connection to a wide area grid (like the Continental European Power System) to explore the control capabilities of the variable speed machines. In this case, the control mechanisms and contributions of all connected generators and loads in the network must be considered. It is assumed that the influence of the control power of a single unit is not decisive in changing the overall frequency deviation. The reason for this assumption is that the indivisible FCR bid size is small (25 MW) compared to the overall tendered FCR provision (3000 MW for ENTSO-E Continental Europe). Hence, a precomputed frequency-response characteristic for different load, generation, and grid inertia scenarios is acceptable. A frequency time series is used as an external input for the SIMSEN model. For the calculation of the frequency signal, the simulation tool MATLAB®Simulink is utilized [17].

The power equilibrium is calculated using

$$\sum_i P_{G_i}(t) - \sum_j P_{L_j}(t) = \omega \cdot J_\Sigma \cdot \frac{d\omega}{dt}\,, \tag{4.20}$$

where P_{G_i} is the power generation of a single unit, P_{L_j} is the power need of a load unit, ω is the electrical angular frequency and $J_\Sigma = \sum J_\nu/p_\nu^2$ the summarized inertia compensated for the initial number of pole pairs as $\omega = \omega_{m,\nu} \cdot p_\nu$, with $\omega_{m,\nu}$ as the individual mechanical angular frequency and p_ν the individual number of pole pairs. The frequency derivation is expressed as

$$\frac{df}{dt} = \frac{\Delta P}{P_\Sigma} \cdot \frac{f_n}{T_A} \cdot \frac{f_n}{f}\,, \tag{4.21}$$

where ΔP is the loss in generation capacity, P_Σ is the overall network power, $f_n = \omega_n/2\pi$ the nominal frequency and T_A the system start-up time constant. T_A which is calculated by

$$T_A = \frac{\omega_n^2 \cdot J_\Sigma}{P_\Sigma}. \tag{4.22}$$

In the following scenario, the frequency response of the ENTSO-E Continental Europe grid is calculated based on [61]. Its static frequency limits are defined by a 50.2 Hz upper and a 49.8 Hz lower boundary. Dynamically, these limits can be exceeded for a short time, but deviations must not be greater than 800 mHz. The frequency containment process is considered using a droop controller with a ± 10 mHz dead zone and a maximum power gradient of 100 MW/s. The frequency restoration process has the task of taking over the remaining frequency and power deviation after 15 to 30 seconds and is modeled as a PI-controller, considering different network power frequency characteristics for different network sizes. Self-regulating effects of the load are considered with 1 % of the load per Hz. Figure 4.7 shows the frequency curves in a simulated case with control mechanisms for a 150 GW network with $T_A = 10$ s, $T_A = 5$ s and $T_A = 1$ s, considering a loss and a surplus in generating capacity of 3000 MW. In addition, the respected trumpet curves [61] are depicted as well. Note that the secondary control will relieve the primary control after 30 seconds and has to restore the frequency within 900 seconds (15 minutes). Figure 4.8 depicts the frequency responses to different losses and surpluses in generating capacity for $T_A = 10$ s and a network size of 150 GW.

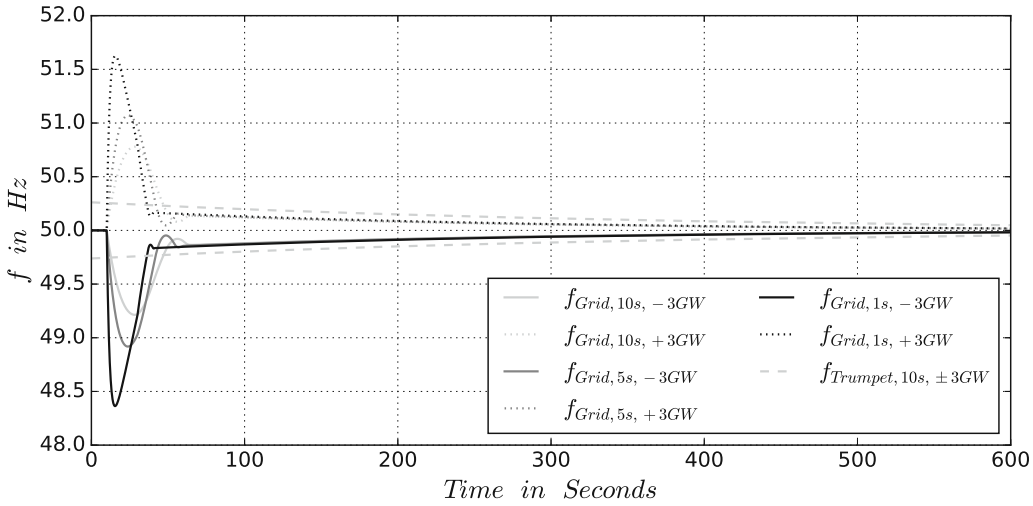

Figure 4.7: Frequency responses to a loss and surplus in generating capacity of 3000 MW and a network size of 150 GW with trumpet curves for different T_A

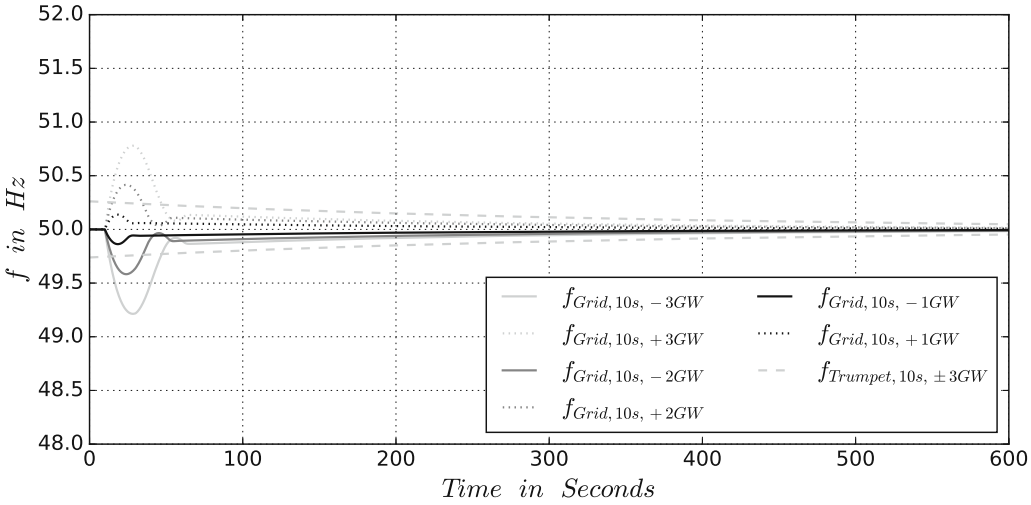

Figure 4.8: Frequency responses to different losses and surpluses in generating capacity for $T_A = 10\,\mathrm{s}$ and a network size of 150 GW (with trumpet curves)

4.5 Overall Model

The overall model includes the electrical and hydraulic model part in one SIMSEN model. This makes an investigation of the PSH behavior during FCR provision, considering electrical and hydraulic aspects, possible. The SIMSEN model represents an PSH with one fixed speed and one variable speed unit with a common head and tail water reservoir. The overall model is featured in figure 4.9.

The FSPT and the VSPT are connected to two mass elements, representing the impeller and generator mass. The motor-generator of the VSPT, modeled as a controlled voltage source, and the synchronous machine of the FSPT are connected to their mass representations. The fixed speed unit is connected to two circuit breakers since phases must be switched for pump and turbine operations. For the connection of the voltage source, only one circuit breaker would be necessary since phases do not have to be changed, but to keep the symmetry to the FSPT unit, two breakers are modeled. The breakers are opened and closed during transition periods between operating modes. To connect the motor-generator to the grid, the line voltage, the frequency, and the phase angle must match, assuming the phase sequence and voltage waveform are correct. Each pumped-storage unit has its transformer and is connected via a power line to the power grid.

The control elements (colored in red) can be divided into following groups:

Inputs external inputs for the model

- electrical power target p_{set}: baseline operating point of the unit
- FCR bid size p_{bid}: indivisible FCR bid size during a 4 h period

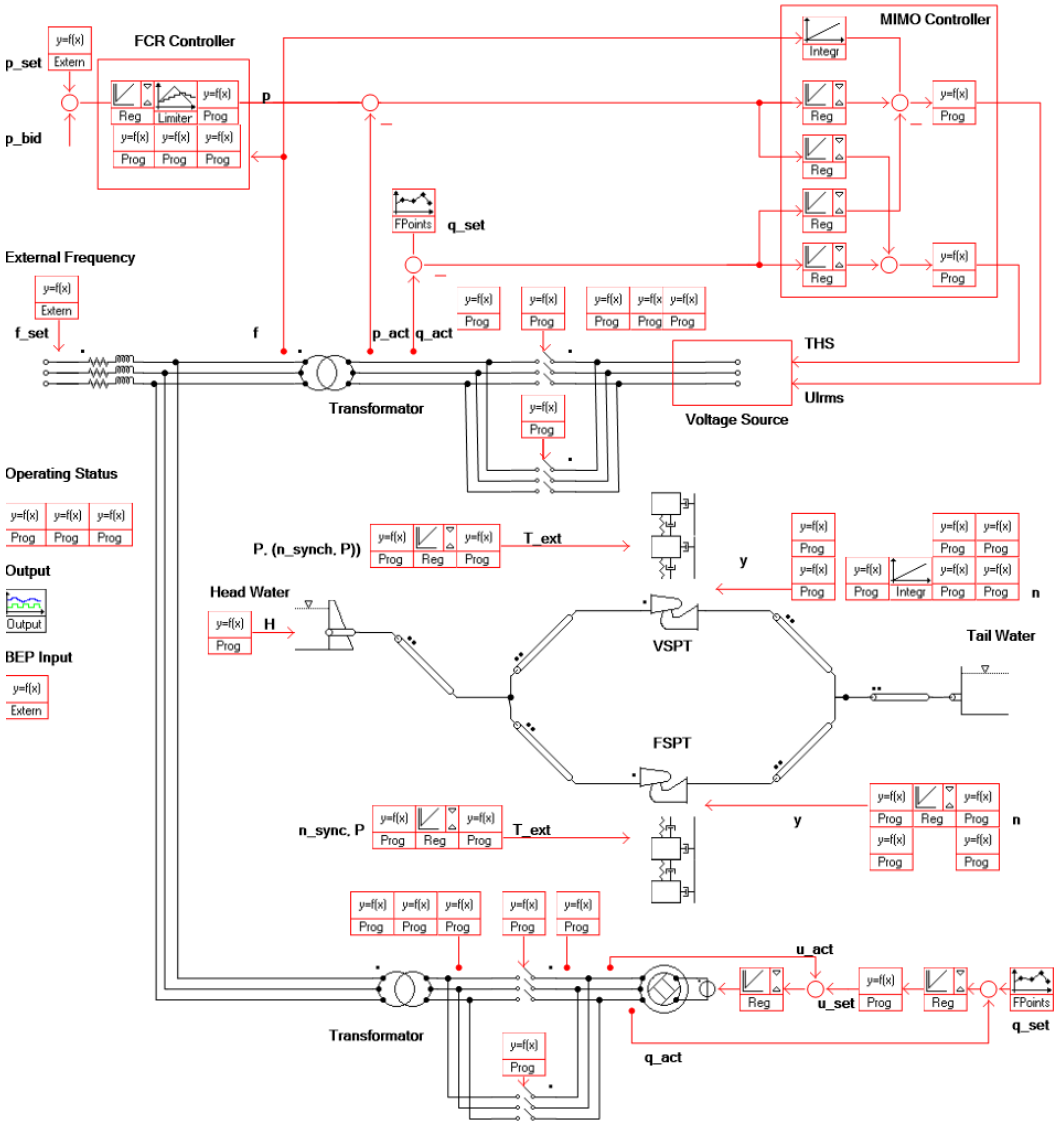

Figure 4.9: Overall model of investigated PSH in SIMSEN

- optimized operating point based on power input/output parameter
- frequency of the power system

FCR Controller The FCR controller delivers the power set-point signal

Operating status The task of these blocks is to determine the operating status of the FSPT and the variable speed pump-turbine schemes.

Hydraulic control

Head water level can be fixed or calculated based on a storage size and flow rate

Circuit breaker control The circuit breakers for the connection of the units to the power system are opened or closed when the synchronization constraints are met. Therefore, the line voltage, the frequency and the phase angle must match, assuming the phase sequence and voltage waveform are correct.

Voltage source control Inputs for the voltage source controller are active and reactive power set-points p_{set} and q_{set} as well as the frequency f. The MIMO controller delivers the correct THS and $U_{L,rms}$ for the voltage source.

Synchronous Machine (FSPT) Depending on the voltage level and reactive power set-point of the motor-generator, the excitation is controlled by an standard model controller.

Mass Elements For the start-up of the FSPT and the VSDFG in pump mode, an auxiliary motor is modeled by the external torque T_{ext}.

5 Validation

Before results can be discussed, the validation of the model's accuracy is necessary. The variable speed pump-turbine models focus on the provision of FCR during turbine or pump operation. One part of the validation thereby centers on the ability of the models to follow different external power reference signals. Furthermore, the start-up processes of the VSDFG and VSFSC scheme in turbine and pump mode are simulated and compared to the FSPT.

The hydropower plant schemes have to operate within certain physical parameter limits. The main parameter restrictions are for the steady and dynamic head and the speed restrictions. The speed limit of the VSDFG is assumed to be -10 % and +4 % of the rated speed [17]. For the VSFSC no lower speed limit is used. However, as mentioned before, to avoid instabilities and cavitation, general efficiency of 80 % is desired.

The steady head limitations are estimated with 0.93 p.u for the lower and 1.06 p.u. for the upper bound. Dynamically, the head can be between 0.8 p.u. and 1.2 p.u.[55]

5.1 Change of Operating Point

First, the changes of operating points in turbine and pump mode are discussed. The investigated parameters are the electrical power output/input, the mechanical power, speed, gate vane opening and net head.

5.1.1 VSDFG

The VSDFG is restricted, as mentioned, to speed limitations due to converter size and mechanical forces. Figure 5.1 shows three examples of changing the current operating point of the VSDFG in turbine mode. In the left column, an instantaneous change in power output is requested. The rapid change of electrical power output can not be compensated by mechanical power increase since the gate vane opening is restricted by a maximum gradient of 20 seconds to full opening. Therefore, the machine is decelerated

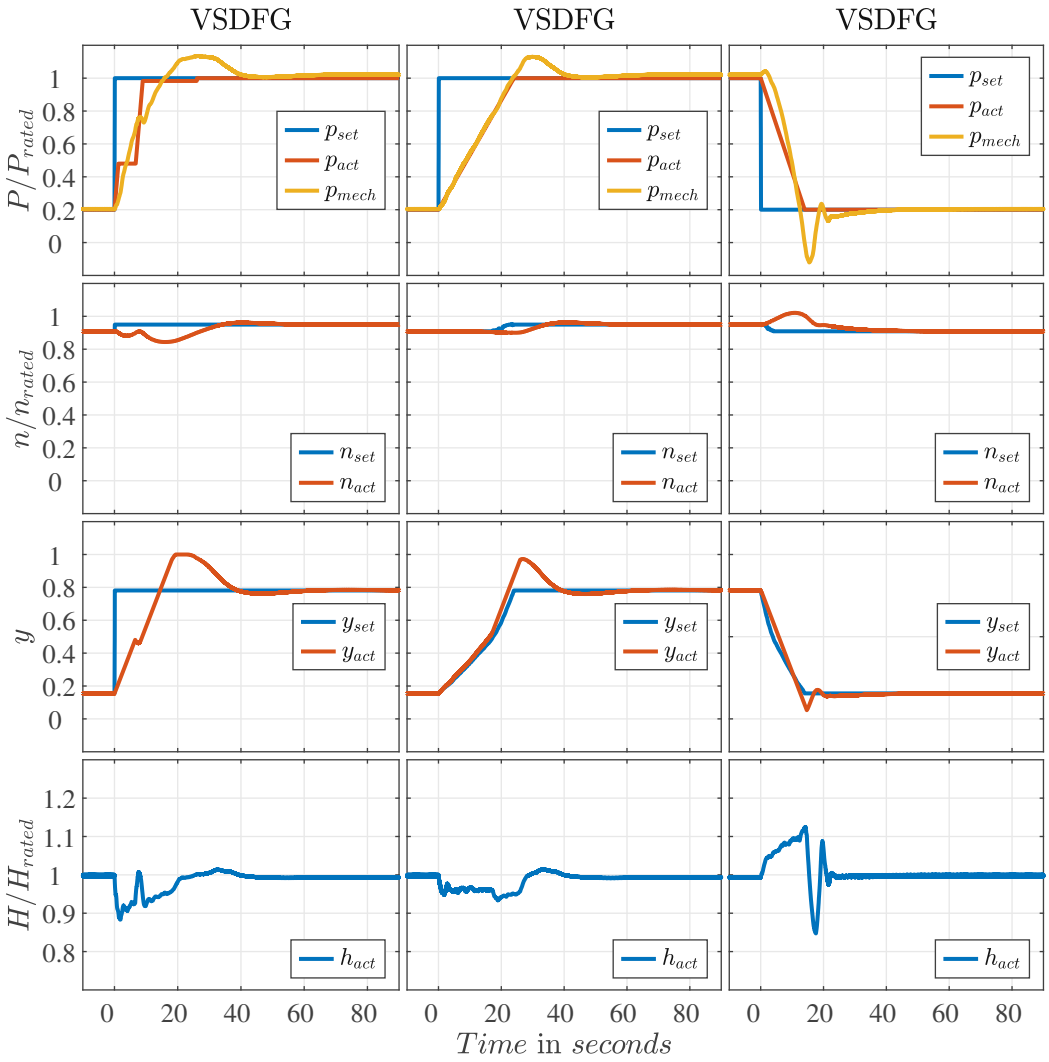

Figure 5.1: Change of operating point of VSDFG in turbine mode

according to the mechanical equations set of the machine [62]

$$T_e - T_l = J \cdot \frac{\mathrm{d}\omega_m}{\mathrm{d}t} \tag{5.23}$$

$$\frac{\mathrm{d}\omega_m}{\mathrm{d}t} = \frac{\mathrm{d}\theta}{\mathrm{d}t}\,. \tag{5.24}$$

In the equations, T_e is the electro-mechanical torque, T_l the load torque, J the inertia of the rotor/load combination, ω_m the mechanical angular rotor frequency, and θ the rotor angle. The deceleration continues until the speed falls under the lower boundary. In this scenario, the machine then stops the increase in power output until the lower boundary is exceeded again. The new set-point is reached after 26 s. This would be fast enough for FCR requirements. However, a power ramp (middle column in figure 5.1) would only require 24 s, and the lower speed boundary is not violated during the process, thus

should be preferred. The right column of figure 5.1 shows the behavior of the VSDFG responding to a decrease of set-point from 1 p.u. to 0.2 p.u.. Reducing the set-point leads to an acceleration of the machine. Therefore, the upper speed boundary needs to be observed. Considering a linear change of electrical power output, the new operating point is reached after 14 s without succeeding the upper speed limit of 1.04 p.u.. In all cases, the dynamic head limits are met.

Figure 5.2 depicts a change of operating point in pump mode. The operating range of the VSDFG during pump operations is smaller than in turbine mode. Hence, a step from -0.6 p.u to -1.0 p.u. and vice versa is shown. In this case, electrical power is drawn from the power grid. The change in operating point is faster than 1 s since the gate vane opening is constant and not a limiting factor. Again, the head stays in its dynamic range.

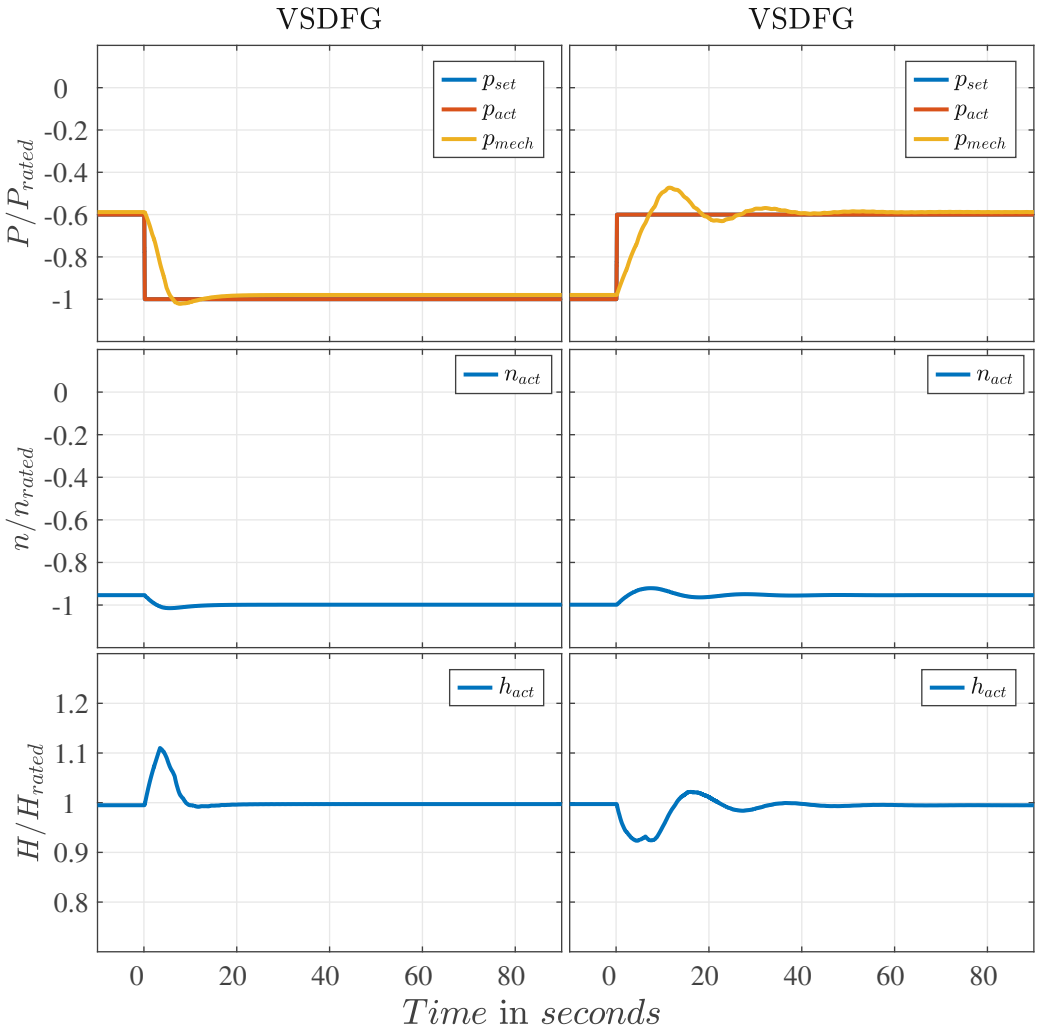

Figure 5.2: Change of operating point of VSDFG in pump mode

5.1.2 VSFSC

The behavior of the VSFSC during a change of operating points is similar to the VSDFG. The left column of figure 5.3 shows a set-point change from 0.2 p.u to 1 p.u. during turbine mode. The VSFSC reaches the new target output after 19 s, which is again fast enough for FCR provision. In this case, a faster transition between operating points is not limited by the lower speed boundary but by the fact that the machine would stall. This happens when the gate vanes are opened to their maximum, but the speed and mechanical power output are rapidly declining. The right-hand side of figure 5.3 depicts the machine's behavior during a decrease of 1.0 p.u to 0.2 p.u.. Here, the upper speed boundary is the decisive factor in limiting the rate of change in electrical power output.

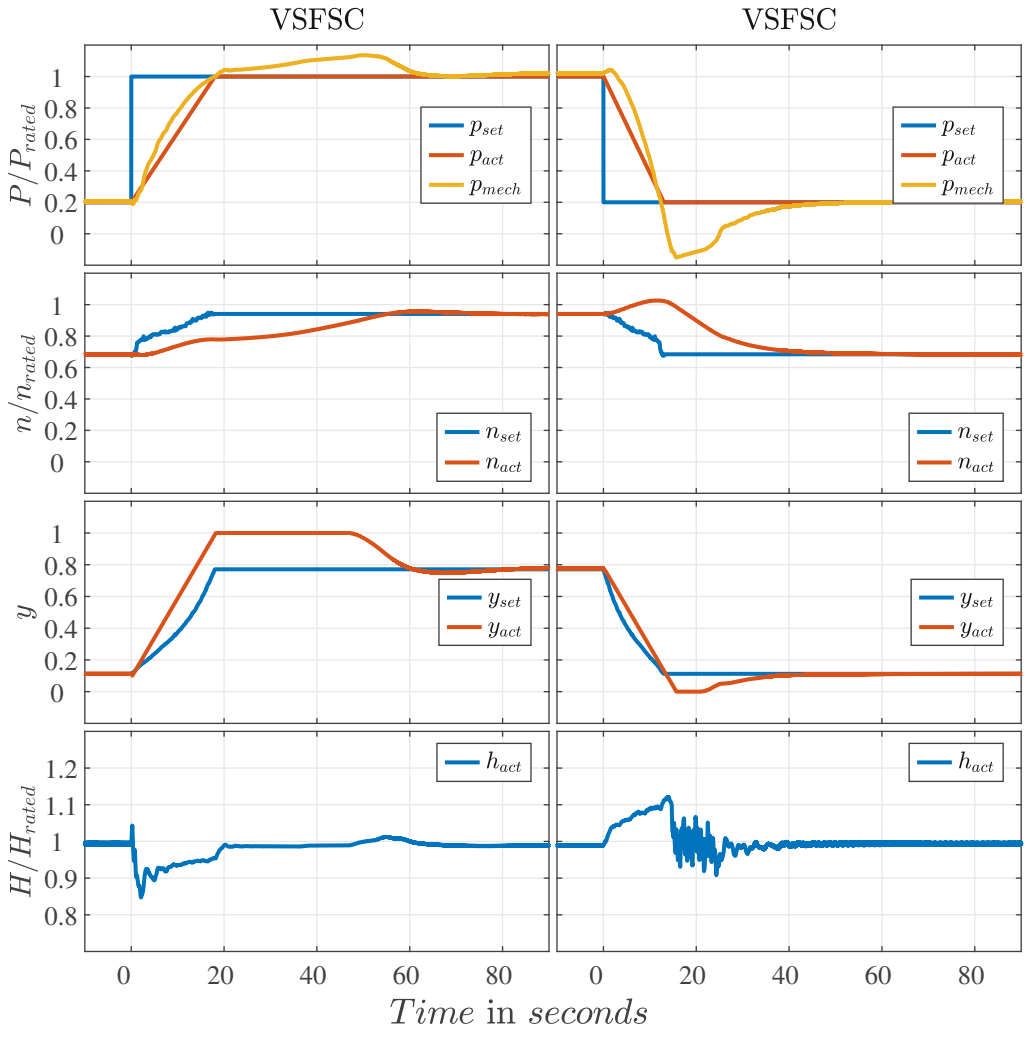

Figure 5.3: Change of operating point of VSFSC in turbine mode

In pump mode, the operating range is larger than the VSDFG. A change of operating point from -0.5 p.u. to -1 p.u is shown in figure 5.4. In both cases, a change of power input can be faster than 1 s, while the mechanical and hydraulic limits are within the

nominal bandwidth.

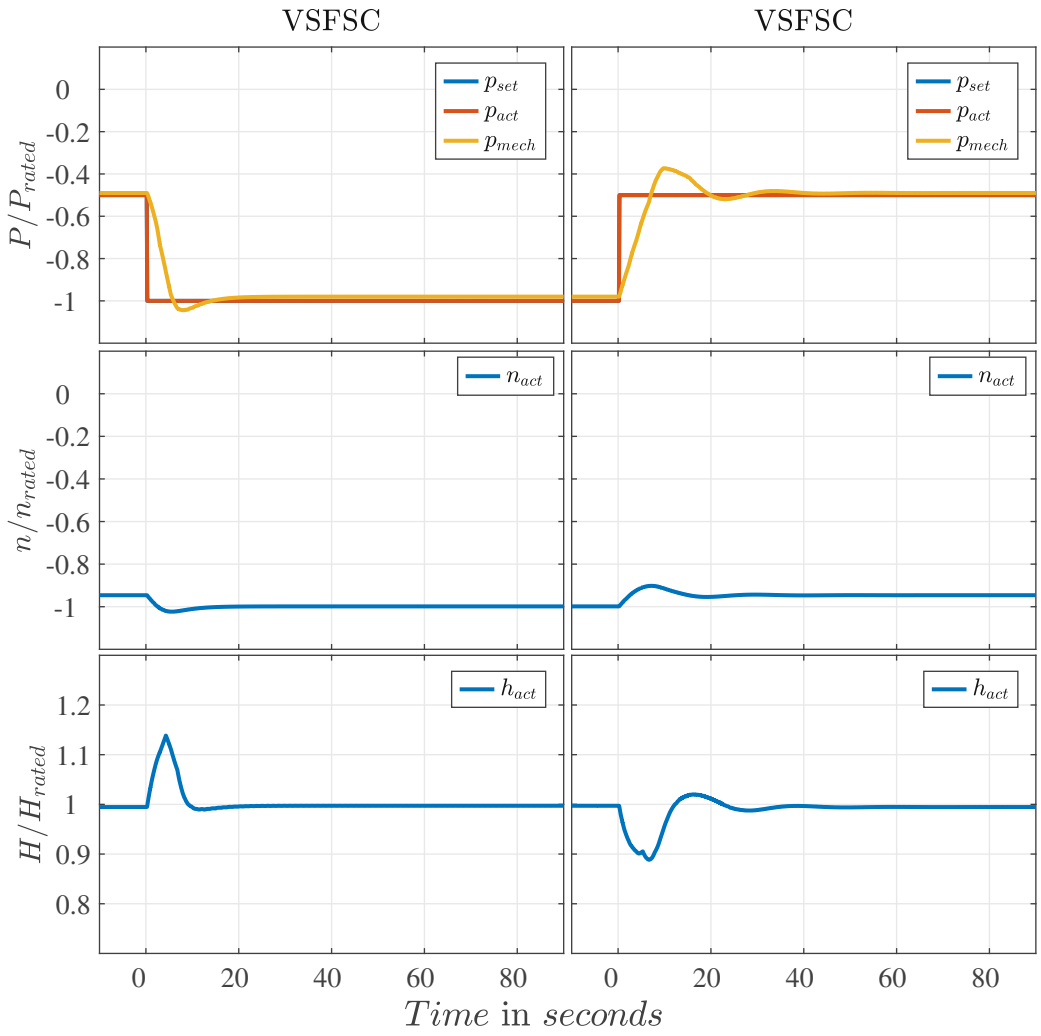

Figure 5.4: Change of operating point of VSFSC in pump mode

5.2 Start-up and Connection to the Power Grid

At the beginning of the start-up process of the machine in turbine mode, the speed of the pump-turbine is zero, and the gate vanes are fully closed. Furthermore, the generator is not connected to the grid, and the circuit breakers are opened. At timestamp zero, a step to nominal electrical power is requested. The following start-up process of the VSFSC, the VSDFG and the FSPT are displayed in figure 5.5. In the first row, the electrical power output p_{act}, mechanical power output p_{mech} and the reference signal for the electrical demand p_{set} are shown for all three investigated schemes. The second row indicates the speed n_{act} and the reference speed n_{set}. The third row shows the gate vane opening y_{set} and the corresponding reference y_{set}. In the final row, the actual net head values are presented.

The start-up for all schemes begins with the opening of the gate vanes to accelerate the pump-turbine. For the FSTP and the VSDFG, the gate vanes are opened around 20 % in the beginning of the synchronization process and are reduced to 10 % close to the synchronization speed. In the case of the FSPT, the synchronization to the power grid is only possible when the nominal speed is reached. Furthermore, the phase and the amplitude of the generator must match with the power system. After connecting to the grid, the gate vanes open to their desired operating point. Concerning the VSDFG, the process is similar. However, since synchronization is already possible at lower speed, the process is faster and requires less water. The fictional VSFSC is demonstrated with a swifter opening of the gate vanes and can connect to the grid at lower speed limits. However, considering the efficiency and that the machine could stall, the synchronization is shown at around 0.9 p.u. Furthermore, the head values need to be observed, as fast changes of the GVO may result in net head values leaving the upper or lower boundary. The opening of the gate vanes leads to a reduction of the head value, whereas closing them produces rising values.

In conclusion, the VSFSC has the ability to start delivering electrical power to the grid after 20 s, followed by the VSDFG after 30 s, and finally, the FSPT requires 40 s.

The start-up of the pump-turbines in pump mode is different from the turbine start-up. An early opening of the gate vanes would result in an acceleration of the generator-machine assembly in the opposite direction. Therefore, a different acceleration approach is required. This may be different for different power plant schemes. [25, 55]

The FSTP requires additional equipment to accelerate the pump-turbine in the pump direction as it always operates at synchronous speed. This can be provided by an auxiliary motor, a start-up turbine or a start-up converter. These devices are typically design to provide only limited amount of power to reduce costs. Therefore, the impeller has to run in air during the acceleration process. The power absorbed in pump model only depends on the head. Hence, no power regulation at a fixed head is available [25].

The VSDFG start-up is similar as the motor-generator can only draw pump power from the grid within its speed limits. However, the existing rotor converter can be used to start-up the rotating assembly when the impeller runs in air. The VSFSC, on the other hand, is not restricted by speed limitations and the converter is designed for rated power input/output. Hence, this scheme would enable a start-up of the impeller while filled with water. [55]. For both variable speed schemes, a change in operating speed leads to a change in absorbed electrical power by approximately $\triangle n^3$. Speed changes are limited by hydraulic cavitation limits, hydraulic stability of operation limits, or generator temperature limits [25].

The exemplary start-up process in pump mode and the synchronization to grid of the VSFSC, VSDFG, and FSPT schemes is shown in figure 5.6.

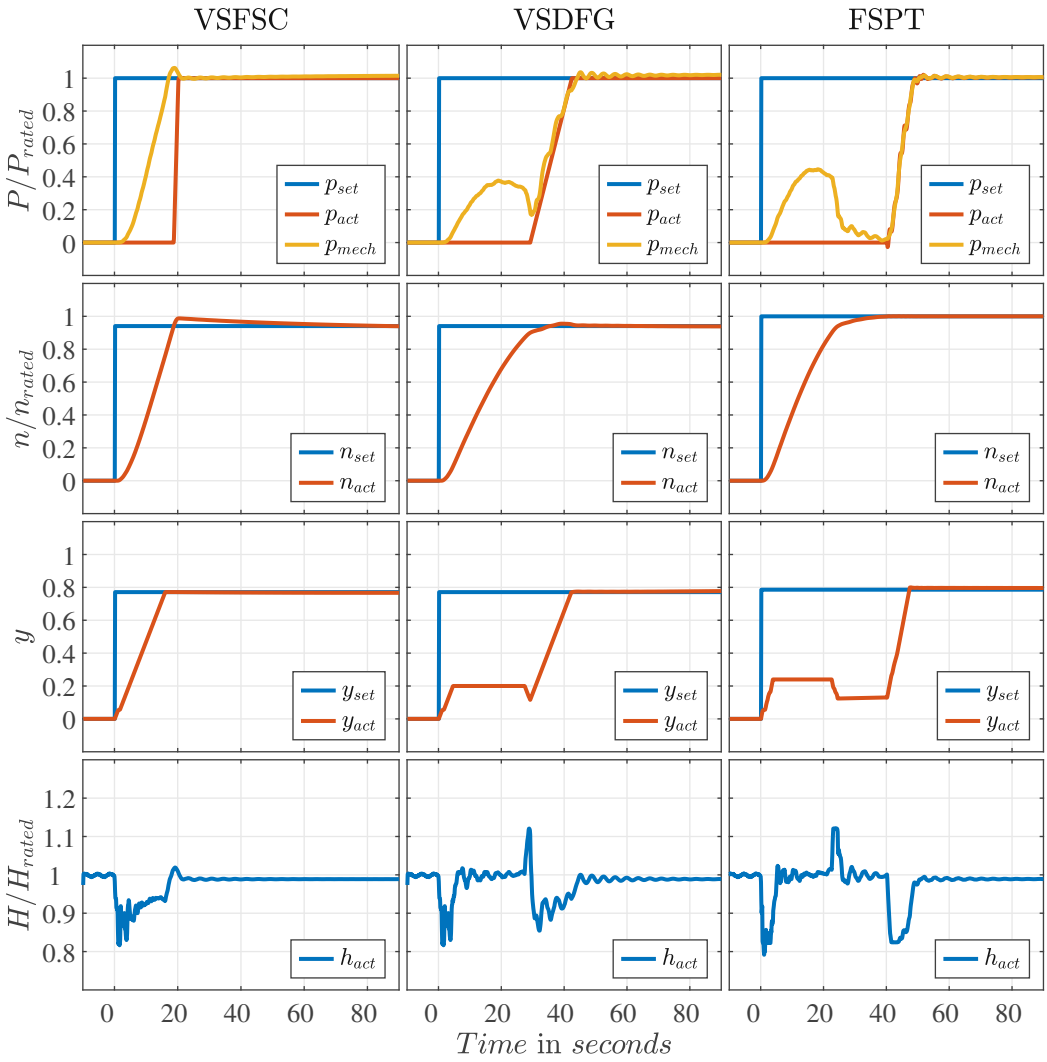

Figure 5.5: Start-up in turbine mode and synchronization to grid of VSFSC, VSDFG and FSPT

The power input is only shown for the main motor-generator assembly. The VSFSC can already draw electrical power for pump operations according to the current speed at the beginning of the change of the reference signal. The pump-turbine can be accelerated in water with rated torque to nominal speed for nominal pump power. The VSDFG's motor-generator assembly is accelerated to a speed of -0.9 p.u. with closed gate vanes. Then, the synchronization to the grid occurs, the gate vanes open, and power input rises to the reference signal. The FSPT start-up is similar to the VSDFG, but synchronization can only happen at nominal speed. Since the acceleration of the pump-turbine needs more time, the FSPT is the slowest of the three schemes to reach the reference signal. The net head during the start-up process remains within its dynamic boundaries.

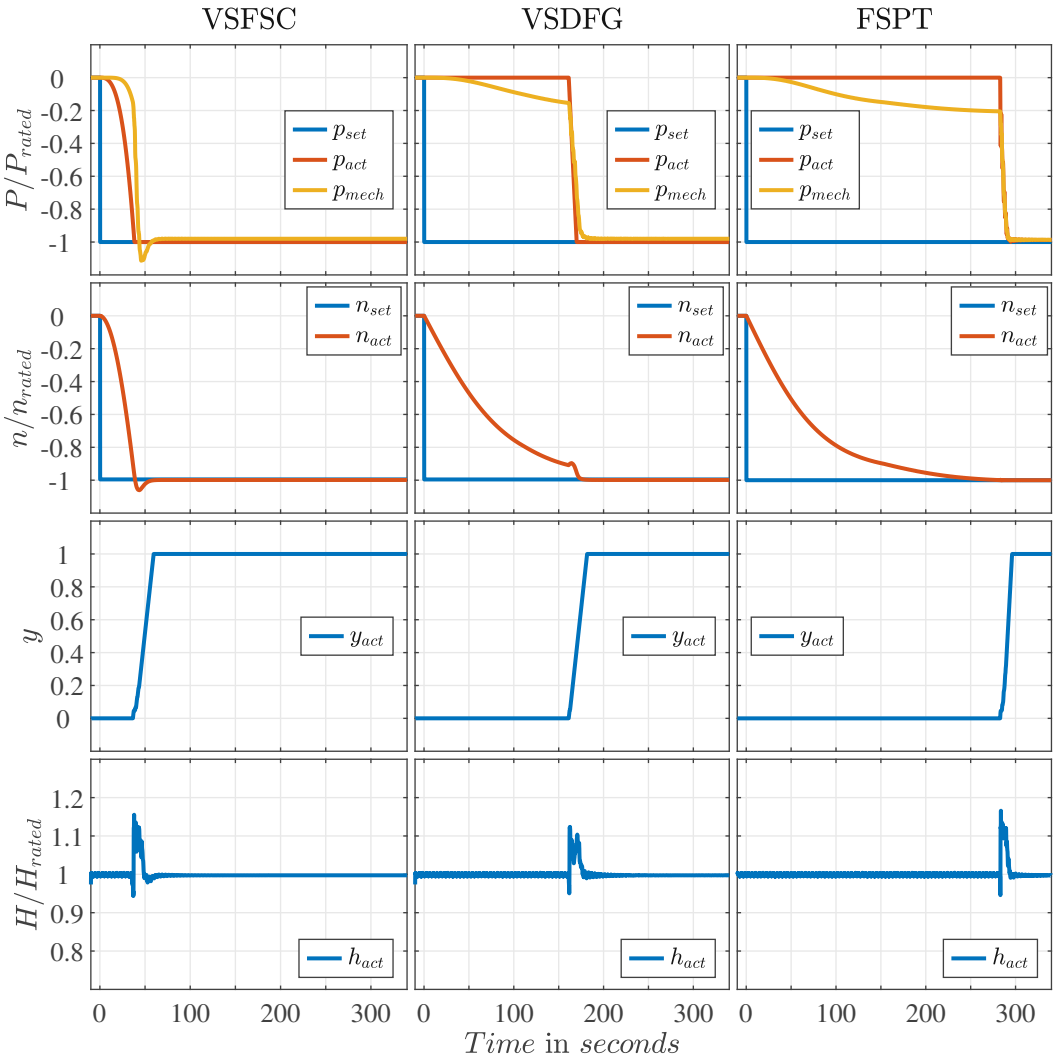

Figure 5.6: Start-up in pump mode and grid synchronization of VSFSC, VSDFG and FSPT

6 Results of Transient Simulations

First, the dynamic behavior of the variable speed pump-turbine schemes is investigated in pump and turbine mode. The goal is to find out how long it takes for the specific technology to change between operating points and what electrical efficiency the schemes have at that operating point. Depending on a minimal mechanical efficiency, the effective operating range is further limited. The results are also analyzed to determine the possible FCR provision range for each scheme and operating mode. Moreover, FCR provisions for a period of 4 hours are simulated, and the correctness of the delivery is investigated using the monitoring methods introduced in subsection 2.2.2.

6.1 Dynamic Behavior

This section determines the dynamic behavior of operating point changes for the VSDFG and VSFSC in pump and turbine mode through transient simulations. The simulated operating point range differs for VSDFG and VSFSC as well as for the operating mode (pump or turbine mode). Changes in the set-point are done by using a ramp power input signal. The minimum ramp-up time for each change between the current and the new set-point is determined. A parameter boundary can be violated if the gradient of the ramp input signal is too high (speed limits and head limits). In this case, the ramp-up time is extended by 1 s and the simulation is done again. The time difference is measured after a successful simulation, when no boundaries are surpassed. Figure 6.1 highlights this approach by displaying the power output, the speed and the net head of the an exemplary set-point change from 0.2 p.u. to 1 p.u. from the VSDFG in turbine mode.

The results are presented for each viable operating point and corresponding $\triangle p$ to reach the next one in the following sections. A distinction between lowering and increasing the current operating point is made. Furthermore, the electrical efficiencies are shown as restrictions due to instabilities, and cavitation are also being made.

6.1.1 VSDFG Turbine Mode

The simulated operating point scope of the VSDFG in turbine mode is between 0.08 p.u. and 1.09 p.u.. Therefore, $\triangle p$ ranges from 0 p.u. to 1.01 p.u.. Figure 6.2 shows the time it takes to change the electrical power output from one operating point by a specific $\triangle p$ value considering a linear change in set-points. Minor changes of around 0.2 p.u. of the set-point can be followed by the VSDFG rather quickly. Bigger leaps lead to a dip in speed as the machine decelerates as more electrical power is fed into the grid than mechanical power can be generated. This can cause the speed to fall under the speed limit of 0.9 p.u.. Since no artificial delay is implemented in the VSDFG reaction to a set-point change, every time value under 30 s can be considered fast enough for FCR delivery. However, a mechanical efficiency of 80 % is desired as mentioned before, but the investigated plants can operate as low as 65 % [55]. Figure 6.3 shows the electrical efficiency after increasing the operating point of the investigated VSDFG in turbine mode. Considering limitations due to the efficiency, the effective operating range is slightly reduced (white dotted line). It is notable, that the efficiency is getting lower for set-points higher that the rated power output.

Figure 6.4 depicts the minimal time values for decreasing the operating point of the investigated VSDFG in turbine mode. Compared to the case of increasing set-points, here, the time it takes to reach the new target value is notable faster. The reason for this is the fact that the optimal speed set-points for lower operating points are close to the lower speed limit. Hence, a decrease in power output leads to the machine's acceleration and more distance from the lower speed limit. For operating points close to rated power, the upper speed boundary is the limiting factor as the speed set-points are closer to the rated speed.

Figure 6.5 shows the electrical efficiency for the simulated operating range and the reduced area due to the minimum efficiency requirement.

6.1.2 VSDFG Pump Mode

The simulated operating area of the VSDFG ranges from -0.55 p.u. to -1.09 p.u.. The time it takes the machine to change operating points in this area is less than half a second. The operating points do not reach the speed, or head limits, and fast set-points transitions are possible especially since the gate vane opening time is not of any concern. Considering the efficiency restrictions of 65 %, the operating range is only slightly reduced and starts from -0.6 p.u.. Figure 6.6 and 6.8 show the time values for the transition from one set-point to another within the defined operating range. .

The electrical efficiency of increasing and reducing the operating points are shown in figure 6.7 and 6.9. Efficiencies from 60 % and up to 85 % can be achieved.

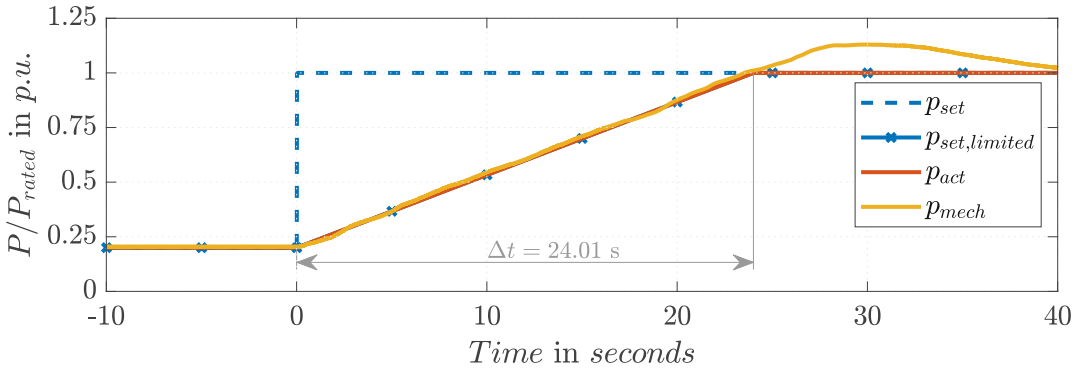

(a) Electrical and mechanical power

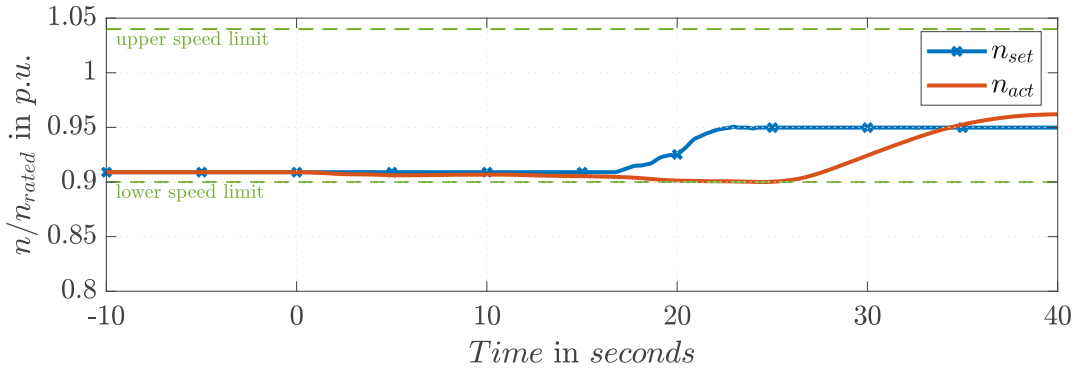

(b) Speed

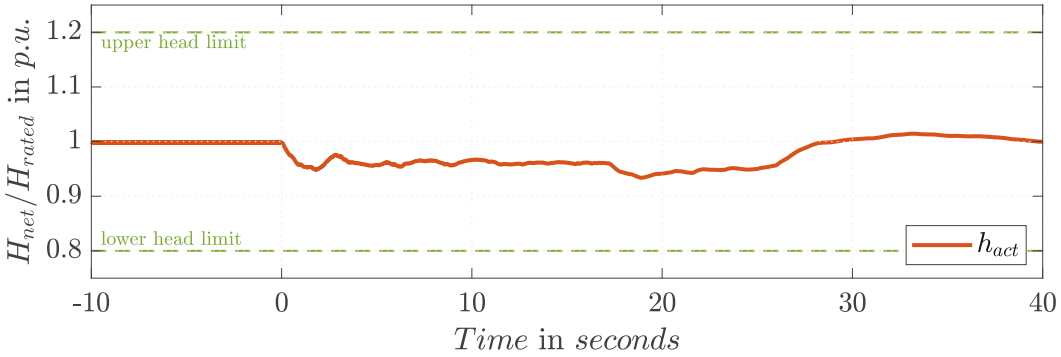

(c) Net head

Figure 6.1: Exemplary set-point change from 0.2 p.u. to 1 p.u. from the VSDFG in turbine mode

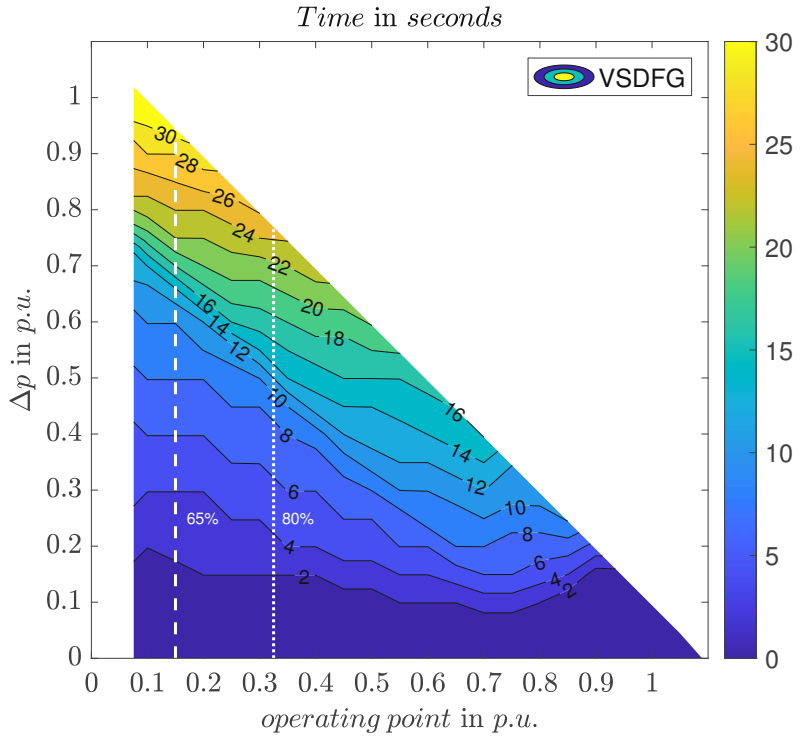

Figure 6.2: The minimal time required (in seconds) for increasing the power output by Δp starting from a specific operating point of the VSDFG in turbine mode

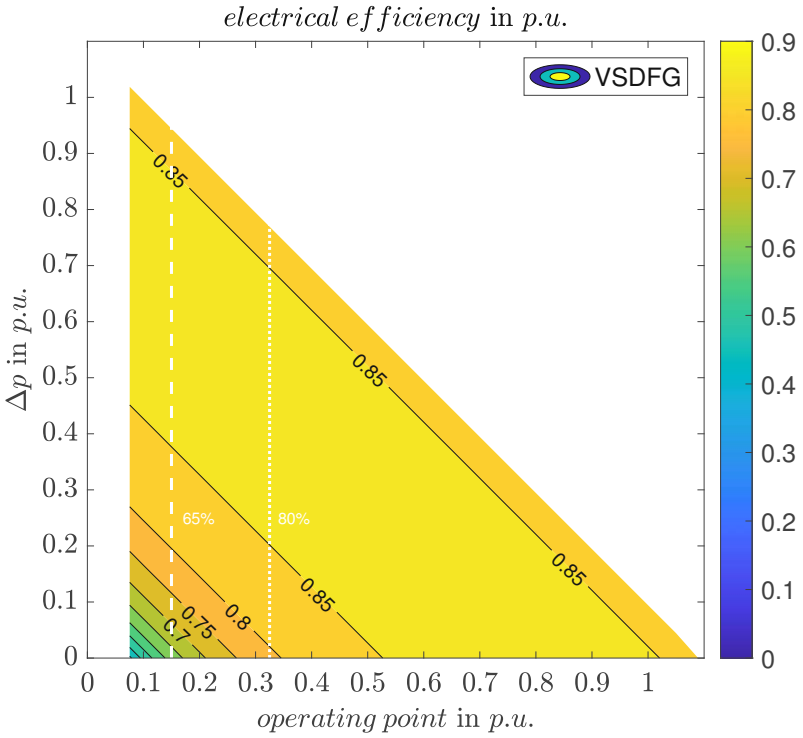

Figure 6.3: The electrical efficiency reached (in p.u.) after increasing the power output by Δp starting from a specific operating point of the VSDFG in turbine mode

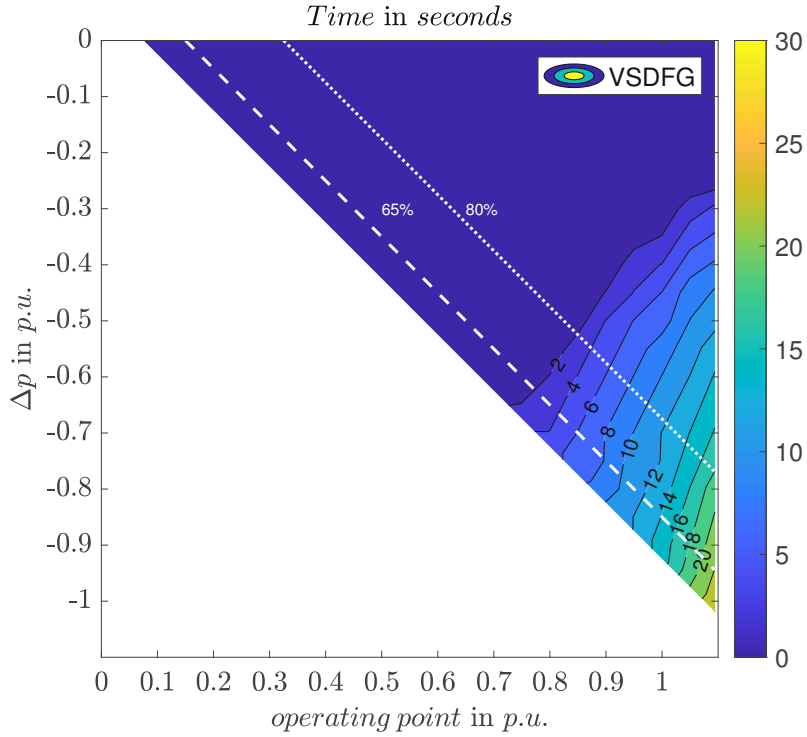

Figure 6.4: The minimal time required (in seconds) for decreasing the power output by Δp starting from a specific operating point of the VSDFG in turbine mode

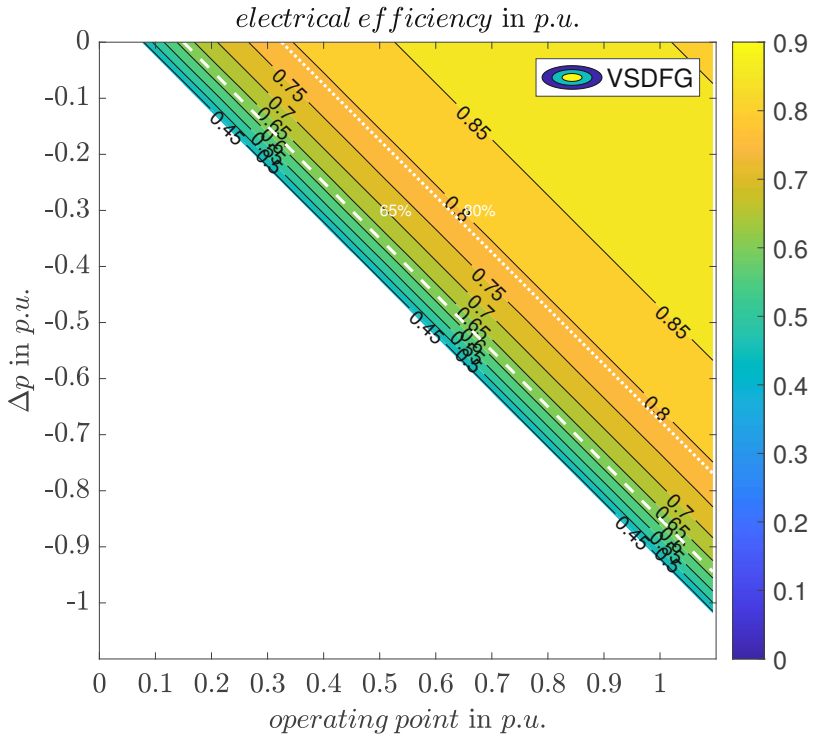

Figure 6.5: The electrical efficiency reached (in p.u.) after decreasing the power output by Δp starting from a specific the operating point (increasing the pump power intake) of the VSDFG in turbine mode

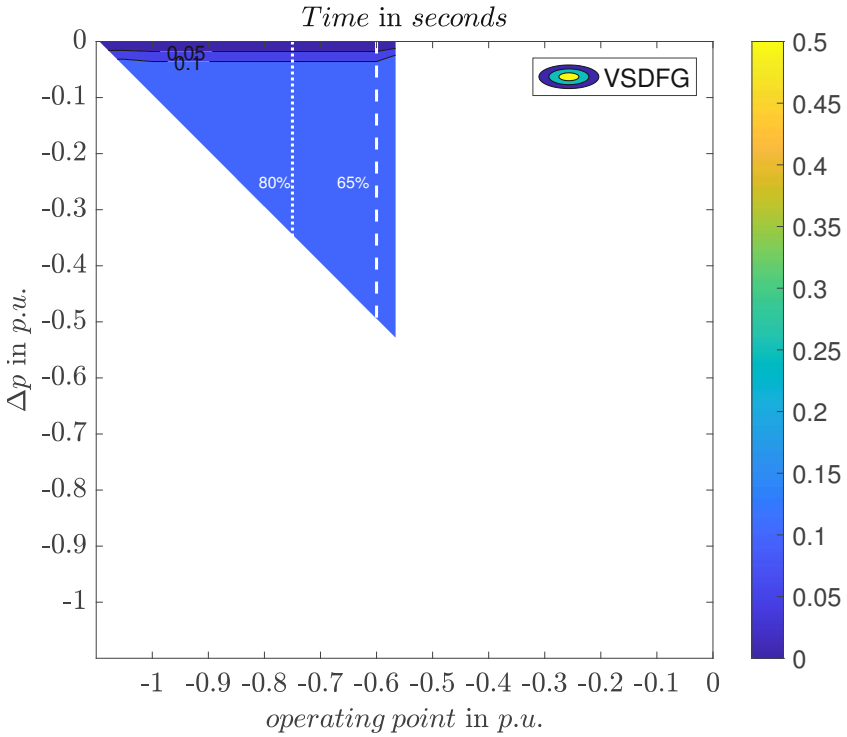

Figure 6.6: The minimal time required (in seconds) for decreasing the power output by Δp starting from a specific operating point (increasing the pump power intake) of the VSDFG in pump mode

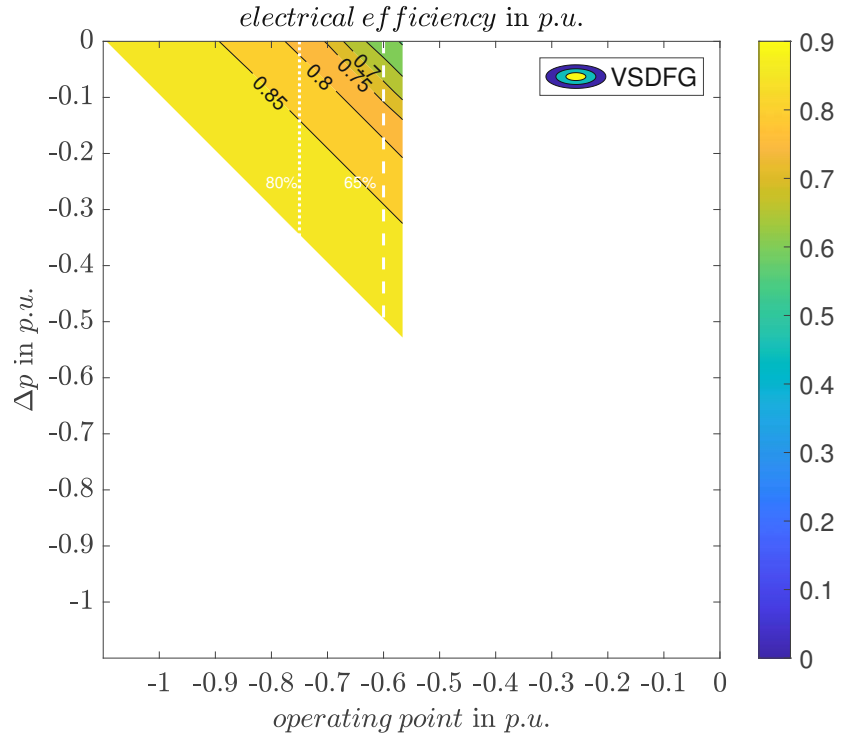

Figure 6.7: The electrical efficiency reached (in p.u.) after decreasing the power output by Δp starting from a specific operating point of the VSDFG in pump mode

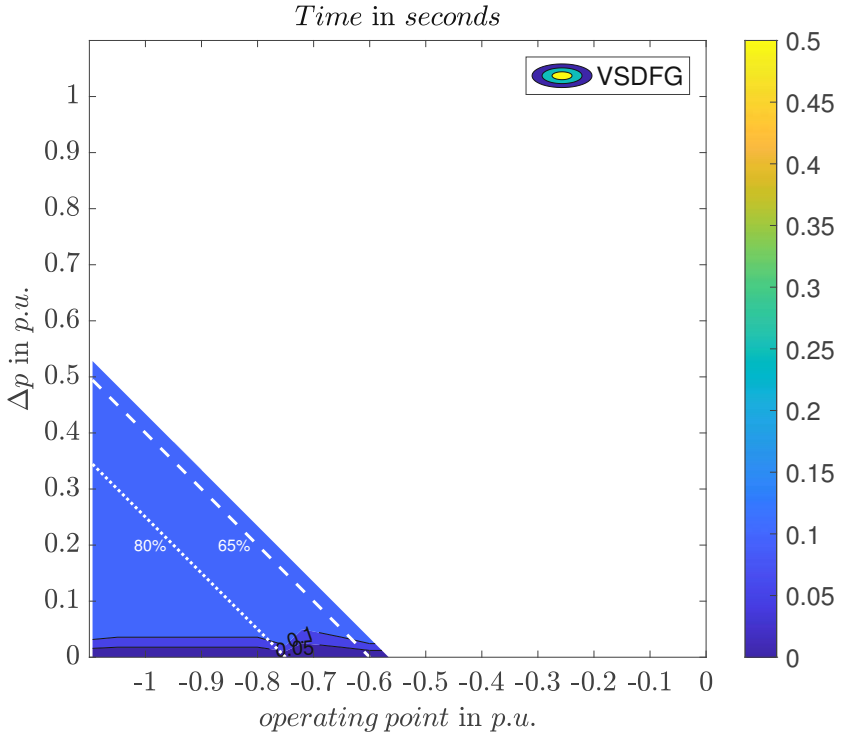

Figure 6.8: The minimal time required (in seconds) for increasing the power output by Δp starting from a specific operating point (decreasing the pump power intake)of the VSDFG in pump mode

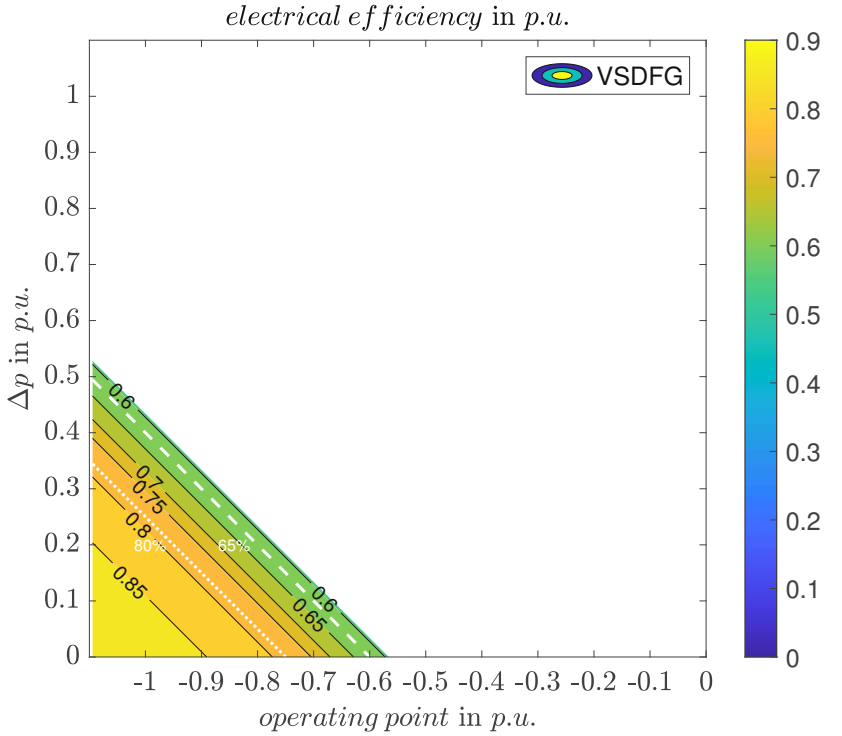

Figure 6.9: The electrical efficiency reached (in p.u.) after increasing the power output by Δp starting from a specific operating point (decreasing the pump power intake) of the VSDFG in pump mode

6.1.3 VSFSC Turbine Mode

The operating range of the VSFSC is simulated from 0.05 p.u. to 1.09 p.u.. Figure 6.10 depicts the time it takes to change the electrical power output linearly from one operating point by a specific $\triangle p$ value. Changes of around 0.3 p.u. of the set-point can be followed by the VSFSC almost instantaneously. Bigger leaps lead to a dip in speed as the machine decelerates as more electrical power is fed into the grid than mechanical power can be generated. Faster transitions between operating points are not limited by the lower speed boundary but by the fact that the machine would stall[55]. Again, since there is no artificial delay implemented in the VSFSC reaction to a set-point change, every time value under 30 s can be considered fast enough for FCR delivery.

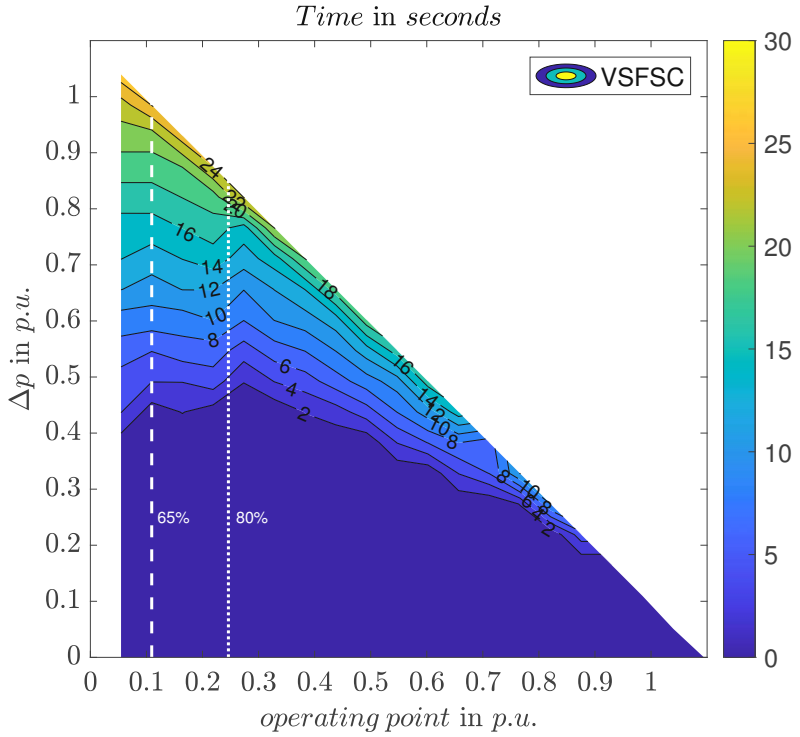

Figure 6.10: The minimal time required (in seconds) for increasing the power output by Δp starting from a specific operating point of the VSFSC in turbine mode

Figure 6.11 shows the electrical efficiency after increasing the operating point of the investigated VSFSC in turbine mode. Considering limitations due to the efficiency, the effective operating range does not start from zero power output but from 0.1 p.u.. Again, the white dotted line indicates this boundary. Notably, the efficiency is getting lower for set-points higher than the rated power output.

Figure 6.12 depicts the minimal time values for decreasing the operating point of the investigated VSFSC in turbine mode. Compared to the case of increasing set-points, here, the time it takes to reach the new target value is notable faster and within 20 s. For operating points close to rated power, the upper speed boundary is the limiting

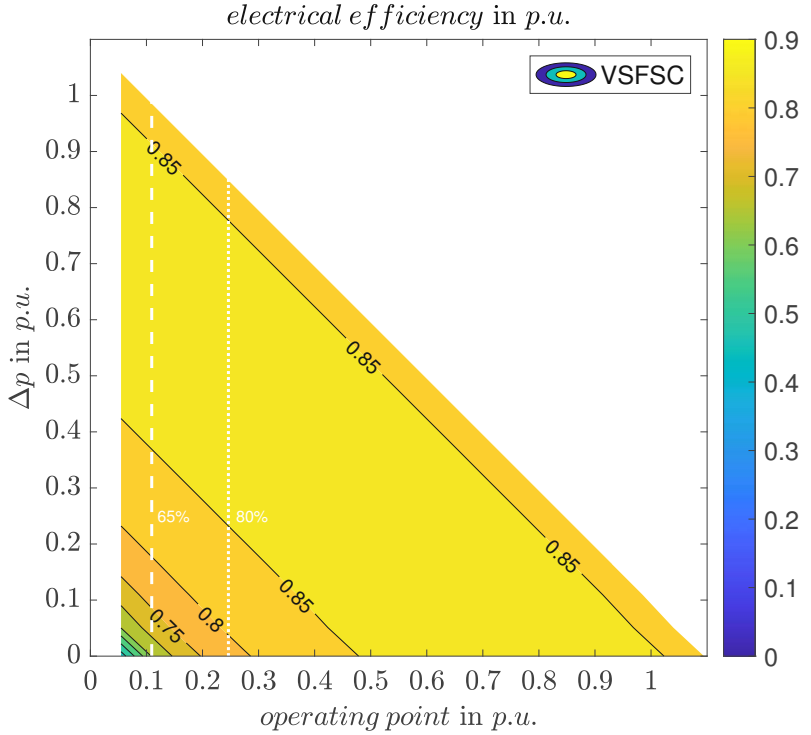

Figure 6.11: The electrical efficiency reached (in p.u.) after increasing the operating point of the VSFSC in turbine mode

factor as the speed set-points are closer to the rated speed.

Figure 6.13 shows the corresponding electrical efficiency diagram after decreasing the operating point of the investigated VSFSC in turbine mode. The efficiency quickly drops for operating points lower than 0.1 p.u..

6.1.4 VSFSC Pump Mode

The simulated operating area of the VSFSC ranges from -0.4 p.u. to -1.09 p.u.. The time it takes the machine to change operating points in this area is less than half a second. The operating points do not reach the speed, or head limits, and fast set-points transitions are possible, especially since the gate vane opening time is not of any concern. Considering the efficiency restrictions of 65 %, the operating range is notably reduced and starts from -0.6 p.u., like the VSDFG. Figure 6.14 and 6.16 show the time values form the transition from one set-point to another within the defined operating range.

The electrical efficiency of increasing and reducing the operating points are shown in figure 6.15 and 6.17. Electrical efficiency at the beginning of the simulated range start from 40 %, while over 85 % can be achieved at rated power.

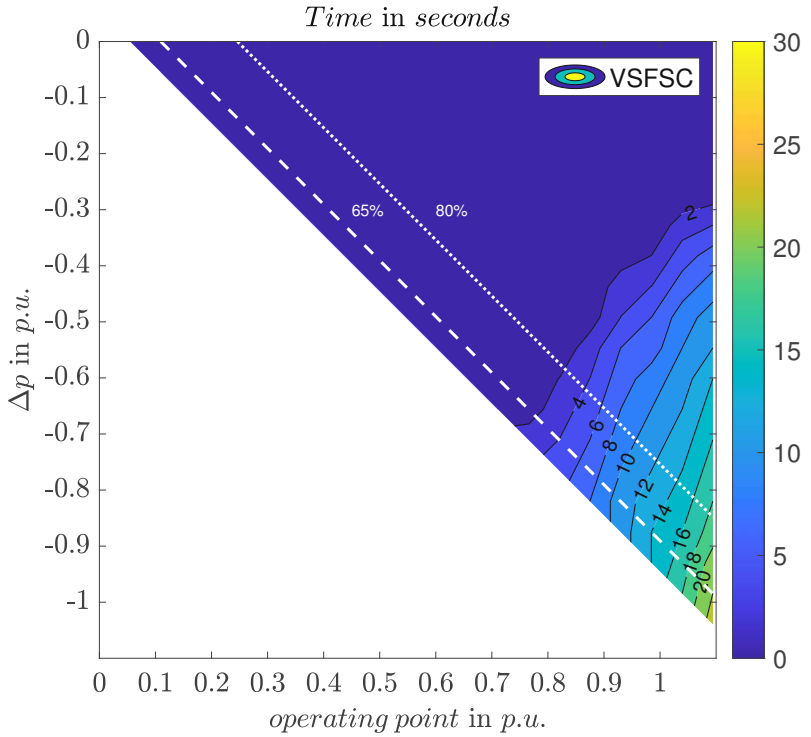

Figure 6.12: The minimal time required (in seconds) for decreasing the power output by Δp starting from a specific operating point of the VSFSC in turbine mode

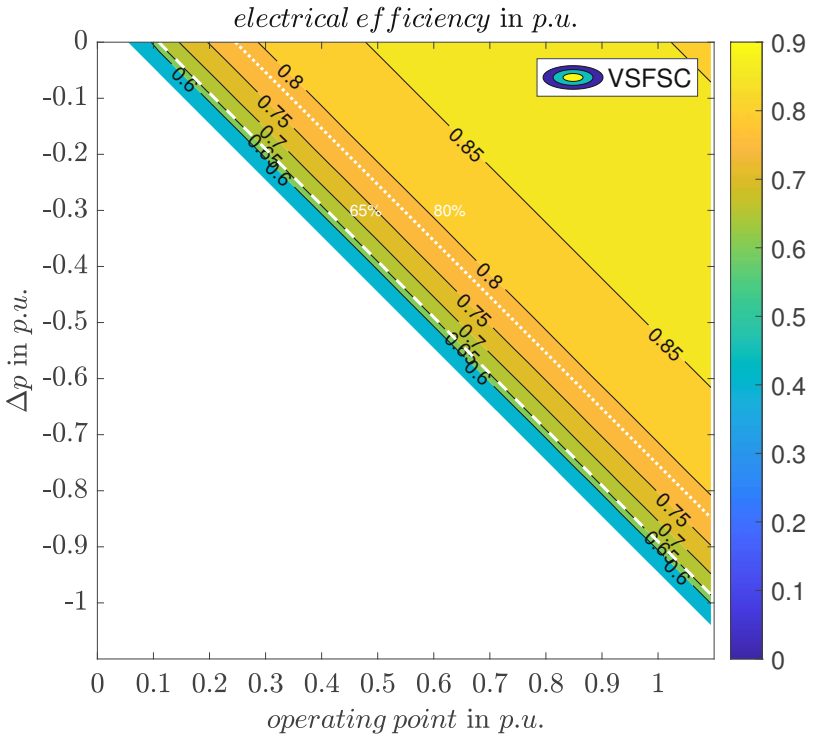

Figure 6.13: The electrical efficiency reached (in p.u.) after decreasing the power output by Δp starting from a specific operating point of the VSFSC in turbine mode

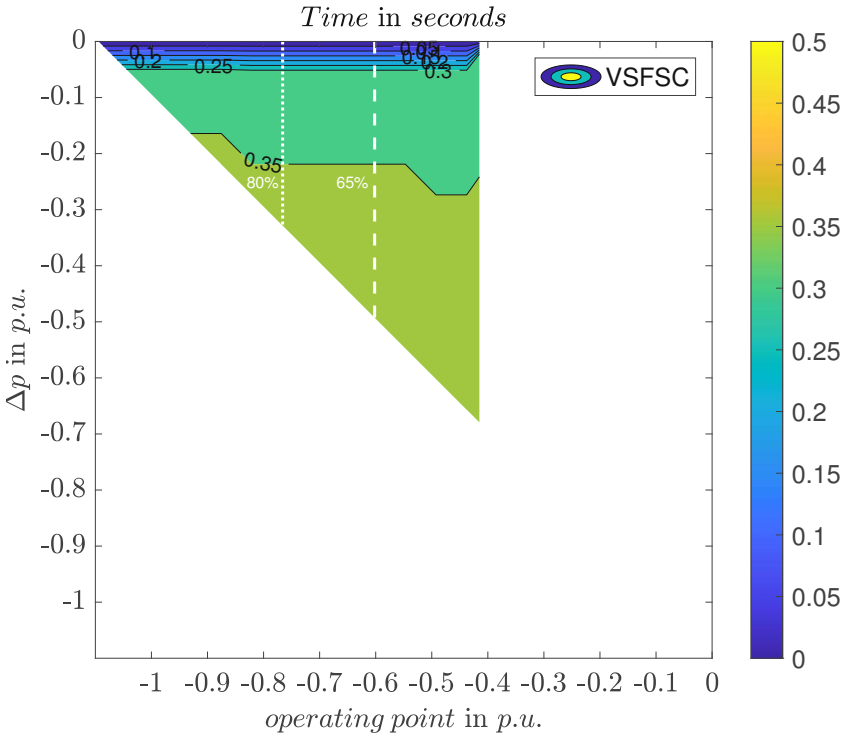

Figure 6.14: The minimal time required (in seconds) for decreasing the power output by Δp starting from a specific operating point (increasing the pump power intake) of the VSFSC in pump mode

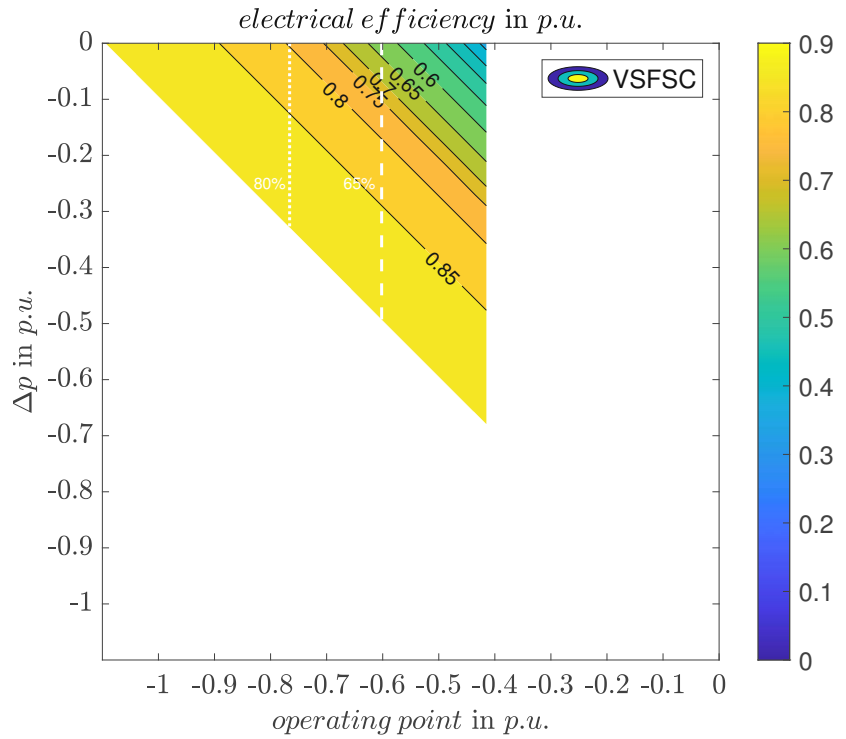

Figure 6.15: The mechanical efficiency reached (in p.u.) after decreasing the power output by Δp starting from a specific operating point (increasing the pump power intake) of the VSFSC in pump mode

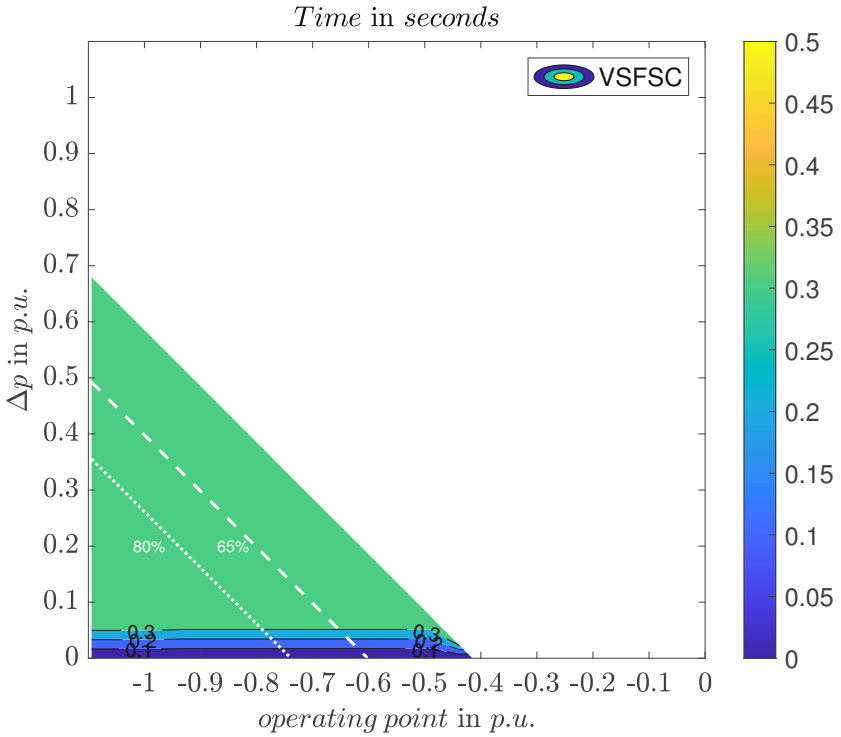

Figure 6.16: The minimal time required (in seconds) for increasing the power output by Δp starting from a specific operating point (decreasing the pump power intake) of the VSFSC in pump mode

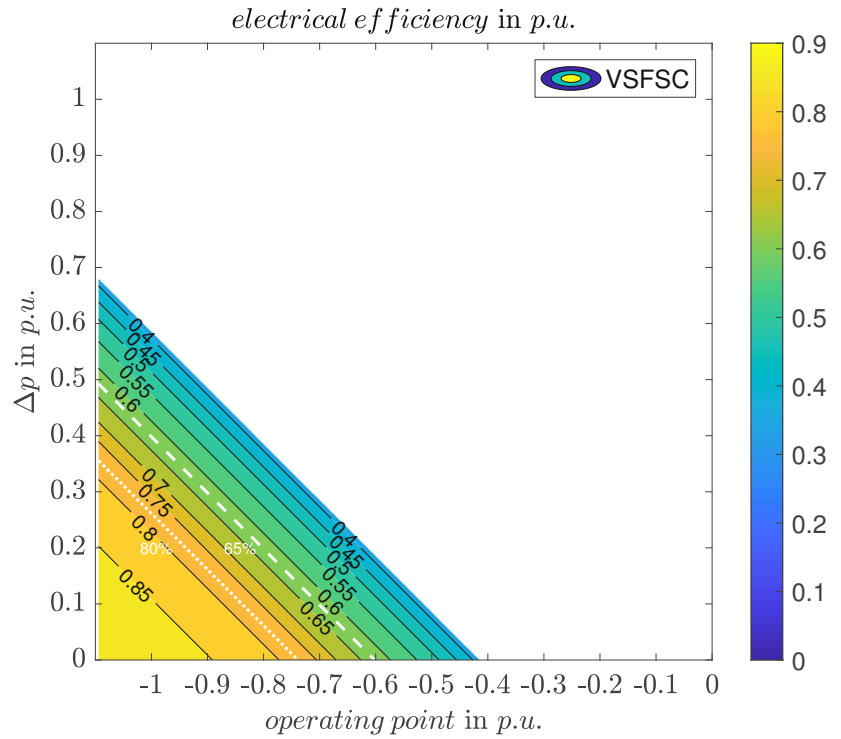

Figure 6.17: The electrical efficiency reached (in p.u.) after increasing the power output by Δp starting from a specific operating point (decreasing the pump power intake) of the VSFSC in pump mode

6.1.5 Comparison of VSDFG and VSFSC

A four quadrant plot of the VSDFG and the VSFSC is put together by adding all figures from turbine and pump mode of the investigated variable speed machines. Figure 6.18 depicts the four quadrant plot of the VSDFG and figure 6.20 shows the plot for the VSFSC. In both displays, the effective operating range for mechanical efficiencies greater than 65 % and 80 % are indicated. It is notable that the effective operating area in pump mode for efficiencies over 65 % are the same for both schemes. For turbine operations, the effective set-point range of the VSFSC is larger for 65 % and 80 % mechanical efficiencies. This originates in the fact that the VSFSC can operate at lower speed at lower operating points, which improves the efficiency. Figure 6.19 and 6.21 show the corresponding four quadrant electrical efficiency charts. Again, they include dotted lines that indicate when the mechanical efficiencies are greater than 65 % and 80 %.

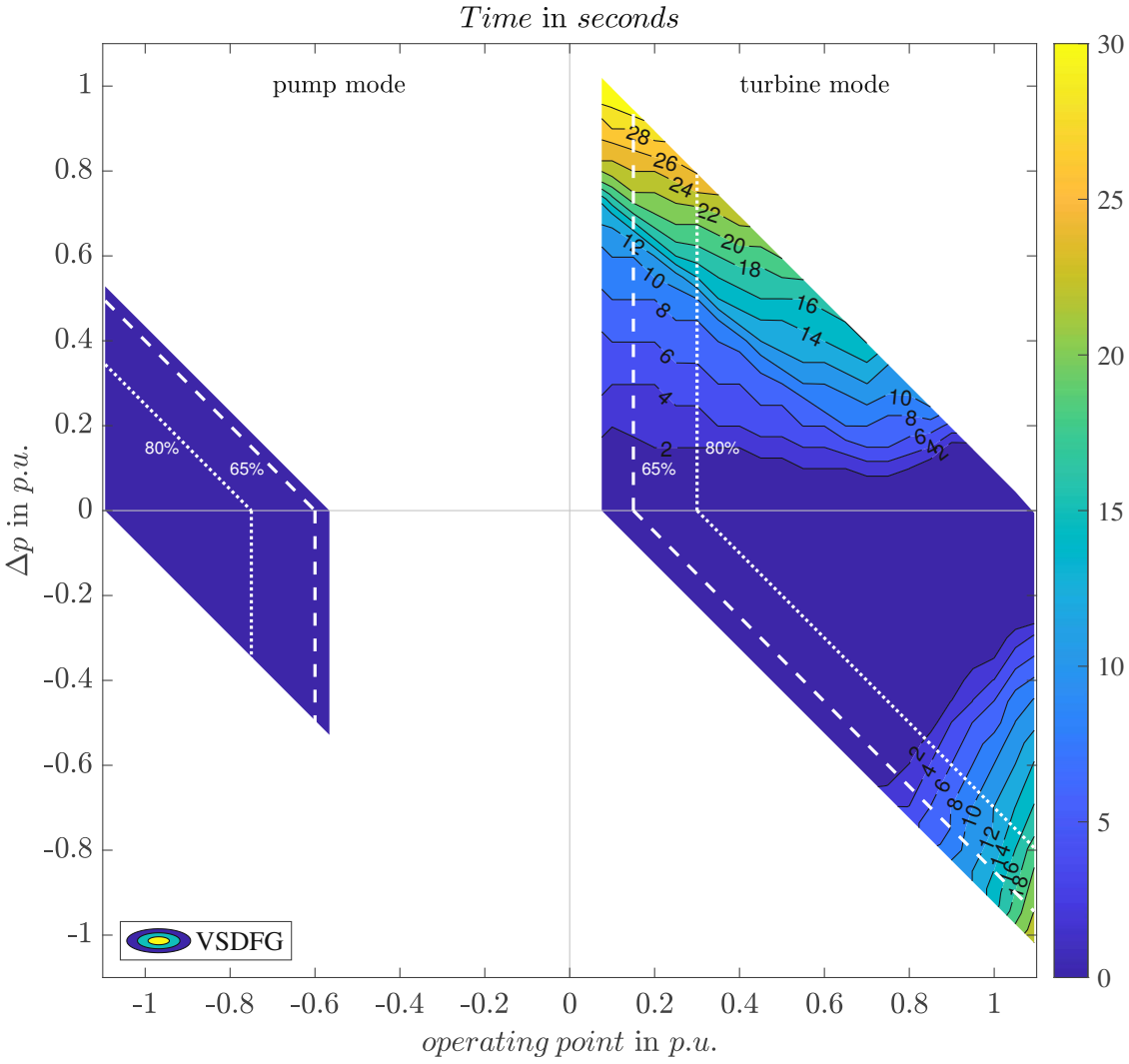

Figure 6.18: The minimal time required (in seconds) for changing the power output by Δp starting from a specific operating point of the investigated VSDFG in turbine mode and pump mode

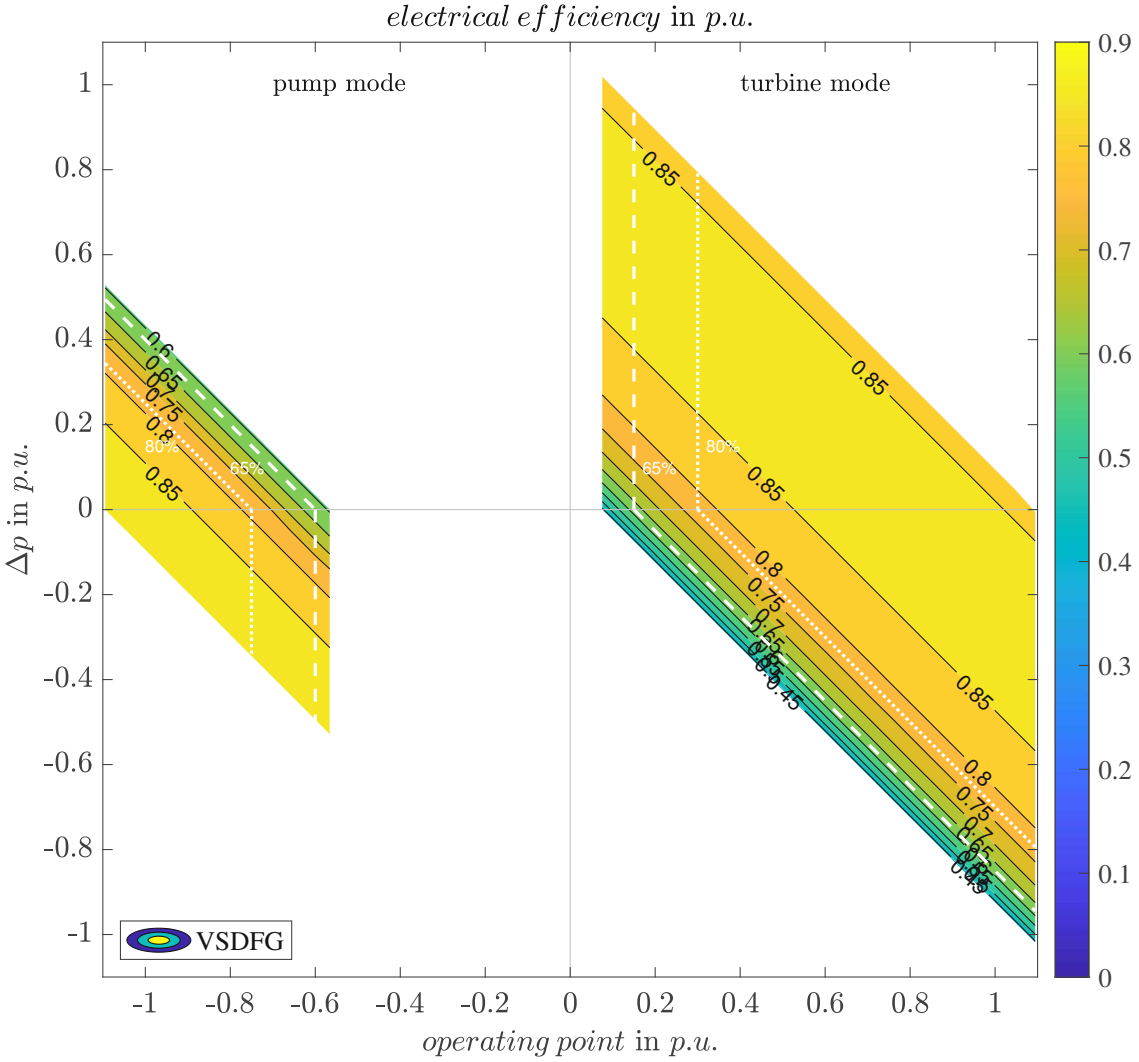

Figure 6.19: The electrical efficiency reached (in p.u.) for changing the power output by Δp starting from a specific operating point of the investigated VSDFG in turbine mode and pump mode

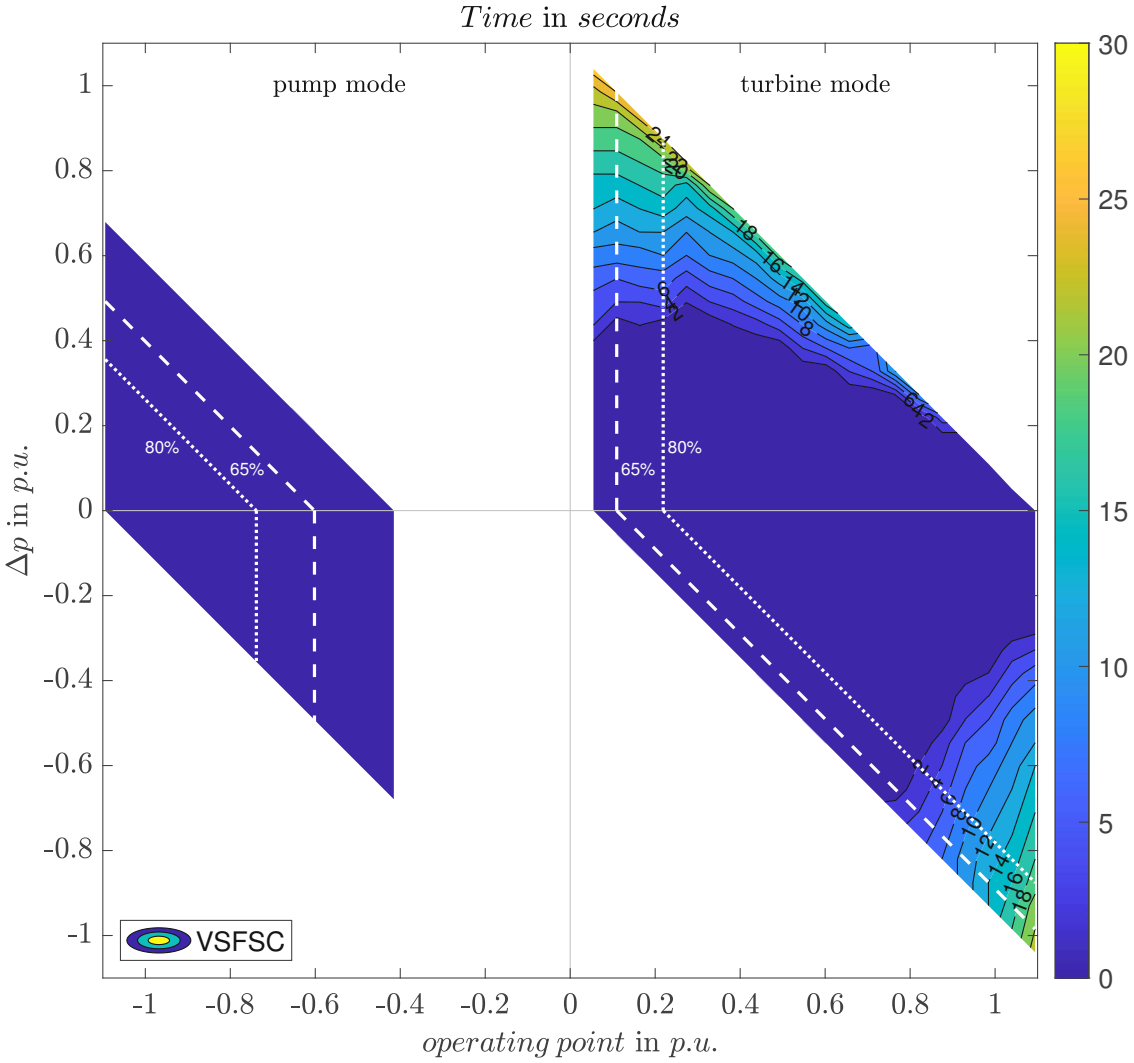

Figure 6.20: The minimal time required (in seconds) for changing the power output by Δp starting from a specific operating point of the VSFSC in turbine mode and pump mode

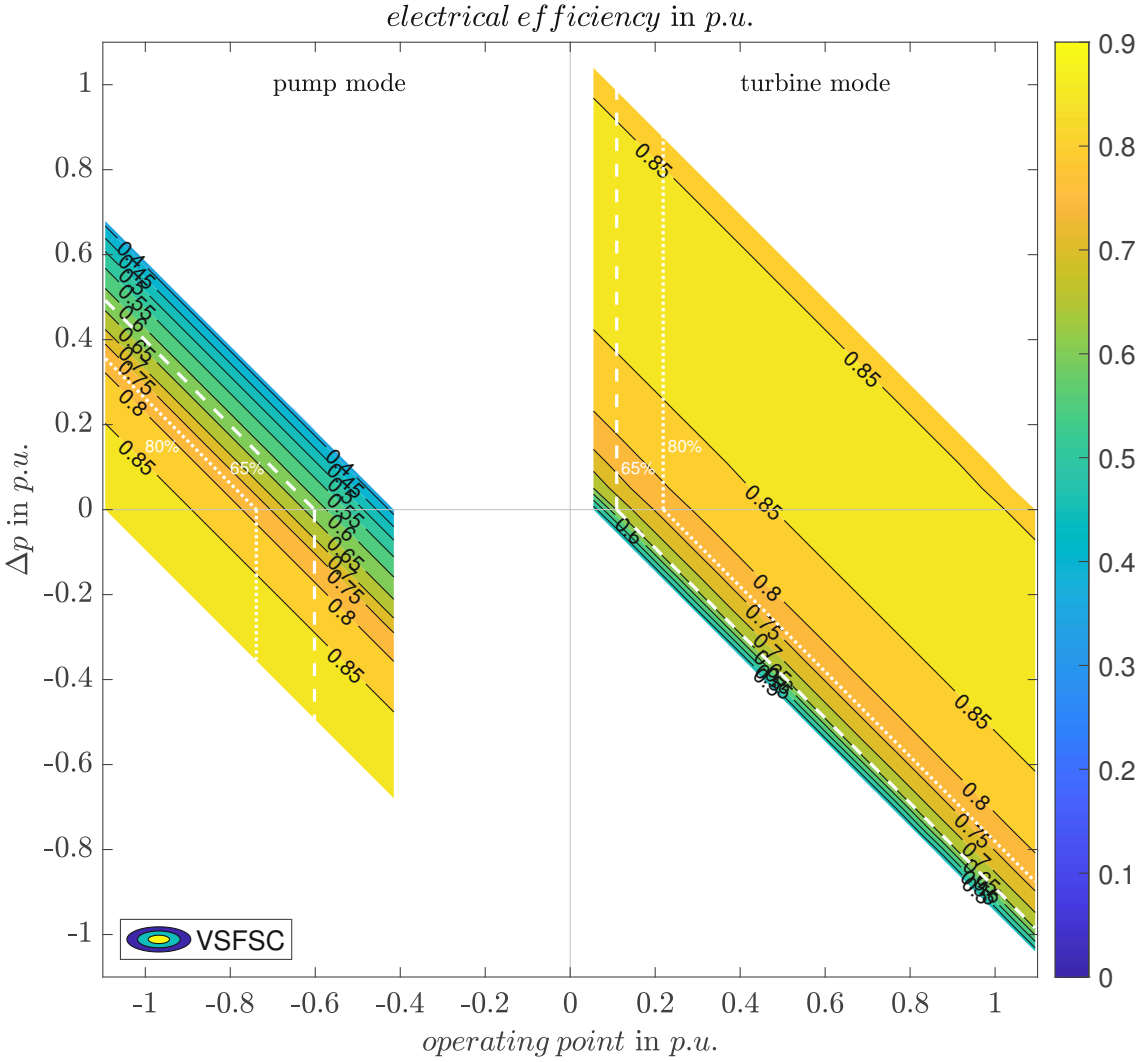

Figure 6.21: The electrical efficiency reached (in p.u.) for changing the power output by Δp starting from a specific operating point of the VSFSC in turbine mode and pump mode

6.2 Frequency Containment Reserve Provision

In this section, the ability of the VSDFG and VSFSC to provide FCR in turbine and pump mode is investigated. A change of operating modes from pump to turbine or the other way around during FCR provision is not considered, as the switch-over times are too high for the investigated power plant configuration.

Since FCR provision has to be done symmetrically, the effective operating range for FCR provision is slightly smaller than the overall range. At the lowest and highest power output/input points, no FCR bidding is possible, while the minimum FCR bid requirements further reduce the area. Furthermore, the scheduled set-point limits the FCR bid size. For lower operating points, the FCR bid is defined by distance to the minimal set-point, while for operating points around rated power, the distance to the maximum power output/input defines the maximum bid size. Finally, the current maximum FCR bid size is also taken into consideration.

6.2.1 Frequency Signal based on Design Hypothesis

For a realist assessment of FCR capability during turbine and pump operations, the grid model of section 4.4 is used as input frequency signal. Every frequency deviation influences directly connected rotating machines in their speed. The frequency event based on the design hypothesis presents the current worst case scenario for FCR provision, as full deployment of FCR resources is triggered. Furthermore, it indicates the highest and steepest frequency gradient. In the following sections, a positive (triggers a negative FCR provision) and negative (triggers a positive FCR provision) frequency deviation, according to the design hypothesis is used as f based on a 150 GW network with $T_A = 10$ s and considering a loss and a surplus in generating capacity of 3000 MW. The FCR target is calculated based on f according to equation 2.6. The same principle described in section 6.1 is utilized to determine the time needed for full activation of FCR at a specific operating point and FCR bid, using the FCR target as power input/output signal.

VSDFG

First, the FCR bid range of the VSDFG in turbine mode is analyzed. Figure 6.22 shows the simulated area of FCR provision with the time values to reach a full activation of Δp after a positive or negative frequency deviation according to the design hypothesis. Full activation is possible in any case within the 30 s limit. However, as mentioned before, the effective FCR provision range is reduced when it is subject to minimal mechanical efficiency requirements. Figure 6.23 depicts the electrical efficiency values for the investigated operating range. For lower efficiency

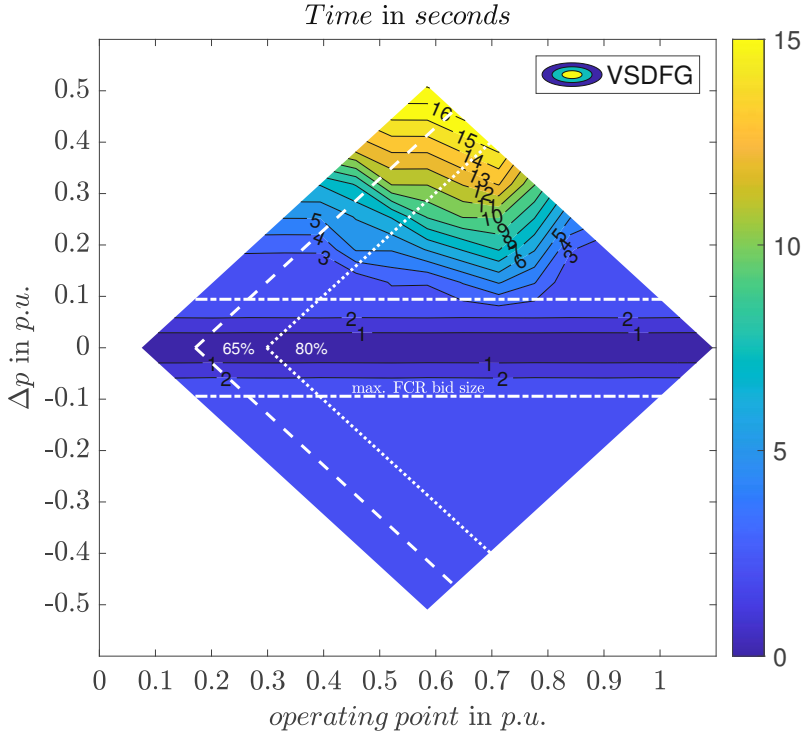

Figure 6.22: The minimal time required (in seconds) by the VSDFG in turbine mode for delivering FCR at a specific power output

boundaries of 65 % (white dashed line) and 80 % (white dotted line), the FCR bid area is notably reduced, also reducing the maximum FCR bid of the plant. The operating point, where most FCR provision is possible ($P_{FCR,max}$), is shifted to the right. However, when applying the current maximum indivisible bid size of 25 MW for this rated power output configuration, possible FCR bids are limited to a small band around the current operating point.

For pump mode, the effective FCR operating range is shown in figure 6.24. Again, the FCR bid area is notably reduced for lower efficiency boundaries of 65 % (white dashed line) and 80 % (white dotted line). The current maximum indivisible bid size for possible FCR bids has a less limiting effect concerning the FCR operating range since the overall operating area is smaller compared to the turbine mode. Figure 6.25 displays the corresponding electrical efficiency diagram.

VSFSC

The VSFSC has a wider operating range for the turbine process, as previously discussed. This also affects the operating area for FCR provision. Figure 6.26 shows the time values and the FCR bid range for the VSFSC in turbine mode. Again, the whole simulated range, as well as restrictions due to efficiency limits of 65 % and 80 % are marked. Compared to the VSDFG, the maximum possible FCR bid is larger, and the

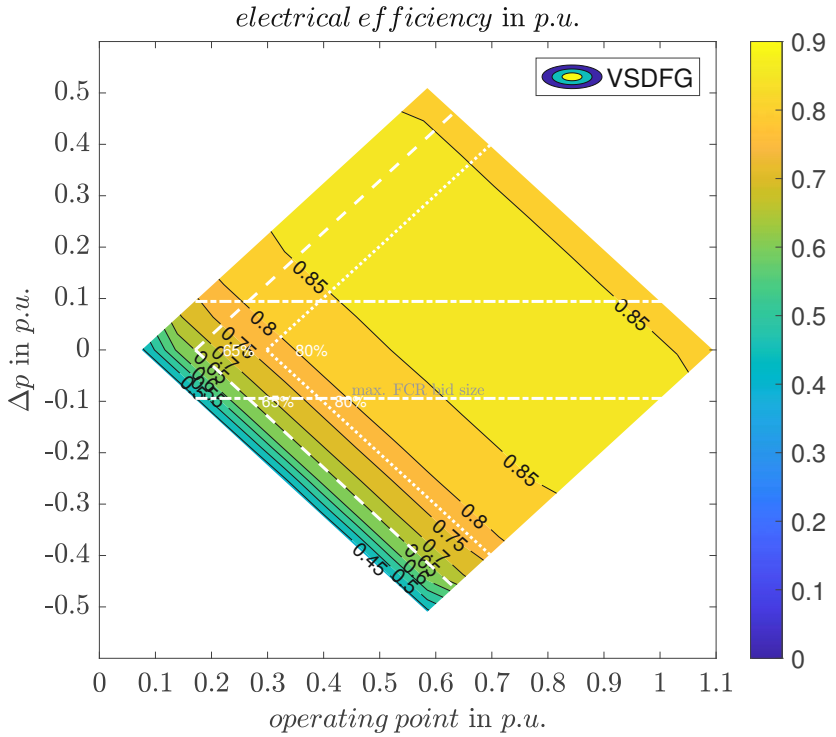

Figure 6.23: The electrical efficiency (in p.u.) of the VSDFG in turbine mode at different operating points considering FCR provision

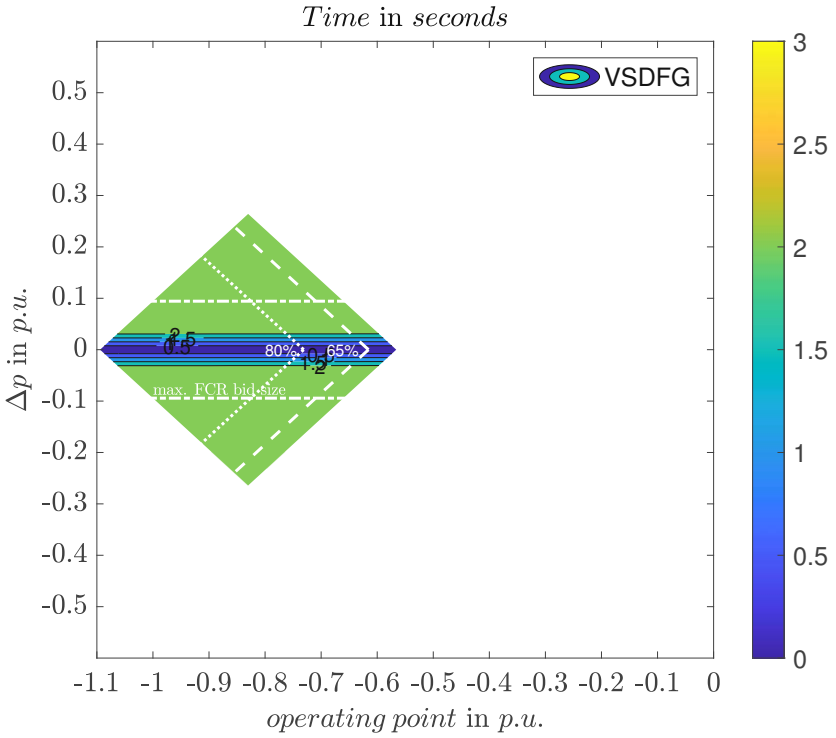

Figure 6.24: The minimal time required (in seconds) by the VSDFG in pump mode for delivering FCR at a specific power output

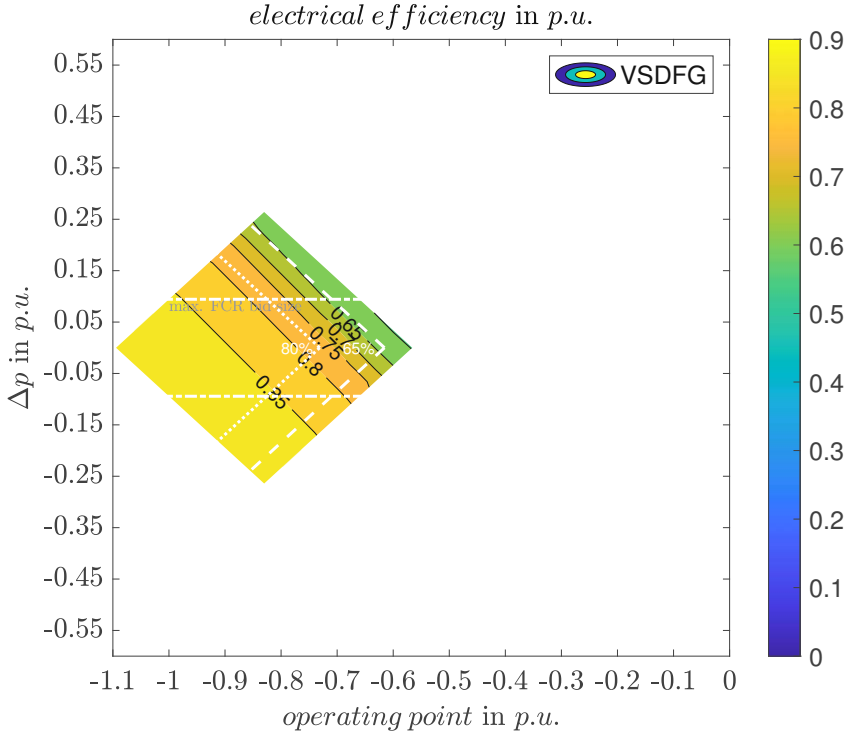

Figure 6.25: The electrical efficiency (in p.u.) of the VSDFG in pump mode at different operating points considering FCR provision

time values to reach full activation are notable faster. Figure 6.27 depicts the electrical efficiency diagram with the mechanical efficiency boundaries drawn in white dotted and dashed lines.

The FCR operating area for pumping is similar to the VSDFG in pump mode. Figure 6.28 shows the time values needed for full activation of Δp after the frequency event, while figure 6.29 displays the corresponding electrical efficiencies.

6.2.2 Continuous Frequency Containment Reserve Provision

For the investigation and monitoring of continuous FCR provision, a 4 hour long typical exemplary frequency measurement of the ENTSO-E Continental Europe is used. Figure 6.30 depicts the frequency development over the observed time span. The maximum deviation from the nominal frequency of 50 Hz is 40 mHz, while the mean value is 50.0084 Hz. According to the SOGL, the FCR providing unit is permitted an intentional frequency response dead band and an inherent frequency response insensitivity with a combined maximum of ±10 mHz around the set-point frequency. Therefore, the PSH does not need to deliver FCR in this insensitivity area. Within the area, the FCR provision can be zero. There are different strategies possible for how BSPs can operate their units inside this area. In this thesis, a strategy with hysteresis is used. When the VSPT already provides FCR outside of the insensitivity area, and

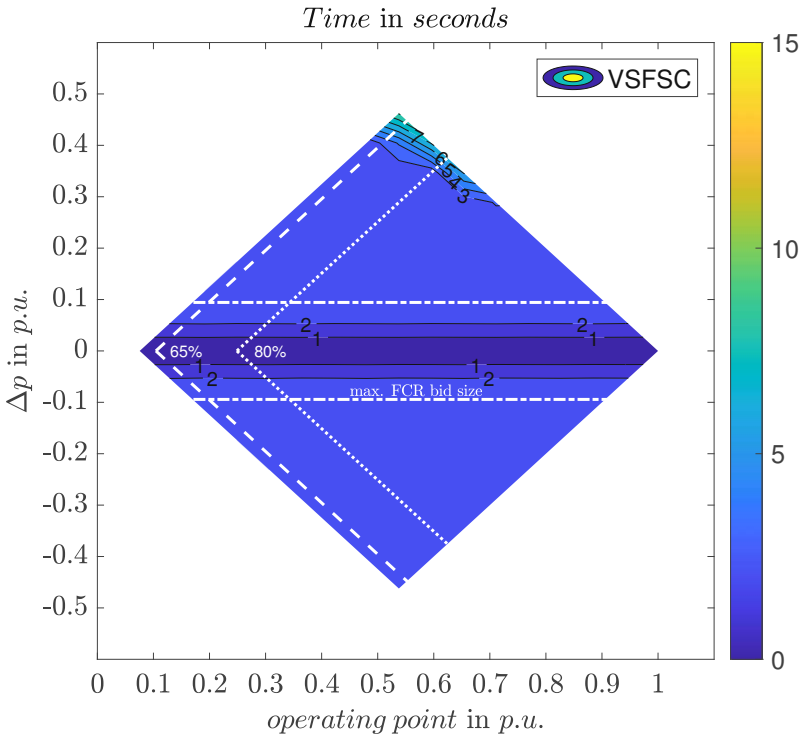

Figure 6.26: The minimal time required (in seconds) by the VSFSC in turbine mode for delivering FCR at a specific power output

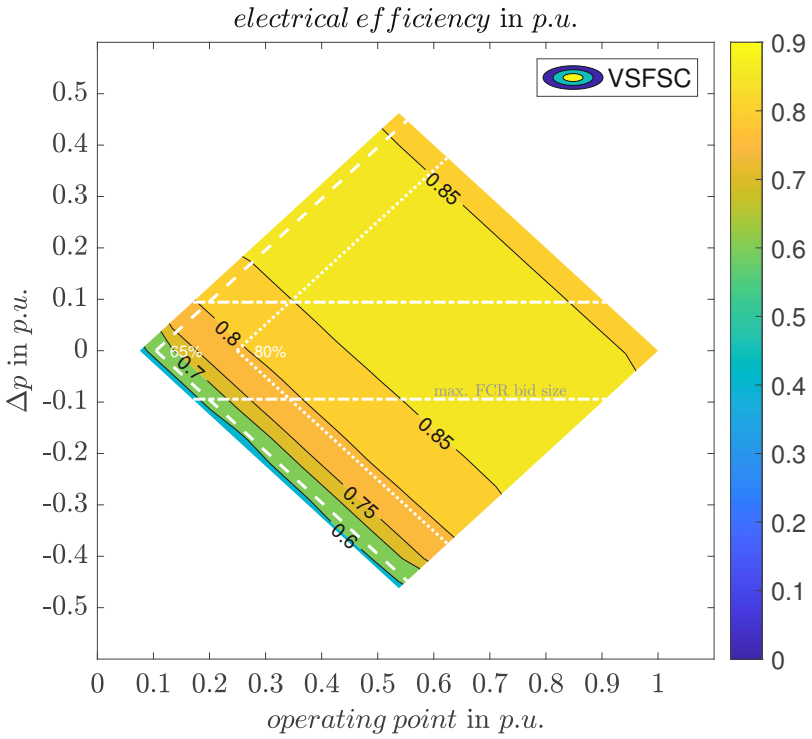

Figure 6.27: The electrical efficiency (in p.u.) of the VSFSC in turbine mode at different operating points considering FCR provision

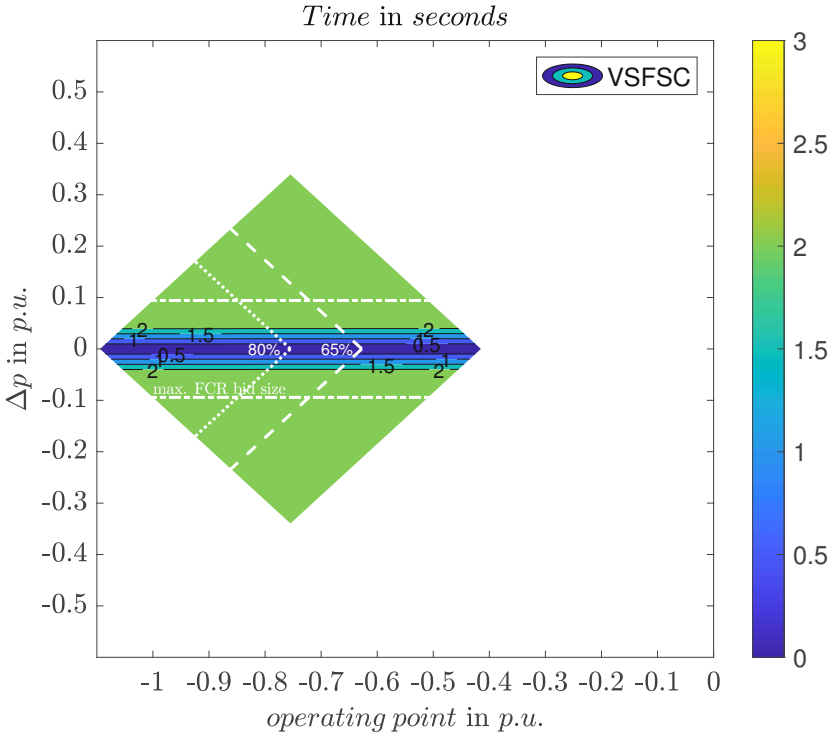

Figure 6.28: The minimal time required (in seconds) by the VSFSC in pump mode for delivering FCR at a specific power output

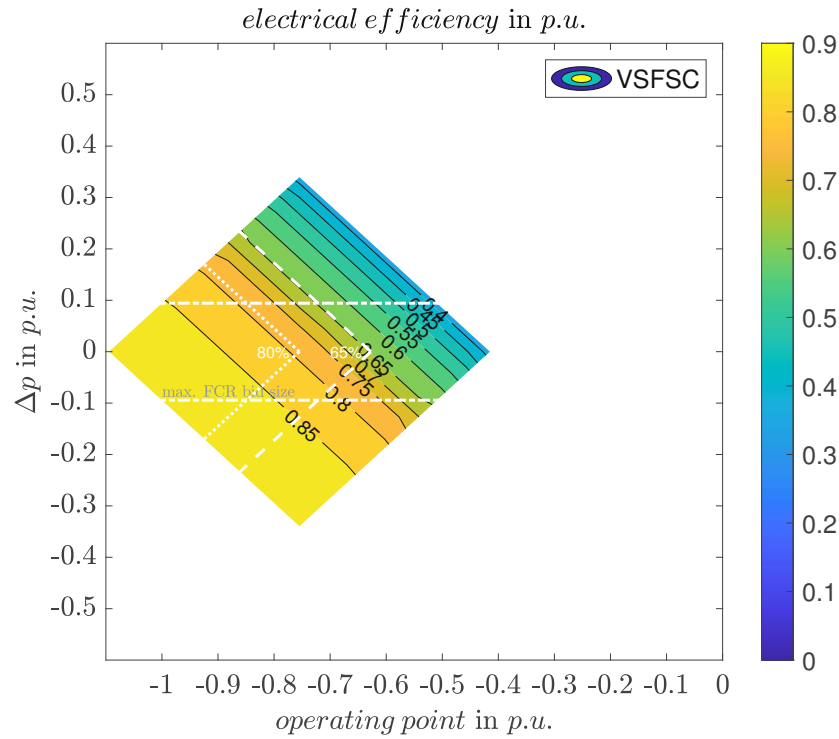

Figure 6.29: The electrical efficiency (in p.u.) of the VSFSC in pump mode at different operating points considering FCR provision

the frequency deviation gets back into it, the FCR provision continues by the BSP even inside the insensitivity area until the set-point frequency is reached again. After that, the BSP is not delivering FCR until the system frequency deviation is greater than ±10 mHz again. Subsequently, this strategy is used in the following FCR provisions of the variable speed schemes in pump and turbine mode.

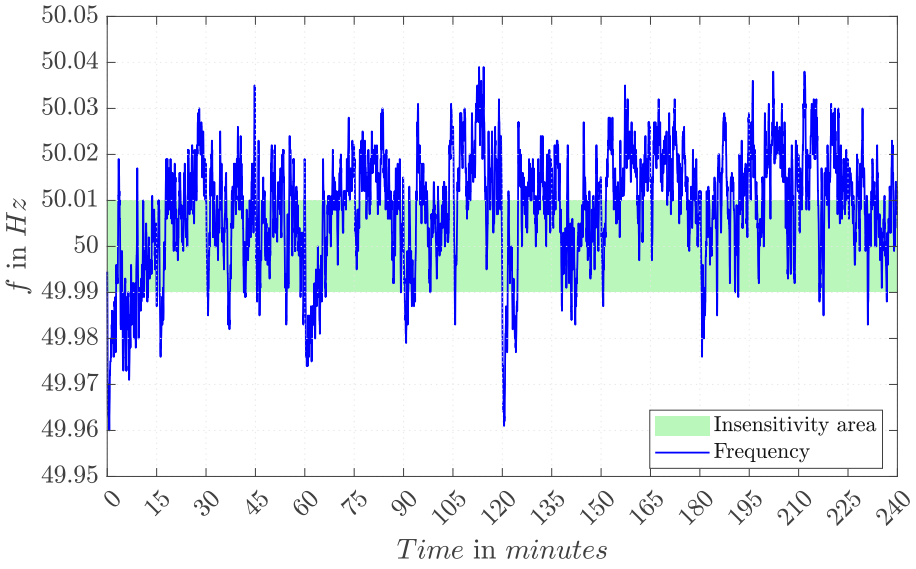

Figure 6.30: Measured frequency of ENTSO-E Continental Europe over a period of 4 hours with insensitivity area

Figure 6.31 shows the FCR provision of the VSDFG in pump ($p_{FCR,BSP,pump}$) and turbine mode ($p_{FCR,BSP,turbine}$) with intentional insensitivity. The figure also indicates that monitoring a correct FCR delivery from a BSP needs enhanced methods to ensure the contracted FCR provision is fulfilled.

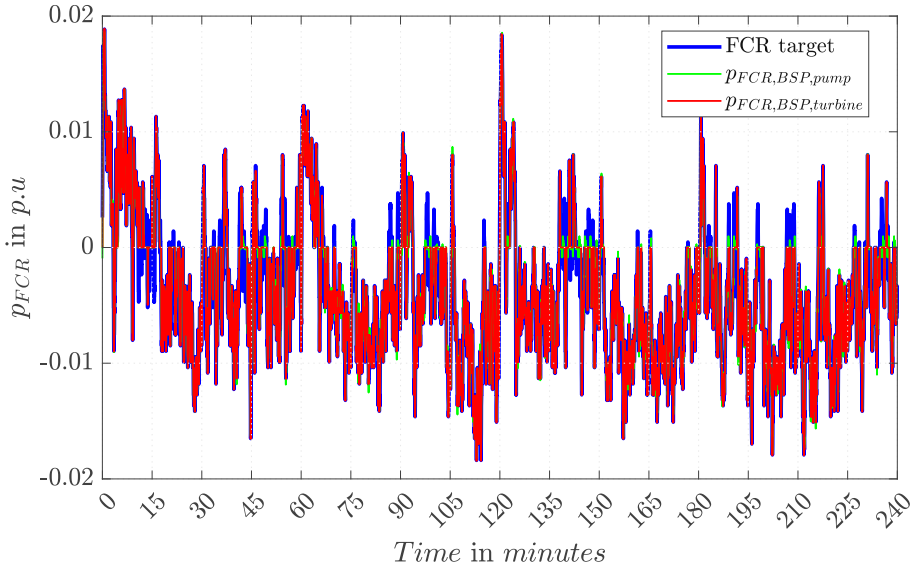

Figure 6.31: FCR provision of VSDFG in turbine and pump mode

6.3 Monitoring of Frequency Containment Reserve Provision

In this section, the three considered monitoring methods are used to check that the FCR provision of the VSDFG and VSFSC in turbine as well as in pump mode is correct and dynamically fast enough. Significant operating points are selected to be subject of the application of the monitoring methods. In turbine mode, the best efficiency point (BEP) and the operating point, where maximum FCR provision is possible (MFP) are considered. In pump mode, the BEP is the highest operating point in both cases (VSDFG and VSFSC). Therefore, if the pump is operated at the BEP, no FCR provision is possible. Hence, only the MFP is used for the monitoring of pump operations. Furthermore, simulations are done with the maximum FCR bid that the machines can deliver at the set-point (BEP or MFP) and the current maximum indivisible FCR bid size of 25 MW. Finally, two different gradient restrictions for full FCR deployment are considered (no restrictions and 30 seconds to full deployment).

6.3.1 Correlation Methodology

The statistic approach of the correlation methodology delivers the linear correlation between the grid frequency and the activated FCR of the balancing service providers (BSP). An indirect proportionality between both values is expected. A $\pm 10\,\%$ tolerance band is added around the diagonal of the correlation diagram to visually indicate a correct activation. Furthermore, two key indicators are calculated to verify the results. First, the slope of the linear regression line is determined by the activated power of the BSP. Secondly, the Pearson's correlation index r is calculated to quantify the rate of linear correlation between the grid frequency and activated FCR.

6.3.1.1 No Gradient Restriction

First, the VSDFG in turbine mode is investigated without any restriction on the gradient of output power change. Figure 6.32 depicts the correlation diagrams as a result of FCR provision at the BEP (0.76 p.u.) and the MFP (0.62 p.u.), each with 25 MW (0.9 p.u.) and maximum bid at the operating point. Since full activation of FCR is not required in the observed 4 hour long frequency window, the activation is only one-fifth at maximum. The slope of the linear regression line indicates in all cases a correct FCR provision. Furthermore, a robust reciprocal correlation between the system frequency and the FCR delivery is determined. Visible is the intentional dead-band around 10 mHz of the nominal frequency.

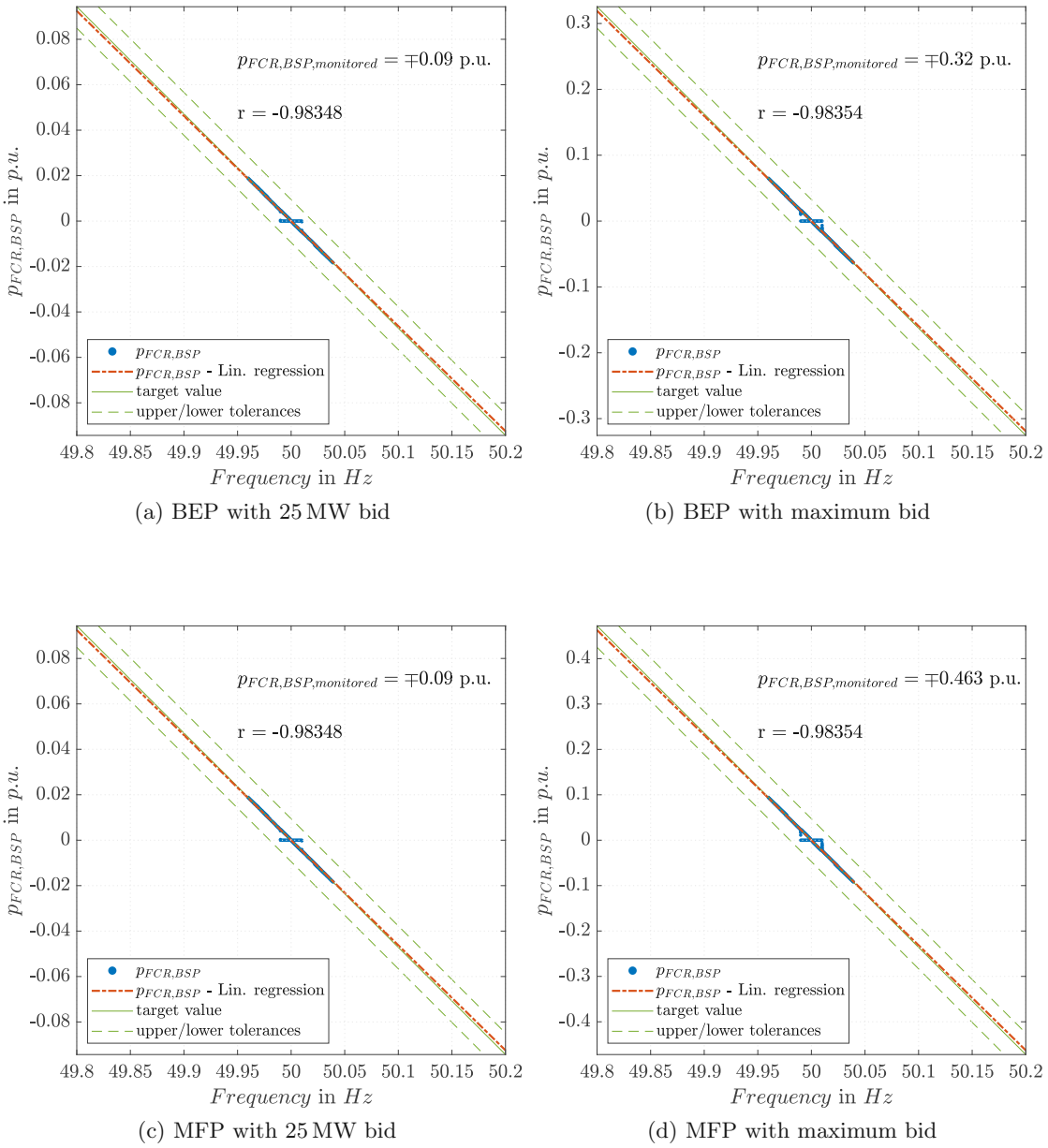

(a) BEP with 25 MW bid

(b) BEP with maximum bid

(c) MFP with 25 MW bid

(d) MFP with maximum bid

Figure 6.32: Correlation diagram of FCR provision of VSDFG in turbine mode

Secondly, the VSFSC in turbine mode is monitored with the correlation methodology. Figure 6.33 shows four cases of FCR provision. At the BEP (0.75 p.u.), the FCR delivery of 25 MW (0.9 p.u.) and the maximum FCR provision of the machine (0.33 p.u.) are investigated. At the MFP (0.60 p.u.), the maximum indivisible bid size limit and maximum FCR provision (0.49 p.u.) are considered. Again, in all cases, a strong correlation with $r \approx 0.98$ is detected and the dead-band around 50 Hz is monitored.

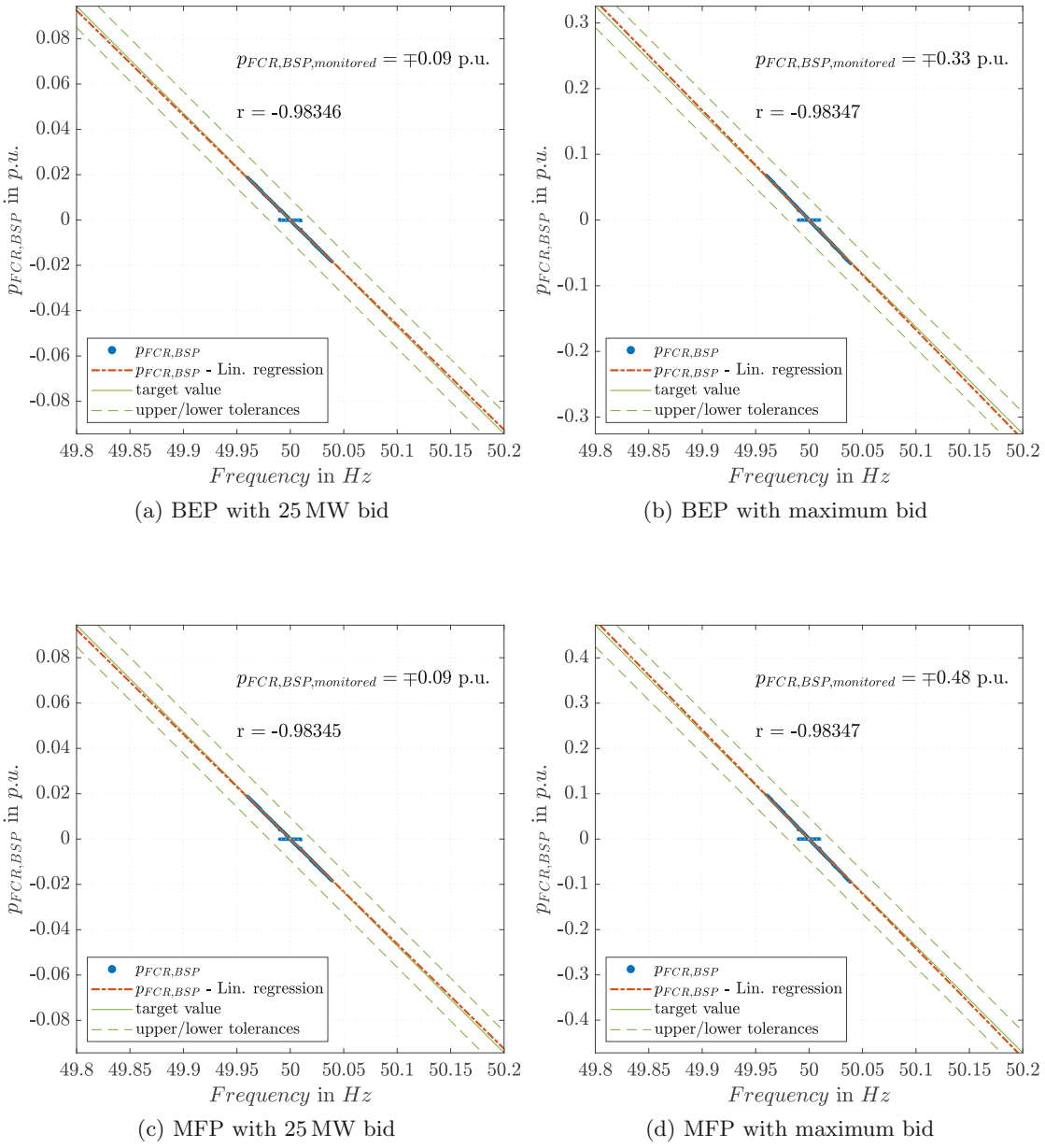

(a) BEP with 25 MW bid

(b) BEP with maximum bid

(c) MFP with 25 MW bid

(d) MFP with maximum bid

Figure 6.33: Correlation diagram of FCR provision of VSFSC in turbine mode

Finally, the pump mode of VSDFG and VSFSC is the subject of the correlation methodology. Figure 6.34 displays the results for FCR provision at the MFP (0.86 p.u.), which is the same for both schemes. The correlation and well as the FCR response of both machine types are correct, but due to numerical noise, the provision is spread out a little more than in turbine mode. This is especially visible at smaller FCR bid sizes.

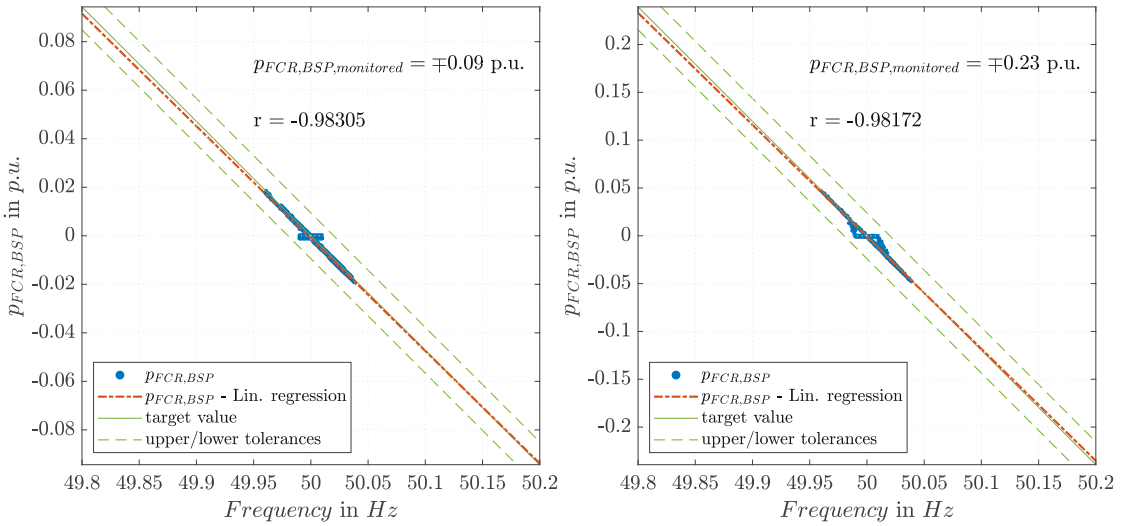

(a) VSDFG: MFP with 25 MW bid

(b) VSDFG: MFP with maximum bid

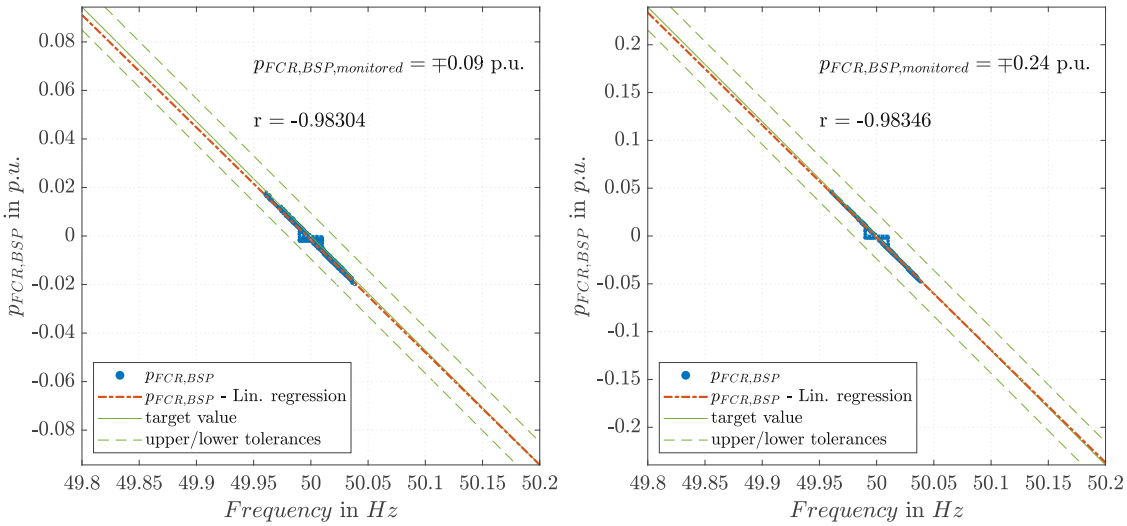

(c) VSFSC: MFP with 25 MW bid

(d) VSFSC: MFP with maximum bid

Figure 6.34: Correlation diagram of FCR provision of VSDFG and VSFSC in pump mode

6.3.1.2 Gradient Restriction

The VSDFG in turbine mode is investigated with a minimum gradient of 30 s to full activation. Figure 6.35 depicts the correlation diagrams as a result of FCR provision at the BEP (0.76 p.u.) and the MFP (0.62 p.u.), each with 25 MW (0.9 p.u.) and maximum bid at the operating point. Again, the slope of the linear regression line indicates in all cases a correct FCR provision. A strong reciprocal correlation between the system frequency and the FCR delivery is determined although the Pearson's correlation index is slightly lower. Compared to the previous case (no gradient restrictions), the intentional dead-band around 10 mHz of the nominal frequency is more distinctive. Still, according to the correlation methodology, in all cases, the FCR provision is assumed to be correct.

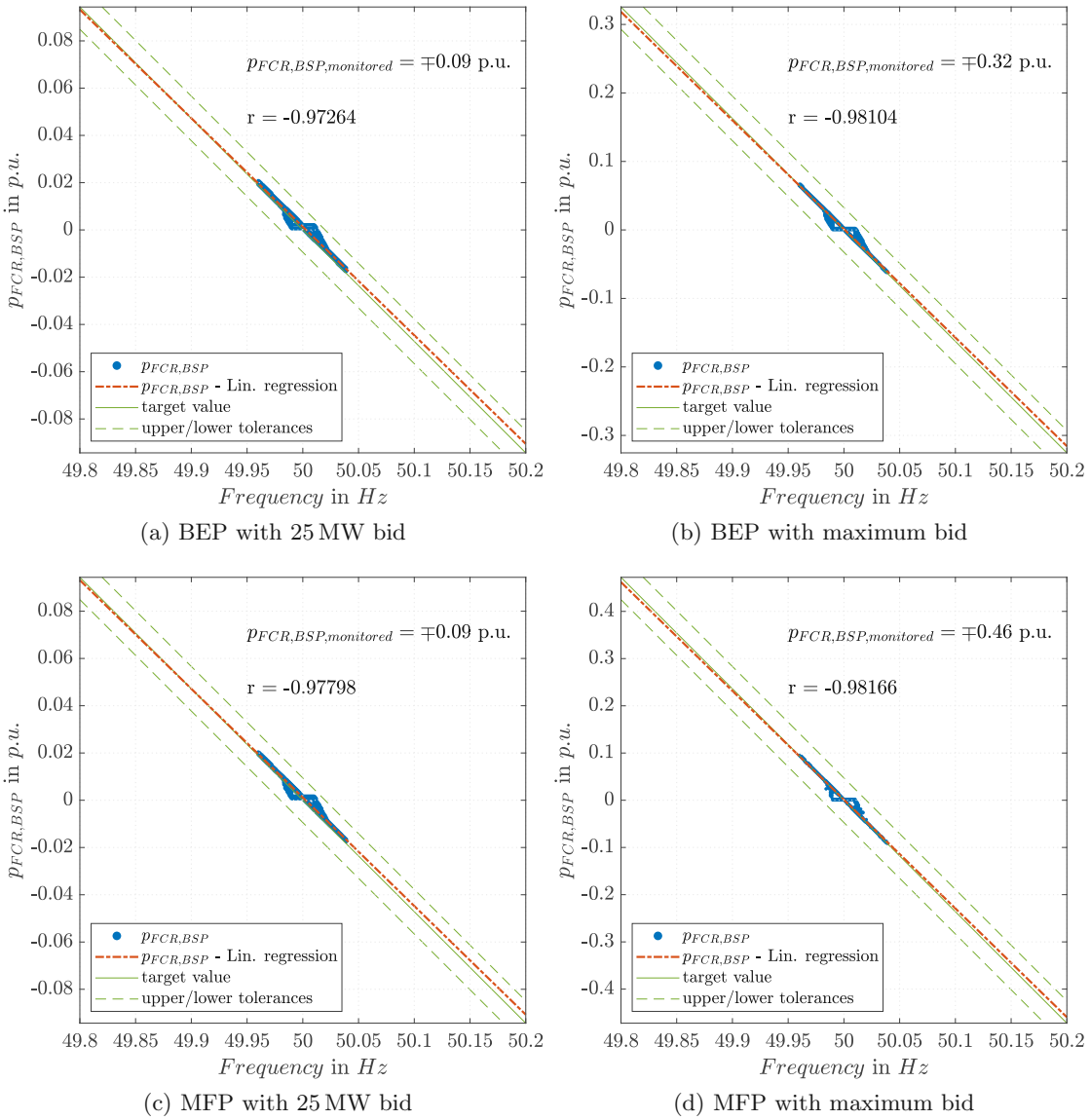

(a) BEP with 25 MW bid

(b) BEP with maximum bid

(c) MFP with 25 MW bid

(d) MFP with maximum bid

Figure 6.35: Correlation diagram of FCR provision of VSDFG in turbine mode

The VSFSC in turbine mode is shown in figure 6.36 for the four cases of FCR provision. At the BEP (0.75 p.u.), the FCR delivery of 25 MW (0.9 p.u.) and the maximum FCR provision of the machine (0.33 p.u.) are monitored with the correlation methodology. At the MFP (0.60 p.u.), the maximum indivisible bid size limit and maximum FCR provision (0.49 p.u.) are considered. Again, in all cases, a strong correlation with $r \approx 0.98$ is detected and the dead-band around 50 Hz is monitored.

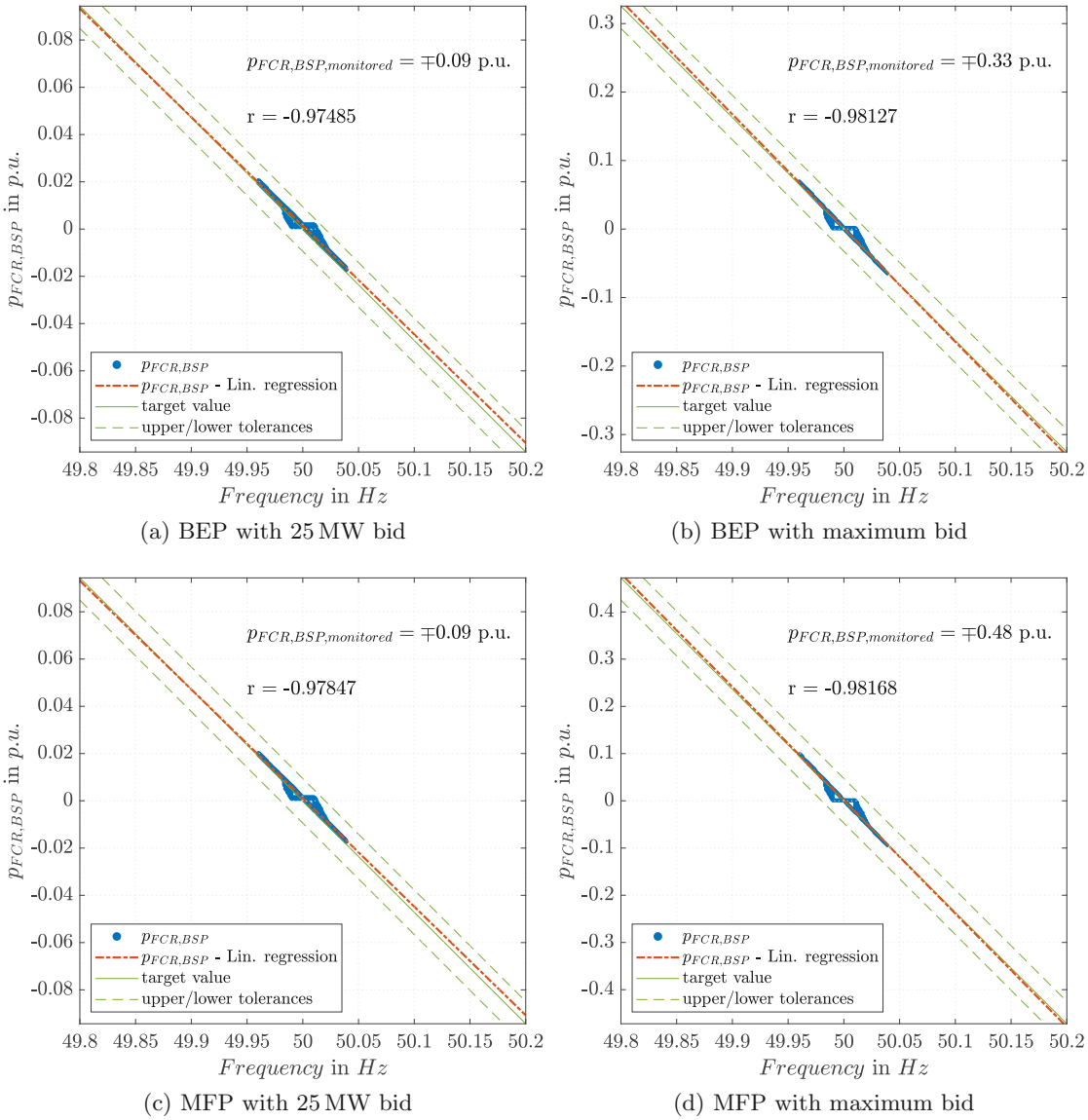

(a) BEP with 25 MW bid

(b) BEP with maximum bid

(c) MFP with 25 MW bid

(d) MFP with maximum bid

Figure 6.36: Correlation diagram of FCR provision of VSFSC in turbine mode

Finally, the pump mode results for FCR provision at the MFP (0.86 p.u.) of the VSDFG and the VSFSC are shown in figure 6.37. The correlation and well as the FCR response of both machine types are correct, but due to numerical noise, the provision is spread out close to the 10 % margin. This is especially problematic at smaller FCR bid sizes.

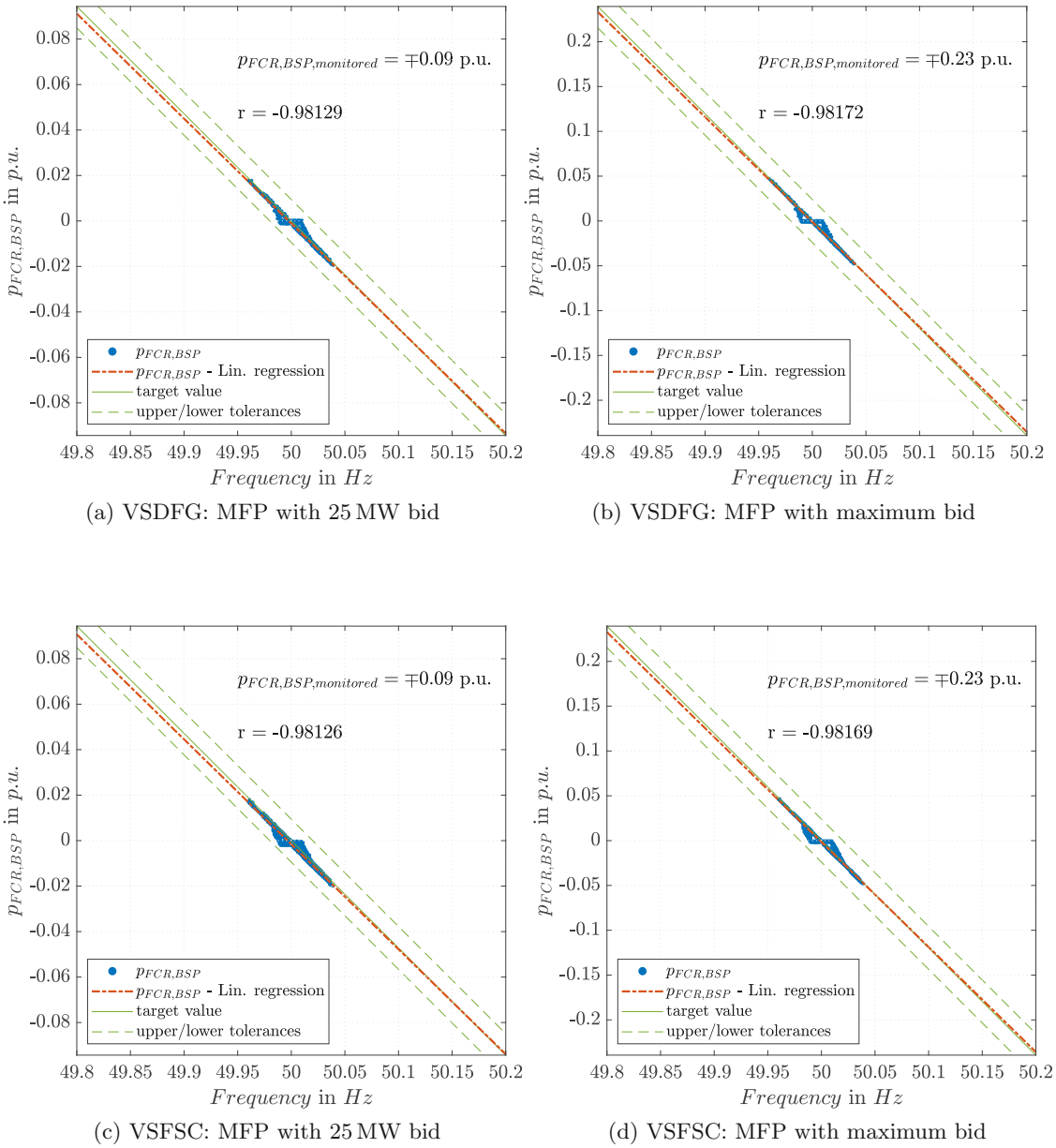

(a) VSDFG: MFP with 25 MW bid

(b) VSDFG: MFP with maximum bid

(c) VSFSC: MFP with 25 MW bid

(d) VSFSC: MFP with maximum bid

Figure 6.37: Correlation diagram of FCR provision of VSDFG and VSFSC in pump mode

6.3.2 Channel Methodology

The dynamic approach of the channel methodology delivers a tolerance channel for each time step. A correct delivery is assumed when the FCR provision stays within these boundaries. To determine a wrong provision, an error signal is generated. This error signal is zero, when the FCR provision is inside the tolerance channel and unequal zero, when the boundaries are left.

Calculations of the tolerance channel for the following deliberations are done with SOGL and SAFA limits for 30 seconds gradients and no restrictions on the BSPs power provision. Results are shown for FCR delivery at BEP with 25 MW and at MFP with the maximum bid for VSDFG in turbine mode. The outcome for pump operations is shown for the MFP with 25 MW and the maximum bid for the VSDFG. Results for the VSFSC are nearly identical and therefore omitted.

6.3.2.1 No Gradient Restriction

First, no gradient restrictions are used on the VSDFG in turbine mode. The tolerance channel is based on the frequency and the awarded FCR bid. Figure 6.38 shows the first 15 minutes of 4 hour long FCR provision of the VSDFG in turbine mode at the BEP with 25 MW bid and tolerance channel based on SOGL and SAFA limits. The reaction of the PSH is fast enough to follow the FCR target signal. Within the insensitivity area, the FCR provision is zero. Therefore, the FCR channel is wider in these cases. The corresponding error signal is zero for the 4 hour period for SOGL and SAFA tolerance channels.

Figure 6.39 depicts the FCR provision at the MFP with the maximum bid size that is possible at this operating point. Results to the previous case are similar, even as the channel and the target gradients are steeper.

The FCR provision during pump operations is the subject of figure 6.40. Since the bid size is the same as in figure 6.38, results are almost identical and the error signal is zero over the course of the observed 4 hour period.

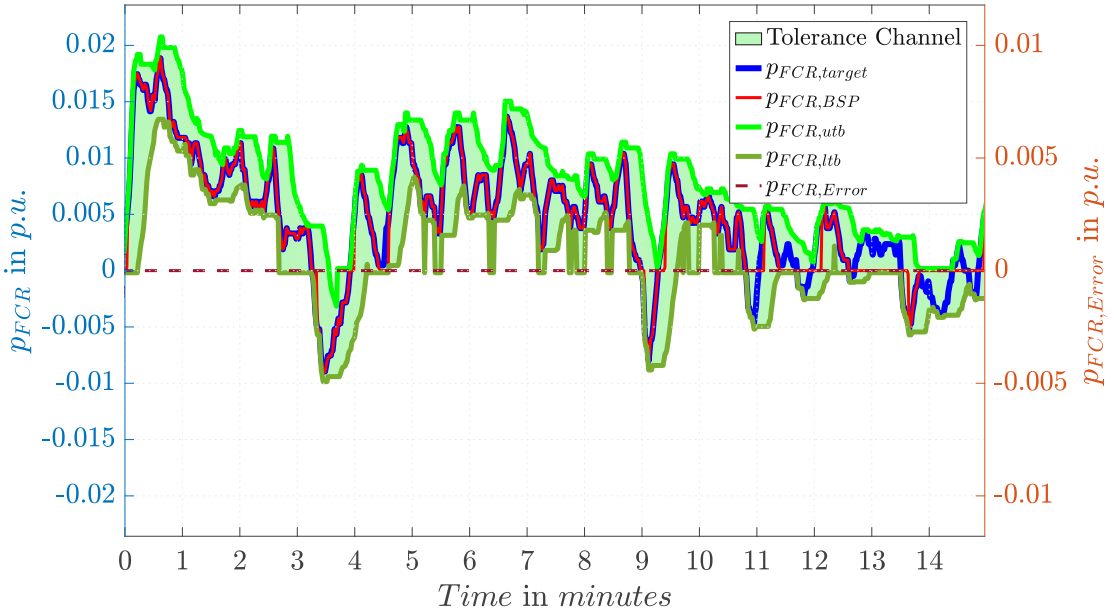

(a) SOGL limits

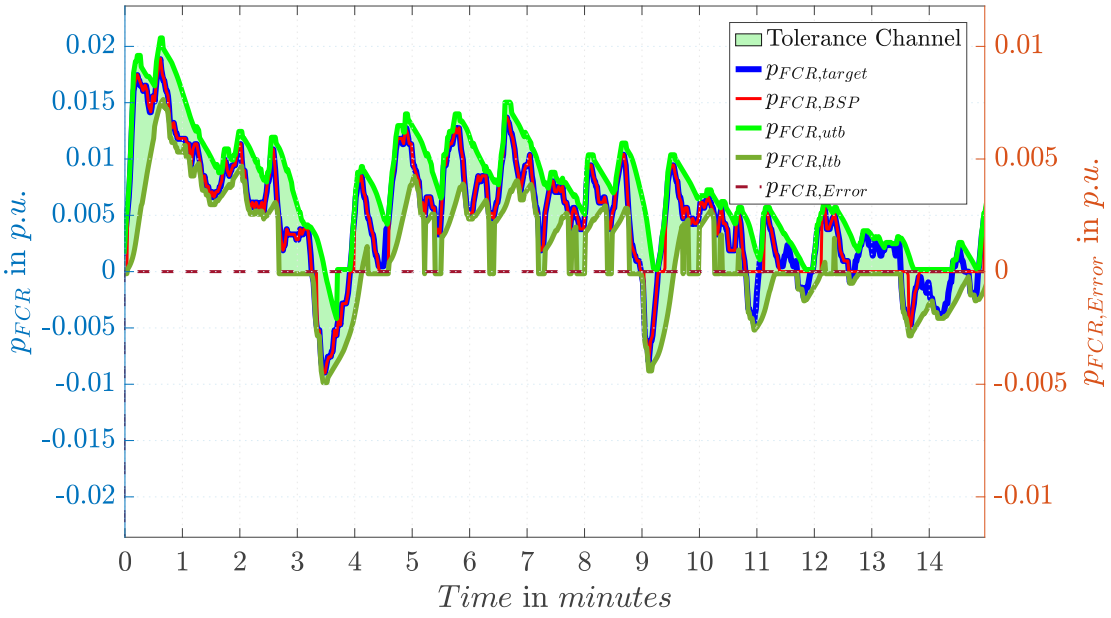

(b) SAFA limits

Figure 6.38: First 15 minutes of 4 hour FCR provision of VSDFG in turbine mode at BEP with 25 MW bid and tolerance channel based on SOGL and SAFA limits

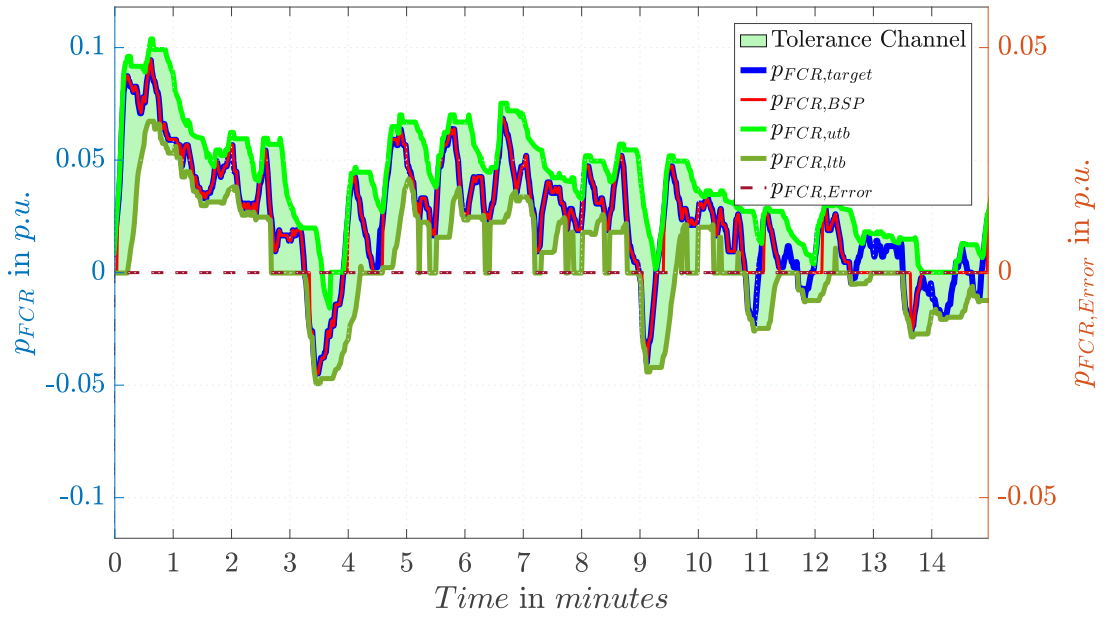

(a) SOGL limits

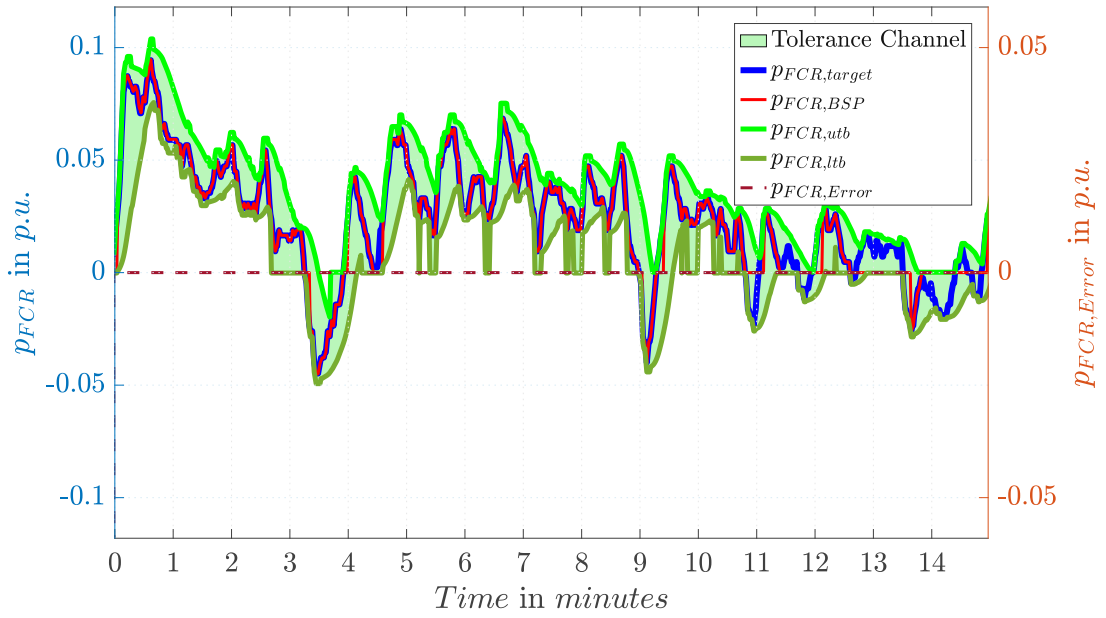

(b) SAFA limits

Figure 6.39: First 15 minutes of 4 hour FCR provision of VSDFG in turbine mode at MFP with maximum bid and tolerance channel based on SOGL and SAFA limits

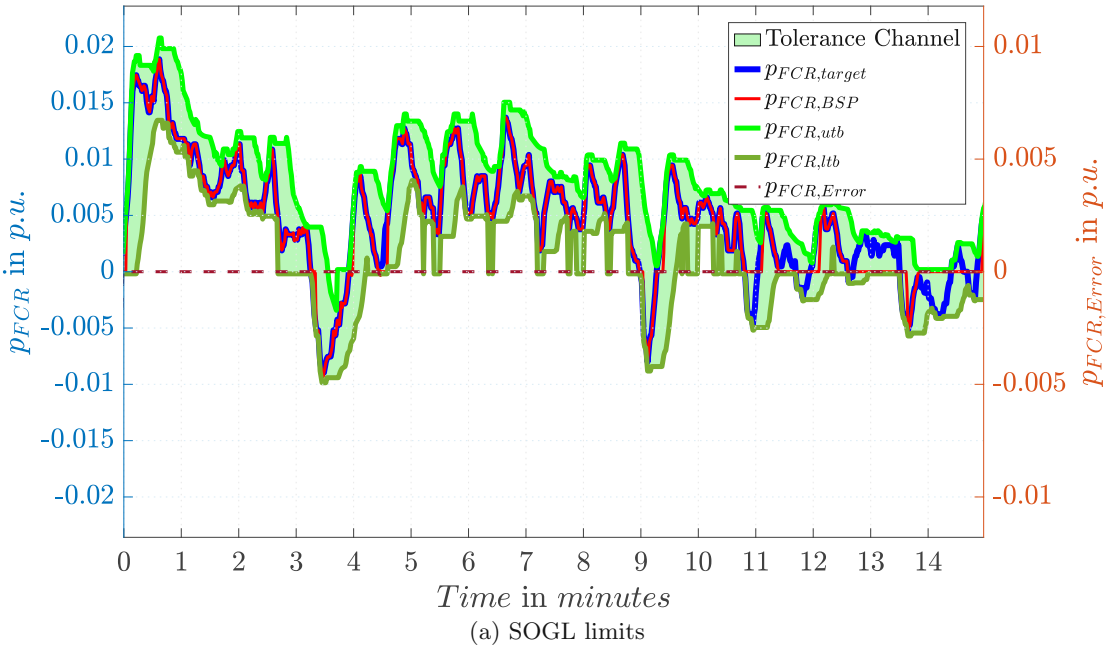

(a) SOGL limits

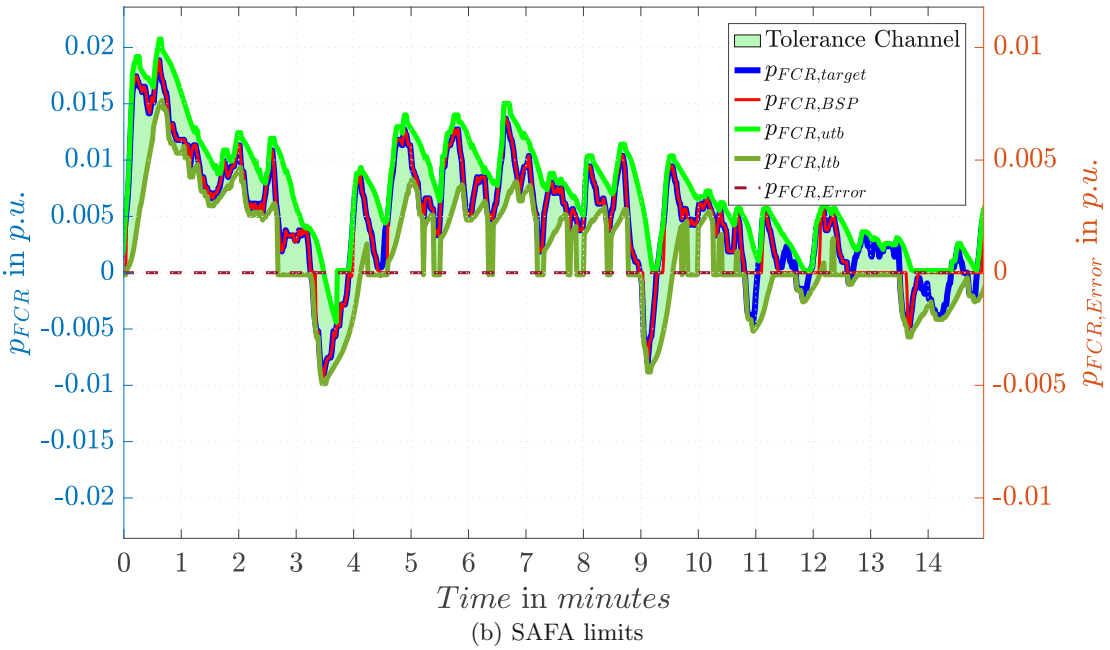

(b) SAFA limits

Figure 6.40: First 15 minutes of 4 hour FCR provision of VSDFG in pump mode at MFP with 25 MW bid and tolerance channel based on SOGL and SAFA limits

6.3.2.2 Gradient Restriction

As established in the previous section, the FCR provision ability of the variable speed drives is fast enough to follow the chosen frequency pattern. Hence, the machines do not have to be stressed to their physical limits to deliver FCR correctly. Therefore, a limiting gradient of 30 s for full FCR activation is tested with the channel methodology. Slower gradients would be possible since full activation does not happen as a step up/down-signal as shown in figure 4.7 and 4.8, but if too slow can become problematic in case of a full activation at frequency deviation greater than 200 mHz. Figure 6.41 depicts the first 15 minutes of 4 hour long FCR provision of VSDFG in turbine mode at BEP with 25 MW bid and tolerance channel based on SOGL and SAFA limits. Again, the error signal is zero over the observed period in both cases with indicated, that the FCR provision is always in the tolerance channel.

Figure 6.42 depicts the results of the first quarter hour at the MFP for the maximum FCR bid that is possible. Again, the most significant deviations from the FCR target happen because of the insensitivity band of 10 mHz, but do not lead to an error signal unequal zero.

Last, the FCR delivery in pump mode is shown is figure 6.43, leading to the same conclusions as the previous cases.

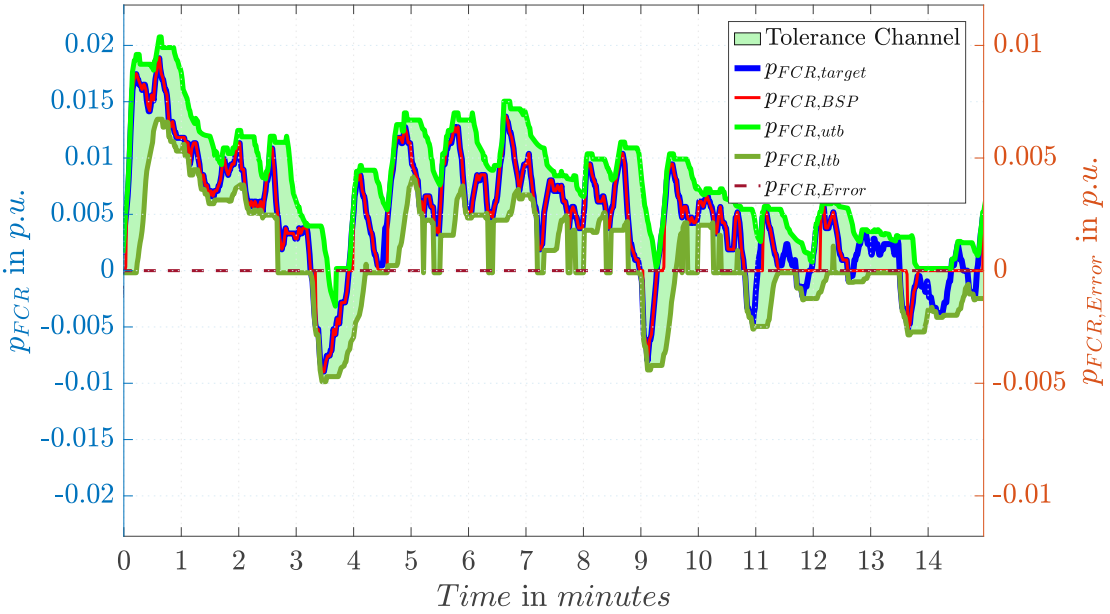

(a) SOGL limits

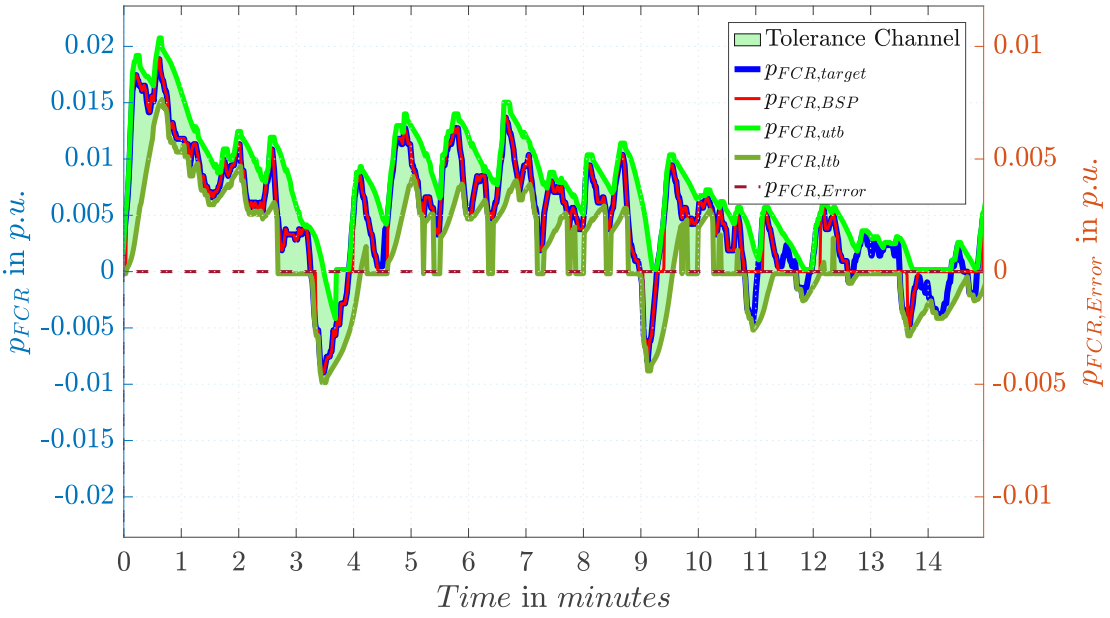

(b) SAFA limits

Figure 6.41: First 15 minutes of 4 hour FCR provision of VSDFG in turbine mode at BEP with 25 MW bid and tolerance channel based on SOGL and SAFA limits

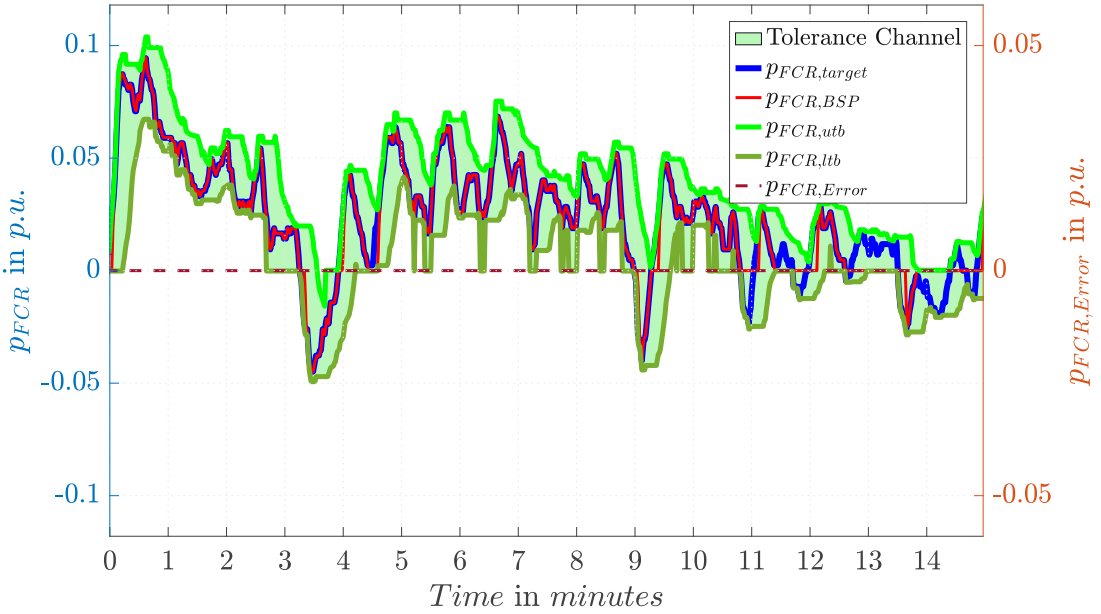

(a) SOGL limits

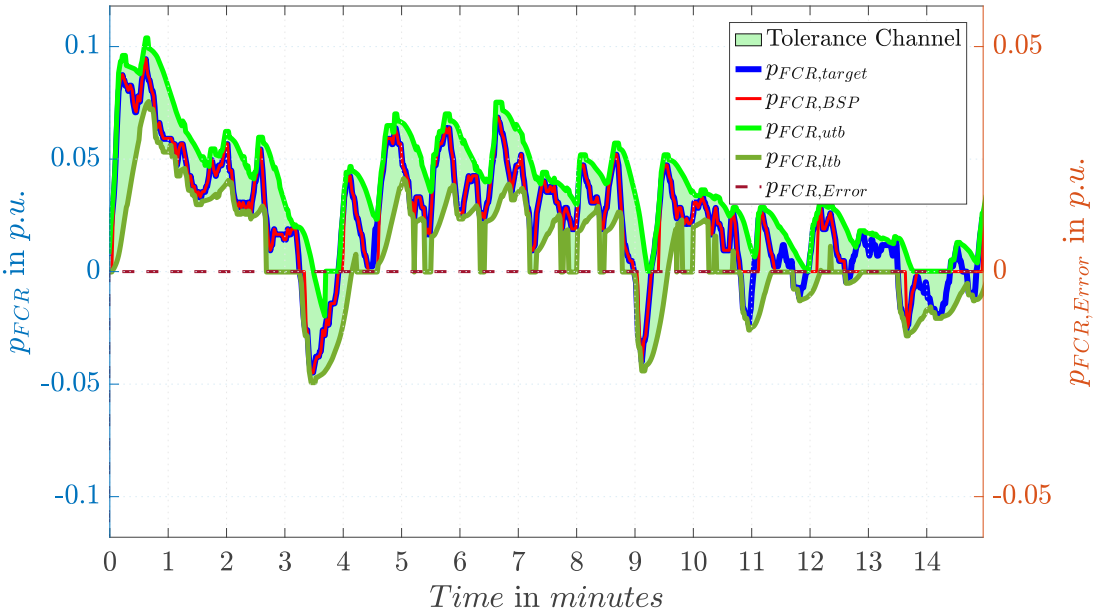

(b) SAFA limits

Figure 6.42: First 15 minutes of 4 hour FCR provision of VSDFG in turbine mode at MFP with maximum bid and tolerance channel based on SOGL and SAFA limits

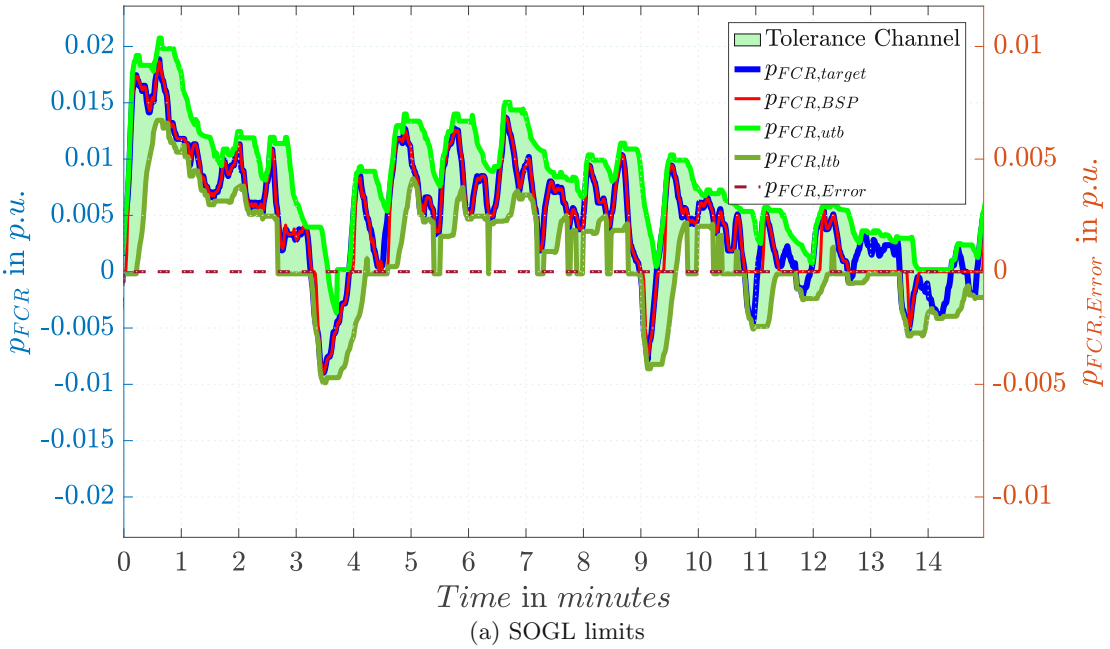

(a) SOGL limits

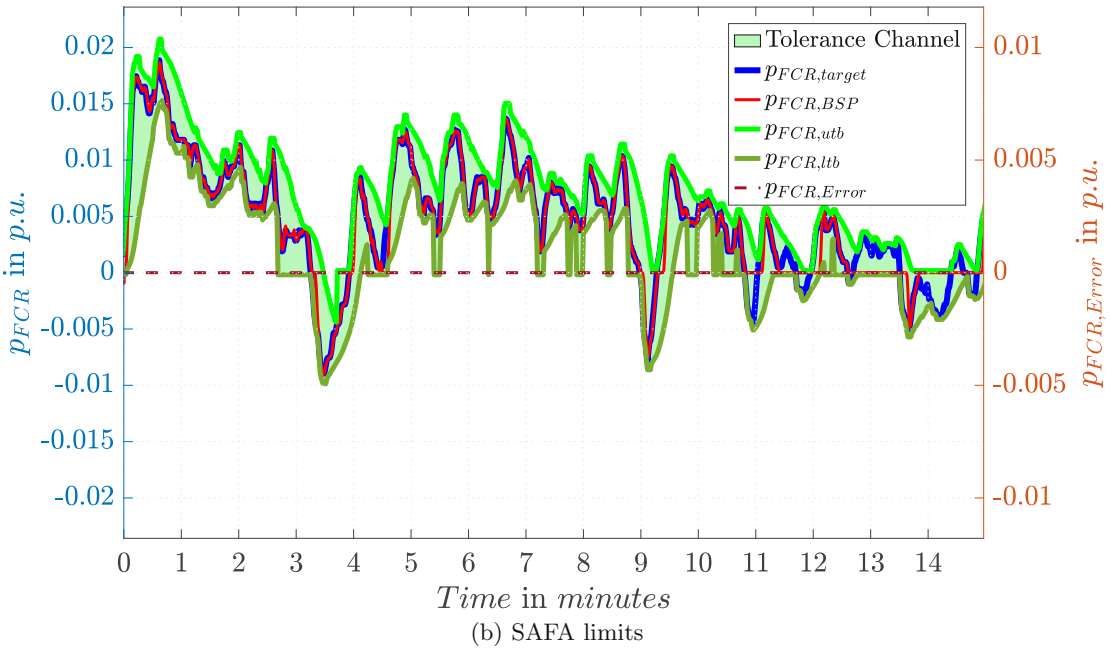

(b) SAFA limits

Figure 6.43: First 15 minutes of 4 hour FCR provision of VSDFG in pump mode at MFP with 25 MW bid and tolerance channel based on SOGL and SAFA limits

6.3.3 Dynamic Normalization Methodology

The dynamic normalization methodology extends the correlation methodology by approximating the requirements of SOGL for the creation of the tolerance channel. Furthermore, a graphic evaluation in the form of normalization is done. Again, results are shown for FCR delivery at BEP with 25 MW and at MFP with a maximum bid for VSDFG in turbine mode. The outcome for pump operations is shown for the MFP with 25 MW and a maximum bid for the VSDFG. Results for the VSFSC are nearly identical, and therefore, omitted.

6.3.3.1 No Gradient Restriction

Sub-figure 6.44a shows the first 15 minutes of an 4 hour long FCR provision of the VSDFG in turbine mode at BEP with 25 MW bid monitored with the dynamic normalization methodology. The tolerance channel is be considerably wider for smaller FCR provisions than the FCR bid size. The reason for this is the fact that the upper tolerance boundary utb and the lower tolerance boundary ltb consider a 5 % tolerance of the total FCR bid $P_{FCR,bid}$ on top of the mean value of the FCR channel MV_0 or the FCR target FCR_{set} [33]. In this case, a 5 % tolerance of 0.09 p.u. FCR bid accounts to 0.005 p.u., as can be seen in sub-figure 6.44a.

Sub-figure 6.44b depicts the normalized deviation of the FCR provision for the full 4 hour period. During this time span, the normalized deviation stays within the predetermined upper and lower boundary. Furthermore, better FCR activation quality is not necessarily indicated by data points closer to the green line, where d_{norm} is zero [33]. The value of d_{norm} is chosen in the dynamic normalization methodology to balance the normalized deviation in a way that all data points can be compared with the same normalized boundaries.

If the additional 5 % tolerance (on top of the FCR target) for the FCR channel is omitted ([33] mentioned, that this option could be considered optional), the tolerance channel is significantly tighter. Figure 6.45 depicts the results for this scenario. Since the dynamic of the FCR delivery of the VSDFG in turbine mode is high, some incidences occur, when $P_{FCR,BSP}(t)$ is overshooting the FCR target, and therefore slightly leaving the tolerance channel. The normalized deviation diagram also detects this fact well.

The following calculations will continue to omit the additional 5 % tolerance (on top of the FCR target) for the FCR channel, as the channels can be better compared to the channel methodology.

Next, the FCR provision of VSDFG in turbine mode at the MFP with the maximum bid is displayed in figure 6.46. Since the frequency signal is the same as in the previous case, the results for the tolerance channel are similar. The normalized deviation scatter

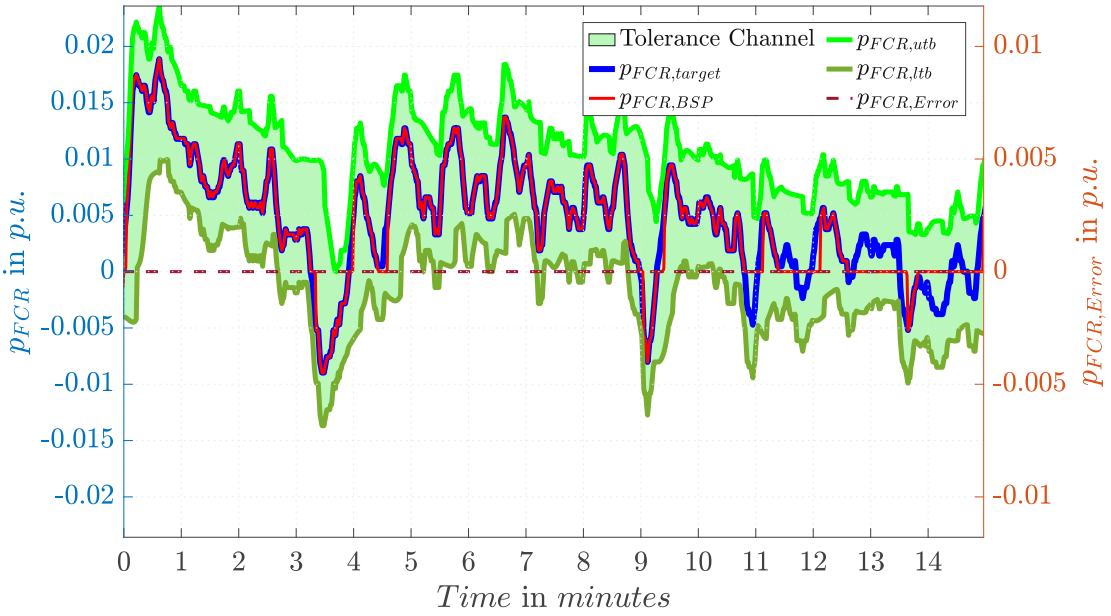

(a) Tolerance channel (15 min of 4 h total)

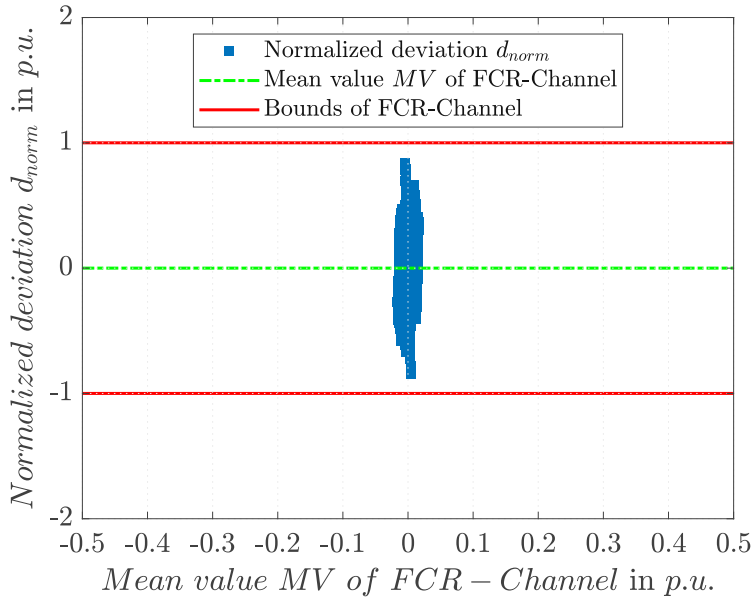

(b) Normalized deviation of the FCR provision

Figure 6.44: FCR provision of VSDFG in turbine mode at BEP with 25 MW bid monitored by dynamic normalization methodology (additional 5 % tolerance on top of the FCR target)

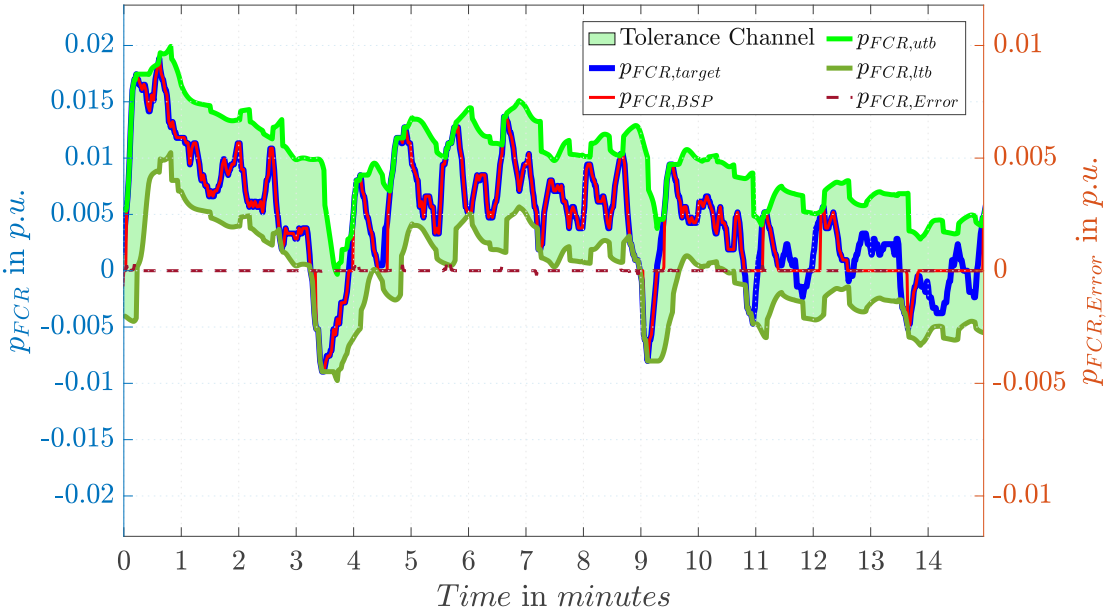

(a) Tolerance channel (15 min of 4 h total)

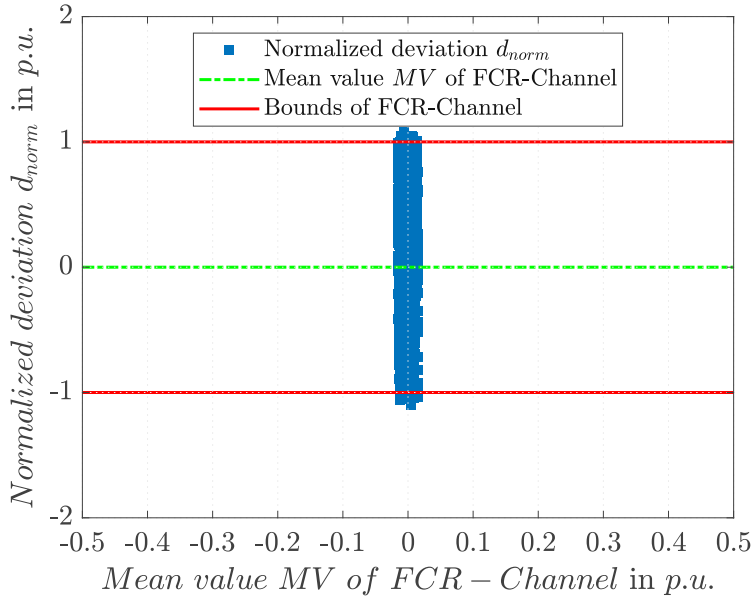

(b) Normalized deviation of the FCR provision

Figure 6.45: FCR provision of VSDFG in turbine mode at BEP with 25 MW bid monitored by dynamic normalization methodology

plots are slightly wider, which indicates a higher deviation for the mean value of the FCR channel at times.

Finally, the results for pump operations are shown in figure 6.47. The results strongly resembles the results of the turbine mode for the same awarded FCR bid size.

6.3.3.2 Gradient Restriction

The following figures 6.48 to 6.50 depict the results, when a 30 s gradient to full FCR activation is considered. The results again strongly resembles the previous ones from the section above.

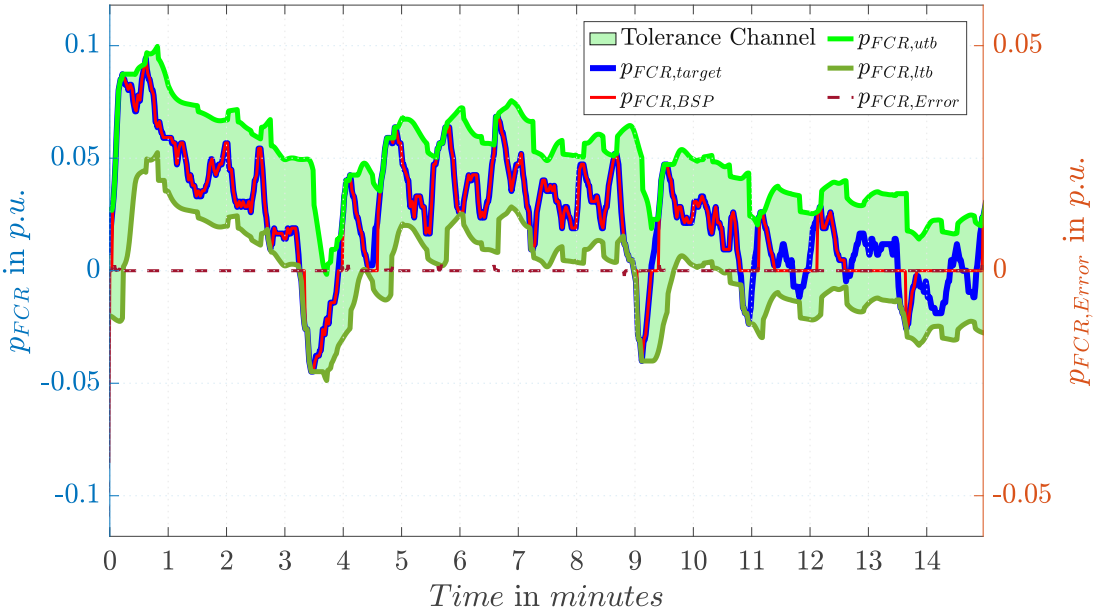

(a) Tolerance channel (15 min of 4 h total)

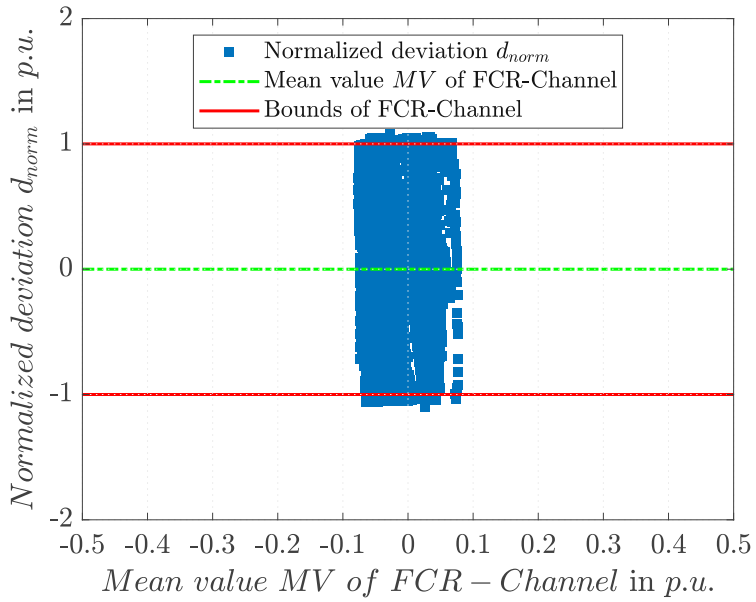

(b) Normalized deviation of the FCR provision

Figure 6.46: FCR provision of VSDFG in turbine mode at MFP with maximum bid, monitored by dynamic normalization methodology

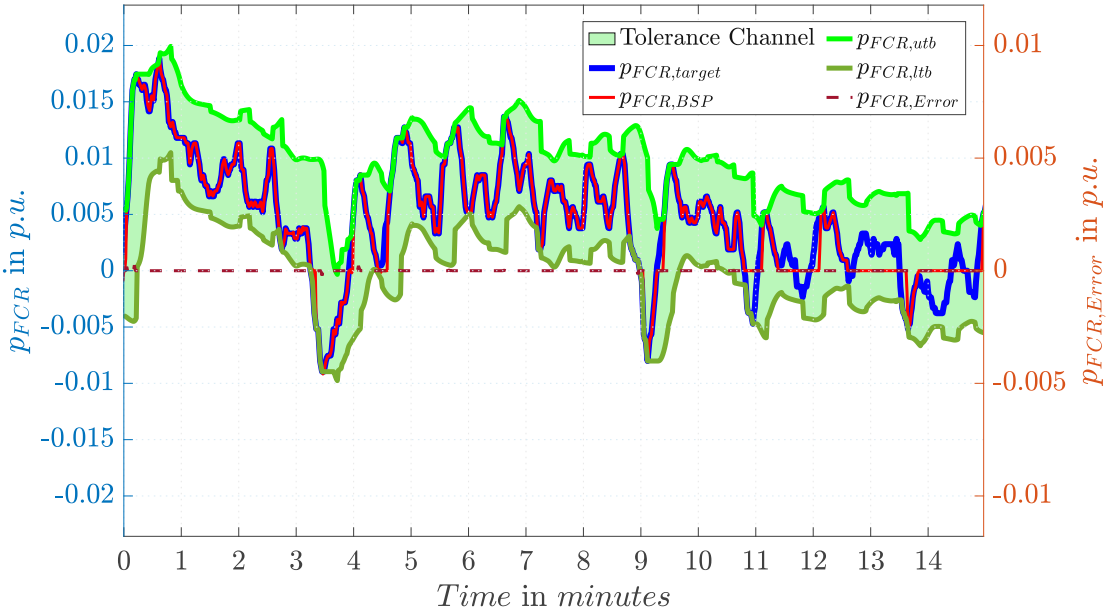

(a) Tolerance channel (15 min of 4 h total)

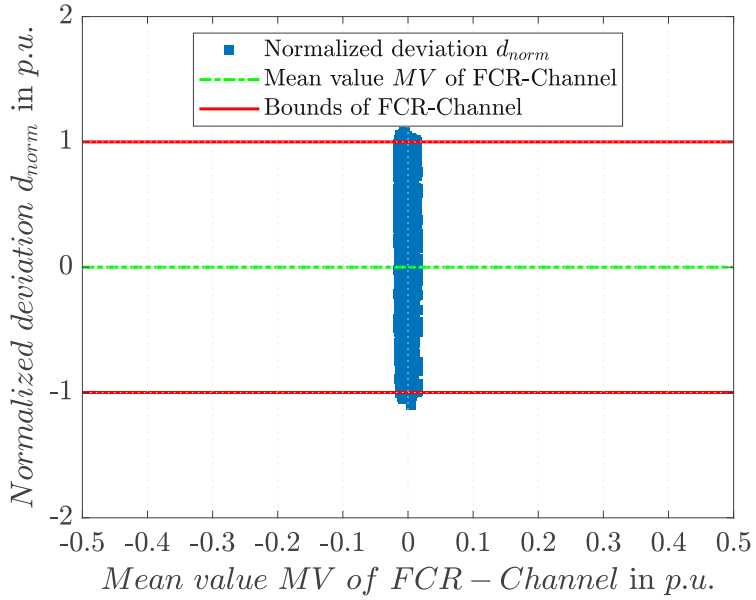

(b) Normalized deviation of the FCR provision

Figure 6.47: FCR provision of VSDFG in pump mode at MFP with 25 MW bid monitored with dynamic normalization methodology

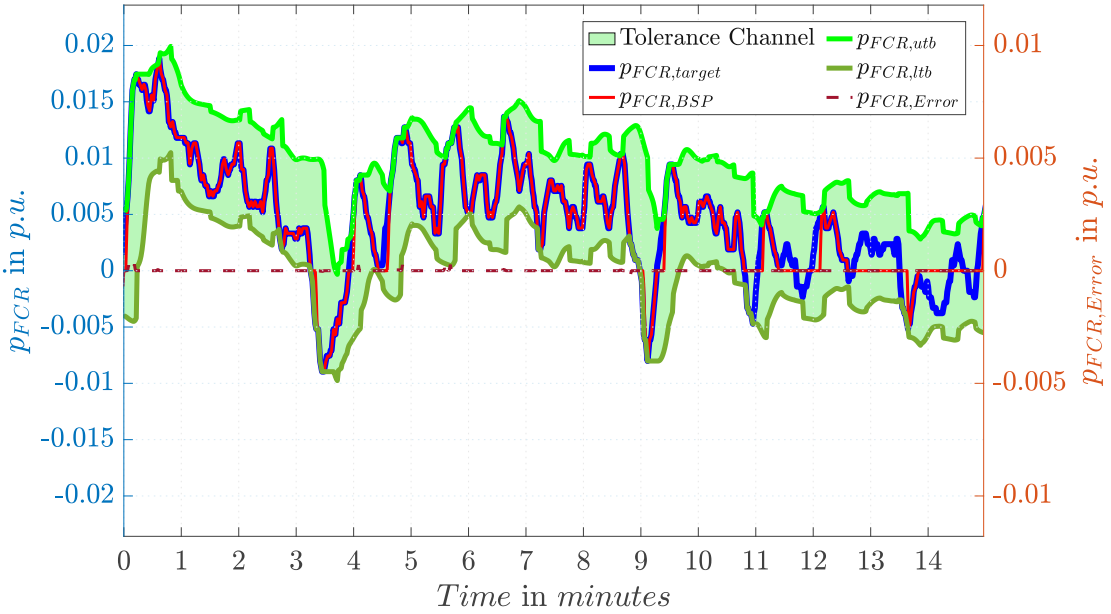

(a) Tolerance channel (15 min of 4 h total)

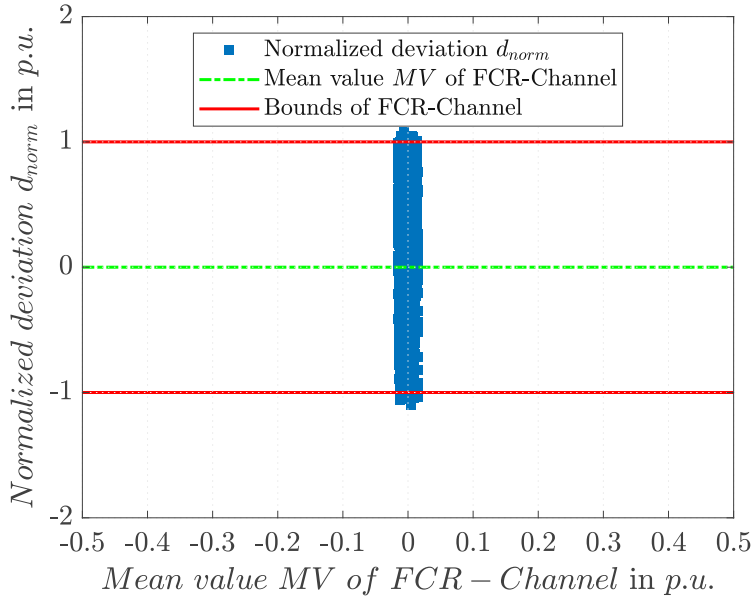

(b) Normalized deviation of the FCR provision

Figure 6.48: FCR provision of VSDFG in turbine mode at BEP with 25 MW bid, monitored with dynamic normalization methodology

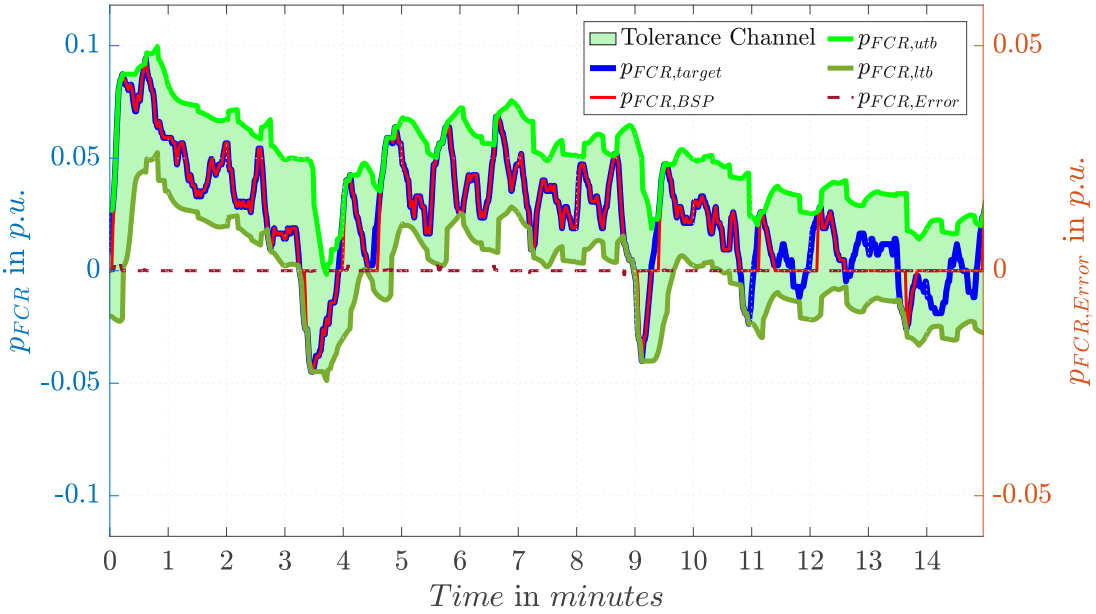

(a) Tolerance channel (15 min of 4 h total)

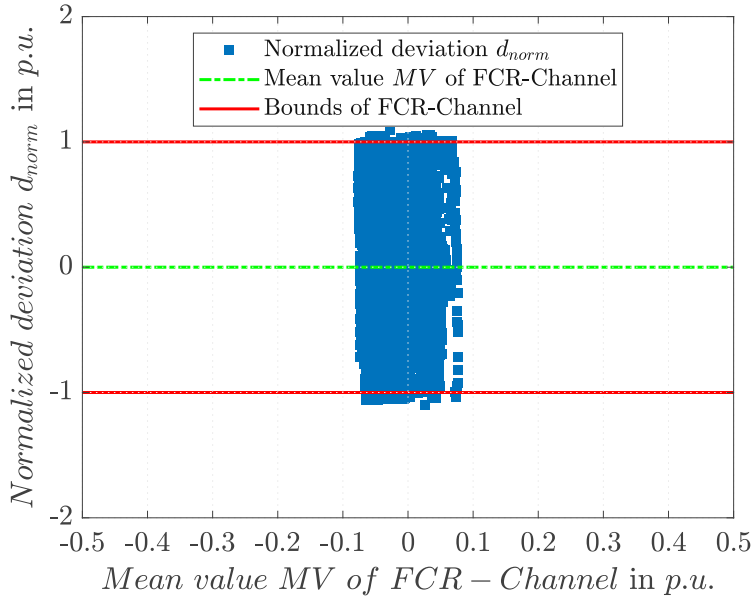

(b) Normalized deviation of the FCR provision

Figure 6.49: FCR provision of VSDFG in turbine mode at MFP with maximum bid, monitored with dynamic normalization methodology

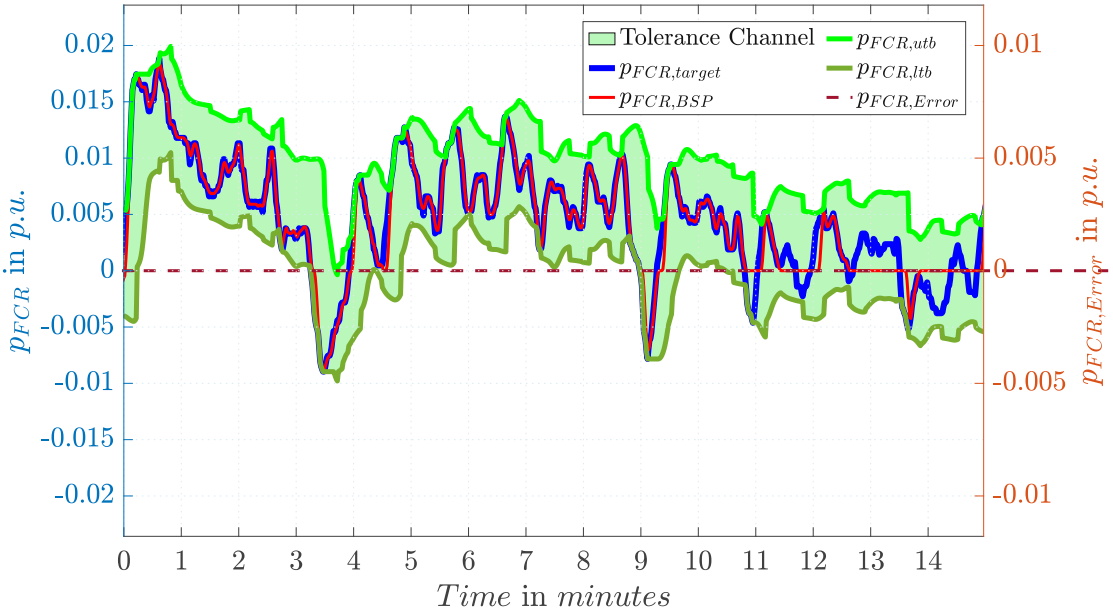

(a) Tolerance channel

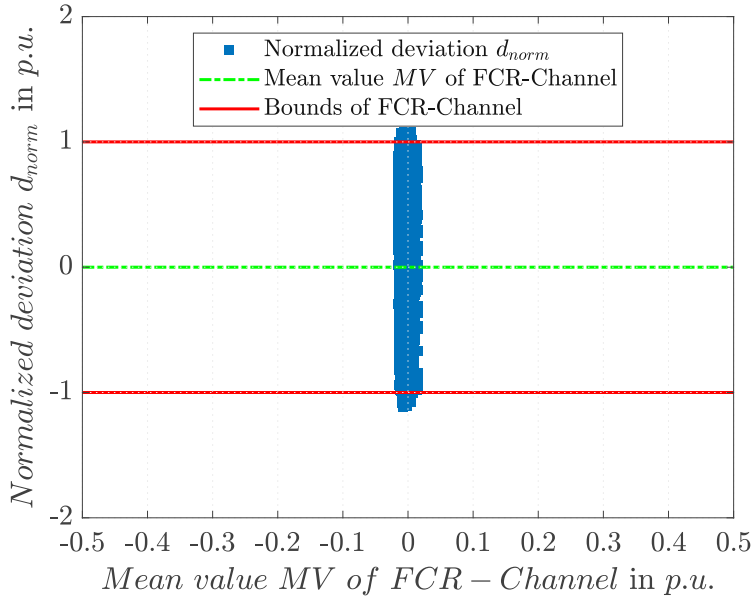

(b) Normalized deviation of the FCR provision

Figure 6.50: FCR provision of VSDFG in pump mode at MFP with 25 MW bid monitored with dynamic normalization methodology

6.3.4 Monitoring of FCR Provision of a large Frequency Event

The correlation, channel and dynamic normalization methodology are applied to a frequency event on 8th of January 2021, when the system frequency of ENTSO-CE rapidly dropped below 49.8 Hz. In this case, full FCR activation is triggered by participating FCR balancing service providers. This highly dynamic frequency signal is used to highlight the differences of the tested monitoring methodologies. The results are presented for the VSDFG in turbine mode at BEP and 25 MW awarded FCR bid, which a maximum gradient of 30 seconds. The findings for the VSFSC and the VSDFG in pump mode are nearly identical, and therefore, omitted. Sub-figure 6.51a shows the frequency development over 30 minutes, the FCR target and the FCR provision of the VSDFG in turbine mode. The FCR target is further limited to the FCR bid size, since the frequency deviation is large than 200m Hz.

First, the correlation methodology is utilized. Sub-figure 6.51b depicts the results, when the maximum frequency deviation is cut off at -200 mHz. Otherwise, the FCR target would be greater than the FCR bid size and the correlation diagram would not represent the FCR target correctly. The FCR provision from the VSDFG is outside of the 10 % limits during the outage, which would indicate a non-compliant FCR provision. Since the observed time span in this case is 30 minutes, which is long compared to the outage, the linear regression line can deliver correct results. The slope of the regression line also provides the correct amount of FCR.

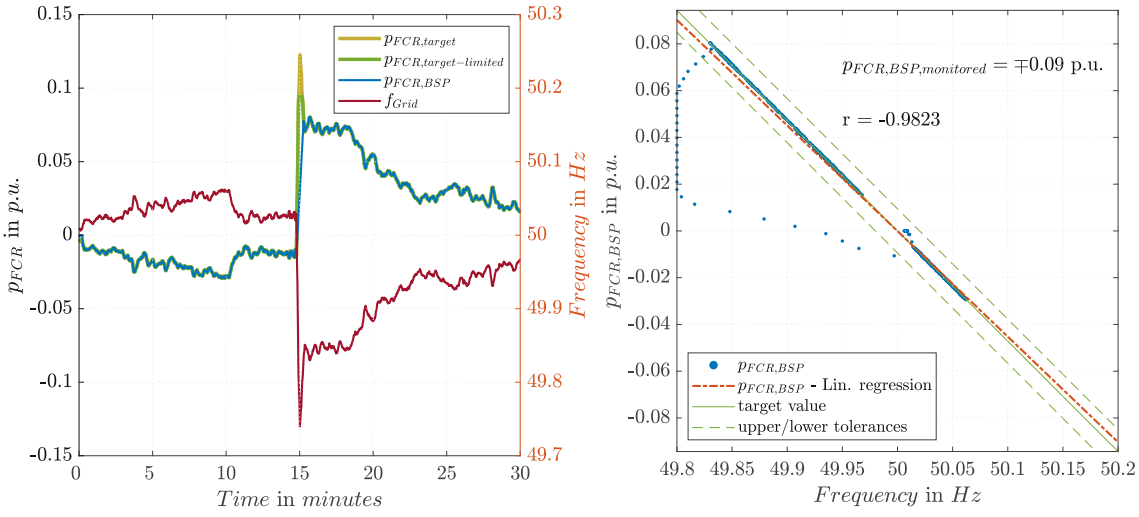

(a) Frequency signal, FCR target and FCR provision (b) Correlation diagram (BEP with 25 MW bid)

Figure 6.51: Frequency signal, FCR target, FCR provision and correlation diagram by the VSDFG in turbine mode

Next, the channel methodology is applied to the frequency signal (see figure 6.52). Again, the FCR target is limited to the maximum bid size. The gradient restrictions of

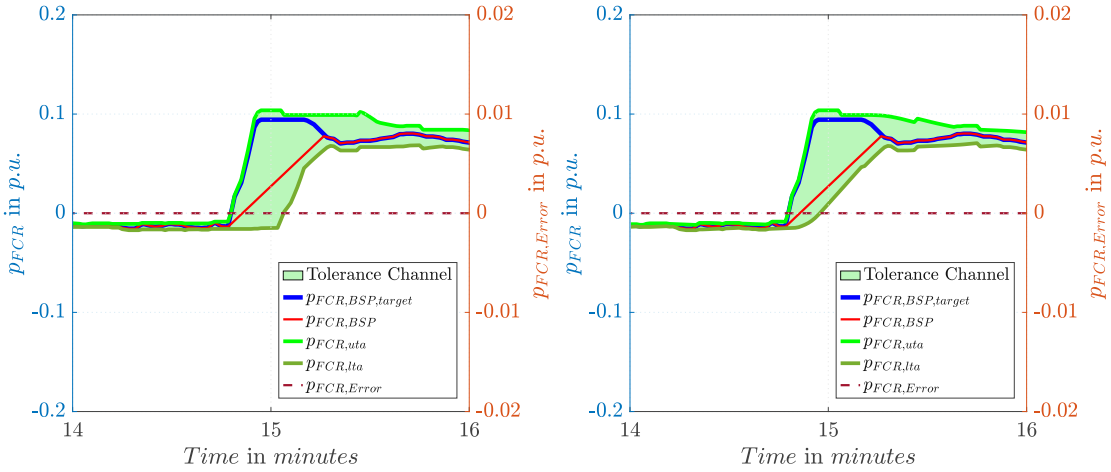

(a) SOGL limits (b) SAFA limits

Figure 6.52: FCR provision of VSDFG in turbine mode at BEP with 25 MW bid and tolerance channel based on SOGL and SAFA limits

the VSDFG can be observed, but are still within the tolerance channel. It can be noted, that the frequency prior to the outage is greater than 50 Hz, so the total change in FCR target is greater than the FCR bid size. The unlikely worst case would be a frequency step from 50.2 Hz to 49.8 Hz, which would trigger a FCR target step of two times the bid size. Then, a 30 seconds gradient restriction would lead to a slower response from BSP than required by the tolerance channel.

Finally, the dynamic normalization methodology is used to determine the tolerance channel (see figure 6.53). The channel distinctively differs during the outage from the one the channel methodology provides. Since the limits do not incorporate an additional tolerance depending on the current FCR target, overshoots from the BSP result in an non-zero error signal. However, these non-compliance is small which can be been the normalized deviation's diagram.

6.3.5 Example of Monitoring of incorrect FCR Provision

The correlation, channel and dynamic normalization methodology are tested if an artificial FCR provision of the VSDFG (in turbine mode) of only 80 % of its original FCR bid is detected correctly. Therefore, the droop of the FCR controller of the VSDFG is set to 80 % of the FCR bid. In this case, the awarded FCR bid is considered 25 MW and the maximum FCR provision of the PSH is only 20 MW at 200 mHz frequency deviation. Results for the VSFSC and the VSDFG in pump mode are nearly identical, and therefore, omitted.

First, the correlation methodology is applied to the power output of the VSDFG. Figure 6.54 shows the result for this monitoring method. The actual droop is detected

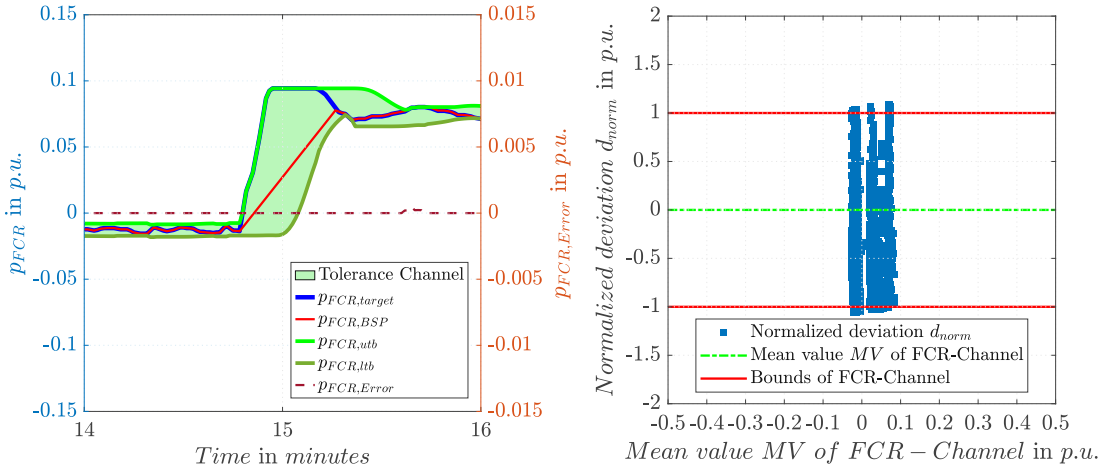

(a) Tolerance channel (2 min of 4 h total)

(b) Normalized deviation of the FCR provision

Figure 6.53: FCR provision of VSDFG in turbine mode at BEP with 25 MW bid, monitored with dynamic normalization methodology

to be 78 % of the FCR bid and therefore, the method delivers a correct indication, that the droop is too low. However, since the frequency deviations from 50 Hz in the frequency test signal are not particularly large, the correlation diagram depicts the FCR provision of the BSP within the ±10 % bandwidth.

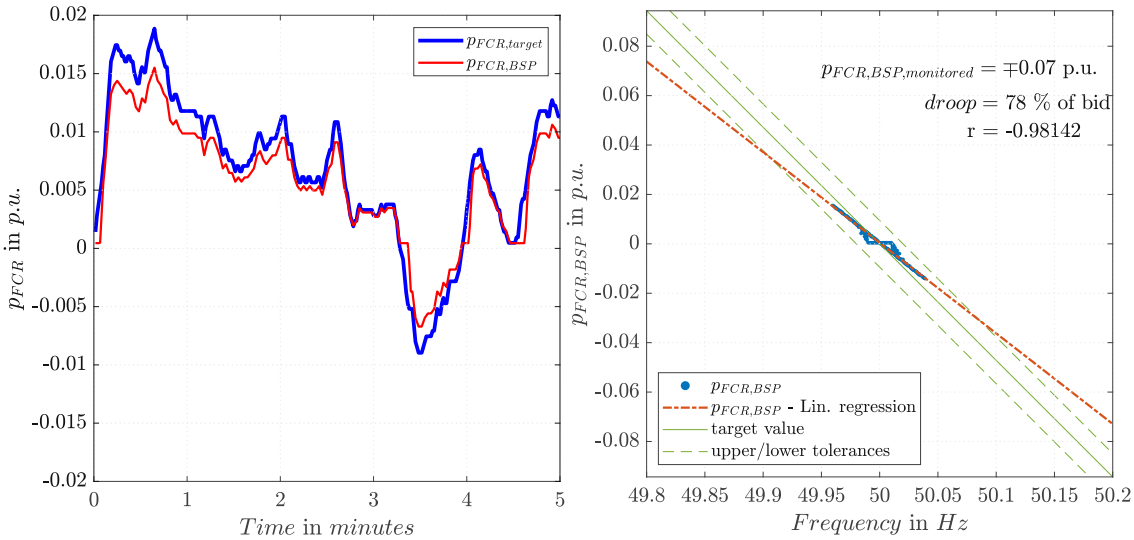

(a) FCR target and FCR provision

(b) Correlation diagram (BEP with 25 MW bid and a droop of only 80 %)

Figure 6.54: FCR target, FCR provision and correlation diagram for the VSDFG in turbine mode at BEP with 25 MW bid and a droop of only 80 %

Next, the channel methodology is applied to highlight, that the FCR provision of the PSH also leave the dynamic limits of the tolerance channel. Figure 6.55 shows the results for a SOGL and SAFA based tolerance channel. The underdelivery of FCR is detected

correctly in both cases as the error signal is different from zero for many incidents during the 4 hour period.

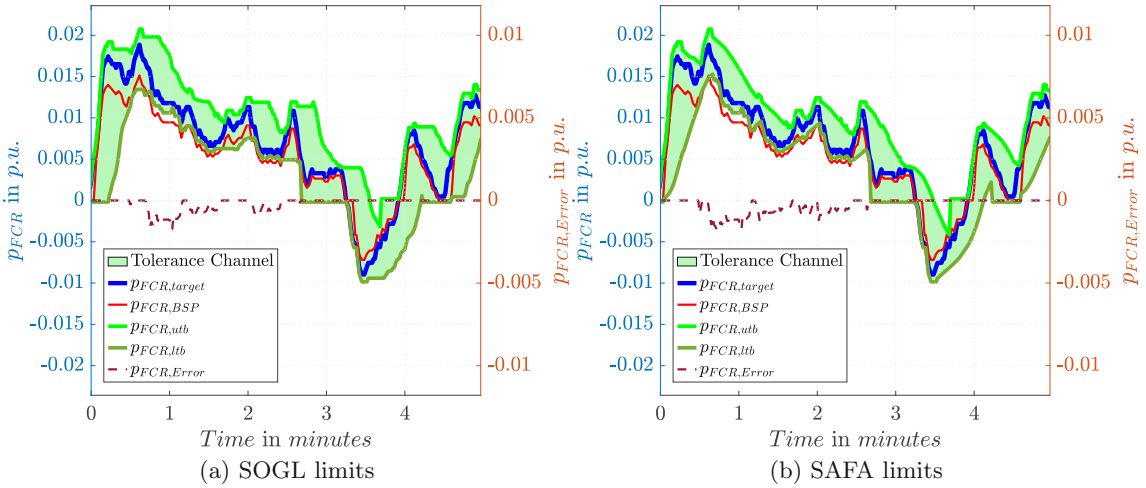

(a) SOGL limits (b) SAFA limits

Figure 6.55: First 15 minutes of 4 hour FCR provision of VSDFG in turbine mode at BEP with 25 MW bid and a droop of only 80 %. The tolerance channels based on SOGL and SAFA limits

Finally, the dynamic normalization methodology is applied to the FCR provision signal. The results are shown in figure 6.56 The error signal in the time series plot is non-zero for many incidents. However, the channel is tolerance considerable wider for many incidences, thus the error signal smaller compared to the channel methodology. Also, the normalized deviation is outside of the bounds of the FCR channel and visibly tilted to the left, which is also an indication of underdelivery.

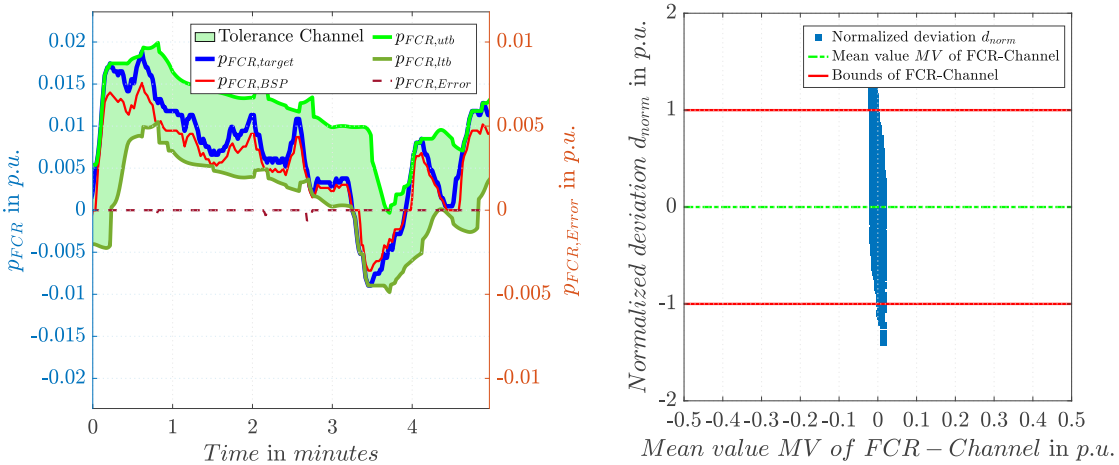

(a) Tolerance channel (15 min of 4 h total) (b) Normalized deviation of the FCR provision

Figure 6.56: FCR provision of VSDFG in turbine mode at BEP with 25 MW bid and a droop of only 80 %, monitored by dynamic normalization methodology

7 FCR Economics

This chapter gives a basic analysis of the economics of FCR in combination with pumped hydro power plants.

For the profitability of pumped storage plants, participation in the control and balancing energy market is important as a complement to just peak/off-peak management. Participation in the balancing energy market is usually limited to aFRR, mFRR and RR provision for PSH. An important question is whether the additional provision of FCR, when technically feasible, makes economic sense.

7.1 Energy and FCR Prices

The average price in EURO per hour for 1 MW of FCR provision was around 7 € in 2020 and 12 € (January - July 2021) in 2021 so far [63, 64]. European wholesale prices for electricity are roughly around $40 - 50$ € on average in the last years [65, 66].

Figure 7.1 shows FCR and electricity price development in the EU over the last years. The FCR tendering periods changed over the years from weekly to daily (from 1st July 2019) and finally to 4 hour periods (from 1st July 2020). Hence, the price resolutions and volatility increased in recent years. The wholesale prices for EU countries (EU27) originate from main markets from spot hub [66].

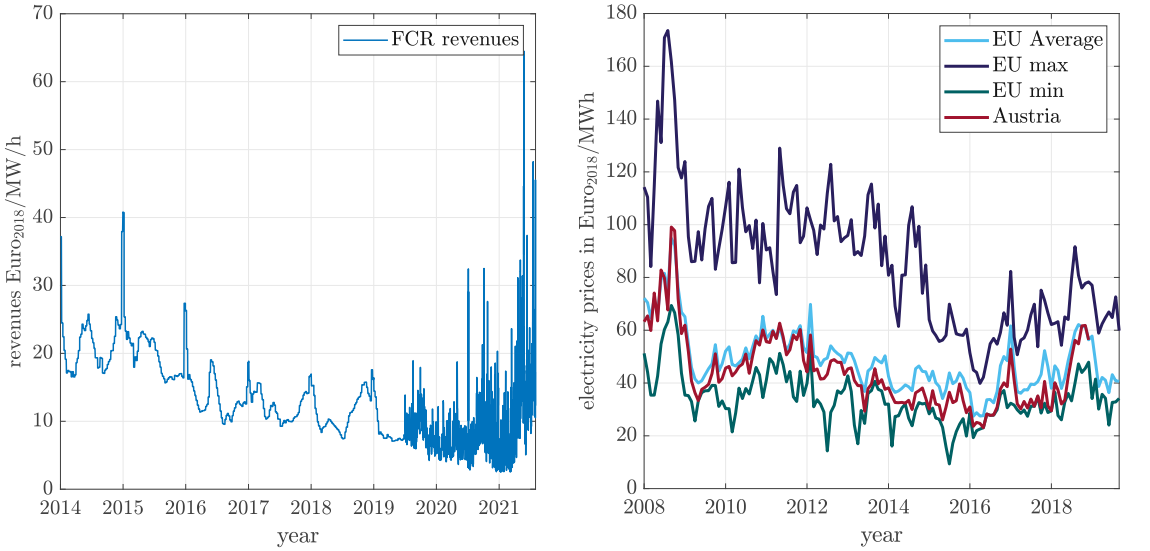

(a) FCR revenues in Euro/MW per hour from 2014-2021 in Austria (data source: [63, 64])

(b) Electricity wholesale prices in EU and Austria (data source: [65])

Figure 7.1: Electricity wholesale and FCR prices

7.2 FCR Provision during normal Operations

An important question is whether it is worthwhile switching to a different operating point, where the PSH may then have poorer electrical efficiency in order to offer more FCR. The following calculations show that this may not always be economically reasonable. The important factors are the change in efficiency due to the shift to a new operating point and the ratio between the attainable FCR price and the electricity wholesale price. Furthermore, the maximum indivisible FCR bid size needs to be considered if a PSH is able to provide more. In the following deliberations, it is also assumed that the PSP is able to provide FCR over a full FCR tendering period (currently 4 hour products). Moreover, mathematical normalization is used to avoid dependencies on power ratings of the PSH, FCR provision, and electricity prices. Table 7.1 lists the nomenclature for the following equations.

The electric power output in turbine mode for a given operating point is represented by P and the electrical efficiency by $\eta_{el}(P)$. The energy necessary to produce the given electrical power output over the time period Δt is

$$E(P) = \frac{P}{\eta_{el}(P)} \cdot \Delta t\,. \tag{7.25}$$

The monetary revenue for the given time period at a specific operating point is calculated by

$$K_{wholesale}(P) = P \cdot \Delta t \cdot \pi_{wholesale}\,. \tag{7.26}$$

Parameter name	Description
P_{rated}	rated power of the PSH
η_{el}	electrical efficiency
P	electric power output of the PSH
P_{FCR}	maximum FCR provision
$\pi_{wholesale}$	wholesale electricity price
π_{FCR}	price for FCR provision
E	released energy from reservoir
K_{FCR}	FCR revenues
$K_{wholesale}$	wholesale revenues
K	total revenue

Table 7.1: Description of nomenclature

After establishing the monetary revenue from normal operations, the revenue from FCR provision is investigated. For a PSP whose maximum FCR provision is smaller than the indivisible FCR bid size, the maximum FCR delivery is

$$P_{FCR}(P) = \begin{cases} 0 & P \leq P_{PSP,min} \\ P - P_{PSP,min} & P > P_{PSP,min} \, and \, P \leq \frac{P_{PSP,max} - P_{PSP,min}}{2} \\ P_{PSP,max} - P & P > \frac{P_{PSP,max} - P_{PSP,min}}{2} \end{cases} . \tag{7.27}$$

Furthermore, if the maximum FCR provision possible of the PSP is greater than the indivisible FCR bid size, the maximum FCR delivery P_{FCR} will be limited to a maximum of 25 MW. Figure 7.2 shows the influence of the maximum FCR bid size on possible FCR provisions for different ratios of $P_{FCR,max}/P_{rated}$. If the indivisible FCR bid size is close to 50 % of the rated power output of a PSH, the bid size limitations have no effect on its FCR provision bid. For PSP with higher rated power, the indivisible FCR bid size needs to be considered for further economic deliberations.

The revenue from FCR provision is

$$K_{FCR}(P) = P_{FCR}(P) \cdot \Delta t \cdot \pi_{FCR} \tag{7.28}$$

The total revenue K consists of the revenues from normal operation and FCR provision

$$K(P) = K_{wholesale}(P) + K_{FCR}(P) \, , \tag{7.29}$$

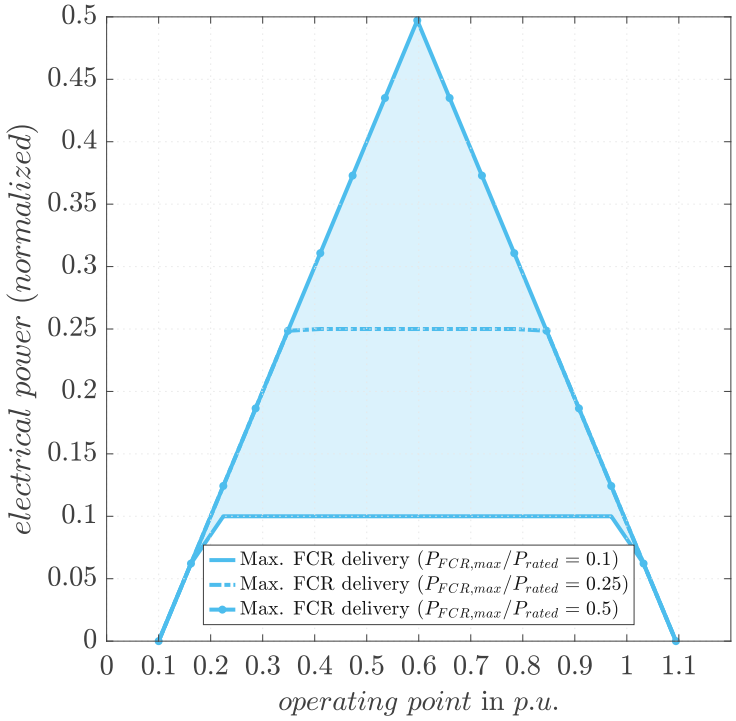

Figure 7.2: Influence of a indivisible FCR bid size on $P_{FCR}(P)$ for a PSH with different rated power output.

and results in

$$K(P) = P \cdot \Delta t \cdot \pi_{wholesale} + P_{FCR}(P) \cdot \Delta t \cdot \pi_{FCR}\,. \tag{7.30}$$

An additional condition for the FCR provision is necessary to advance the calculation by assuming

$$\int_{t=0}^{T} P_{FCR}(P) \cdot \Delta\tau \approx 0 \implies E_{FCR} \approx 0\,. \tag{7.31}$$

This means, that the amount of additional energy during the FCR provision period T is more or less zero. Therefore, the total energy E_{total} can be approximated by

$$E_{total} = E + E_{FCR} \approx E. \tag{7.32}$$

This approximation can be utilized to substitute Δt from equation 7.30 by rearranging equation 7.25

$$\Delta t = \frac{E(P)}{P} \cdot \eta_{el}(P)\,, \tag{7.33}$$

and consequently inserted it into the equation 7.30

$$K(P) = P \cdot \frac{E(P)}{P} \cdot \eta_{el}(P) \cdot \pi_{wholesale} + P_{FCR}(P) \cdot \frac{E(P)}{P} \cdot \eta_{el}(P) \cdot \pi_{FCR}\,. \tag{7.34}$$

Finally, revenue K for turbine operations can be normalized to k by dividing it by E and $p_{wholesale}$ as well as using the normalized values of $p = P/P_{rated}$

$$k(p) = \eta_{el}(p) \cdot \left[1 + \frac{P_{FCR(p)}/P_{rated}}{P/P_{rated}} \cdot \frac{\pi_{FCR}}{\pi_{wholesale}}\right]. \tag{7.35}$$

The ratio $\pi_{FCR}/\pi_{wholesale}$ in equation 7.35 is varied subsequently to show results for different price scenarios, independent of the actual costs of electricity and FCR provision in the following figures. First, figure 7.3 shows the results for FCR provision and total revenue for the VSDFG in turbine mode. The maximum FCR provision from the PSH in sub-figure 7.3a is smaller than the indivisible FCR bid size. Hence, the operating point with the highest possible FCR provision is at 0.62 p.u (considering 65 % minimum mechanical efficiency) and, therefore, in the middle of the operating area of the PSH. Depending on the FCR/electricity price ratio, the figure shows when it is economically reasonable to switch to the operating point of maximum FCR provision (MFP). For a 0.1 price ratio, for example, leaving the maximum efficiency point (BEP) at 0.77 p.u. starts to result in an increase in total revenue for smaller PSH. When the price ratio is even higher, the total revenue increase even further.

In case the available FCR provision capability of the PSH is greater than the cap of 25 MW and assuming a $P_{FCR,max}/P_{rated} \ll 1$, sub-figure 7.3b shows a different picture. Due to higher total losses in efficiency, at smaller price ratios $\pi_{FCR}/\pi_{wholesale} < 0.5$, changing the operating point from the BEP is not economical since the FCR revenue can not be increased much by reducing the power output. However, the flattening curve for higher price ratios is noticeable. This is further investigated in section 7.3.

Since $E(P) = P \cdot \eta_{el}(P) \cdot \Delta t$ for pump operations, the normalized revenue in this operating mode is calculated by

$$k(p) = \frac{-1}{\eta_{el}(p)} \cdot \left[1 + \frac{P_{FCR(p)}/P_{rated}}{P/P_{rated}} \cdot \frac{\pi_{FCR}}{\pi_{wholesale}}\right]. \tag{7.36}$$

Figure 7.4 depicts the results for the VSDFG in pump mode. The best efficiency point, in this case, is the operating point with maximum power input of the pump-turbine. Therefore, no FCR provision is possible at the BEP. When the maximum FCR provision is considered smaller than the indivisible FCR bid size (sub-figure 7.4a), leaving the BEP can result in an increase in actual revenue depending on the price ratio. The actual revenue can be increased further for higher price ratios by reducing the power intake in pump mode until the MFP is reached. If the FCR bid size is capped to

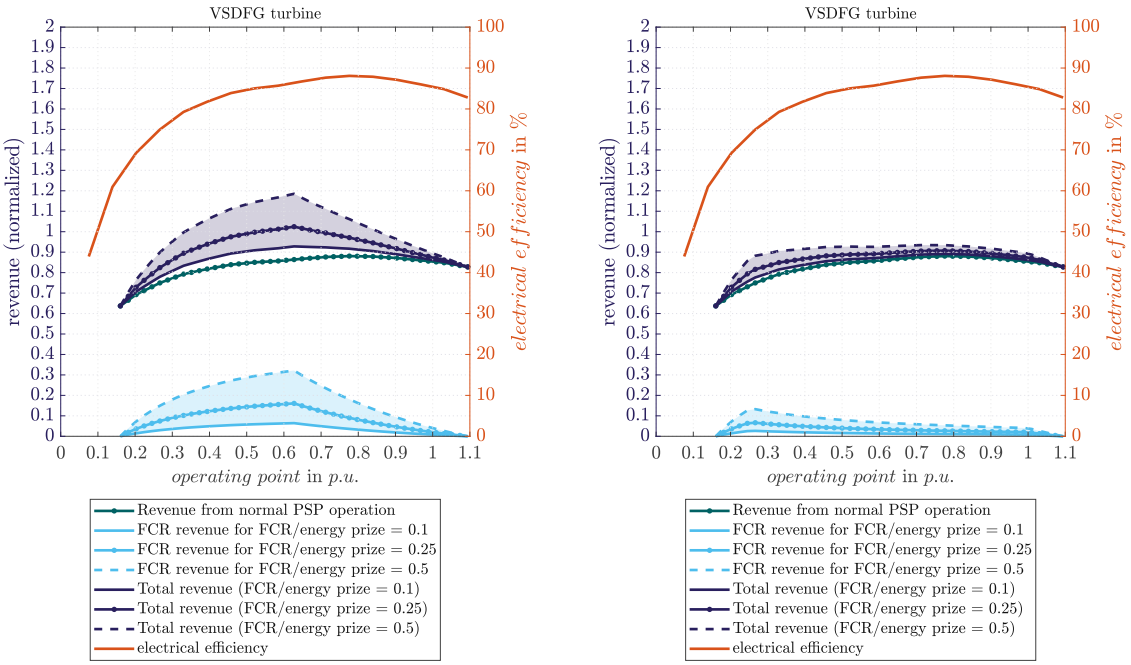

(a) max. FCR provision < indivisible FCR bid size

(b) max. FCR provision > indivisible FCR bid size

Figure 7.3: Normalized revenues for VSDFG in turbine mode (wholesale & FCR provision)

25 MW (sub-figure 7.4b), operating at the MFP to increase revenue is not economically preferable because revenue from FCR provision can not be increased.

The results for the VSFSC in turbine mode depending on the FCR bid size are shown in figure 7.5. The conclusions for changing the operating point to maximize revenue are the same as for the VSDFG in turbine mode. An interesting case, however, can be observed if the FCR bid size is assumed to be capped at 25 MW and the FCR to energy price ratio is very high (sub-figure 7.5b). In this scenario, a very low operating point is preferred to bring in extra FCR revenue. The reason of this is the fact that the VSFSC can operate at higher efficiencies at lower operating points compared to the VSDFG.

For pump mode, results can be found in figure 7.6. Since the effective operating range of the VSDFG and the VSFSC are the same in pump mode, the figures indicate the same conclusions for changing the operating point to increase FCR provision as for the VSDFG.

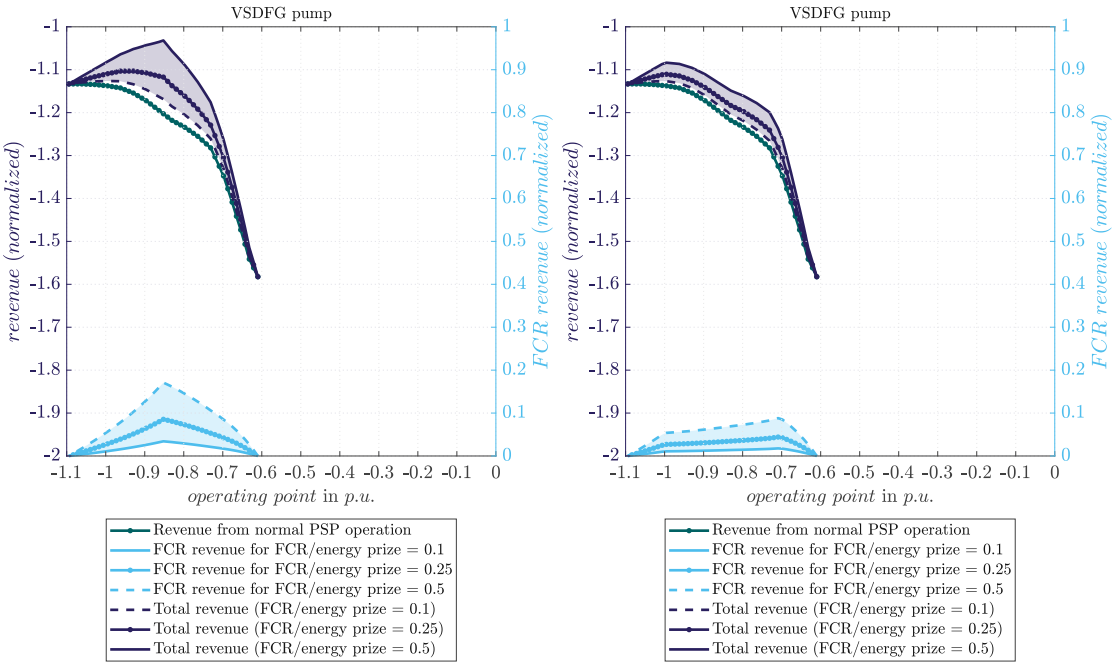

(a) max. FCR provision < indivisible FCR bid size (b) max. FCR provision > indivisible FCR bid size

Figure 7.4: Normalized revenues for VSDFG in pump mode (wholesale & FCR provision)

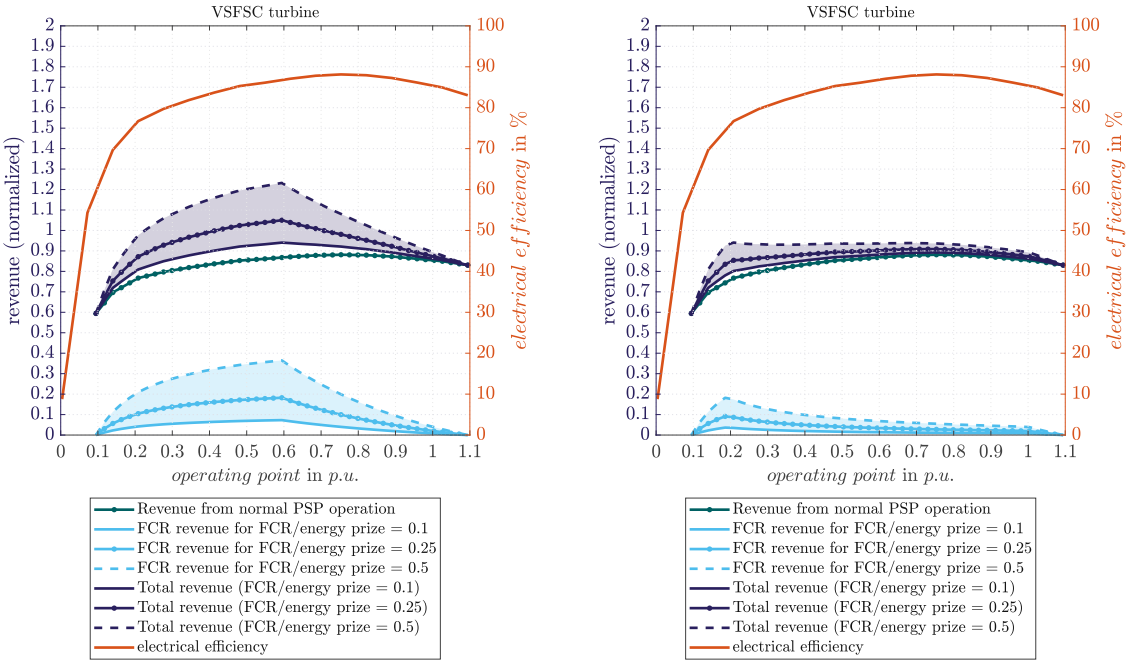

(a) max. FCR provision < indivisible FCR bid size (b) max. FCR provision > indivisible FCR bid size

Figure 7.5: Normalized revenues for VSFSC in turbine mode (wholesale & FCR provision)

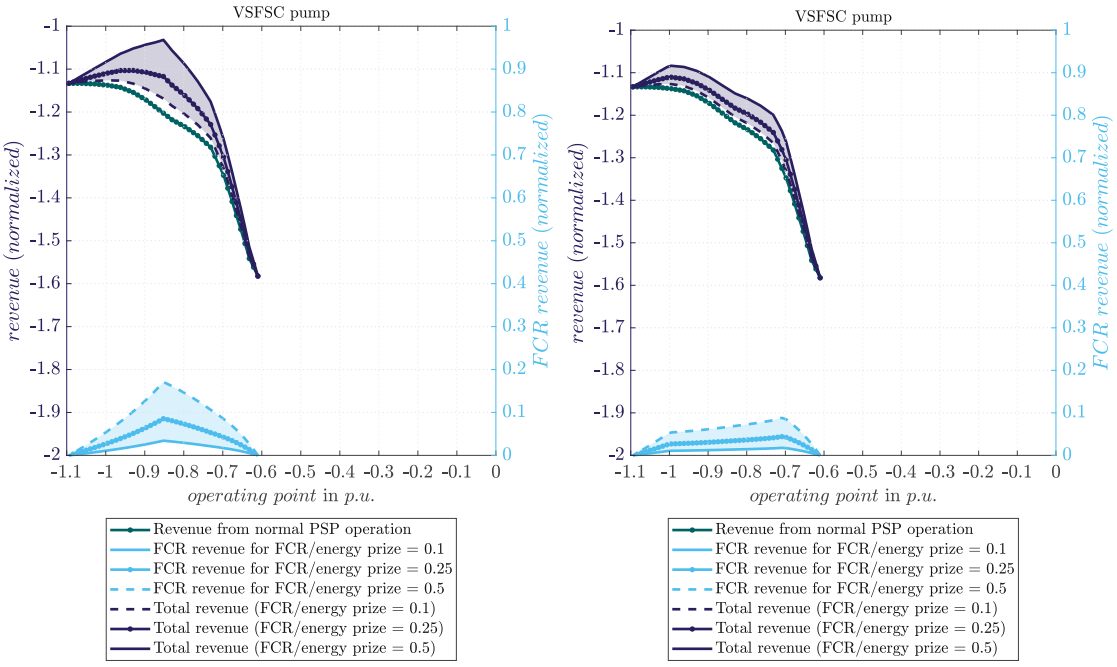

(a) max. FCR provision < indivisible FCR bid size (b) max. FCR provision > indivisible FCR bid size

Figure 7.6: Normalized revenues for VSFSC in pump mode (wholesale & FCR provision)

7.3 Operating Points for Maximum Revenue

In this section, the operating points for maximum revenue for a variety of price and rated power output scenarios based on equation 7.35 are calculated.

First, the VSDFG in turbine and pump mode is investigated. Results for optimal operating point for both modes of operations are depicted in figure 7.7. The x-axis displays the optimal (in regard to the maximum revenue) operating points depending on the price ratio $\pi_{FCR}/\pi_{wholesale}$ (y-axis) for pumped storage plants with different rated power outputs (individual curves). The curves represent PSH with different rated power outputs. The maximum FCR bid size is 25 MW and the rated power outputs of the PSH is a multiple of it. In these deliberations, it is assumed that the electrical efficiency curve is the same for PSH with different rated power outputs.

In turbine mode, the optimal operating point for PSH varies significantly depending on the FCR to wholesale energy price ratio and the rated power output. The BEP is the optimal operating point for lower price ratios for PSH with high rated power compared to the indivisible FCR bid size. As the FCR price increases, lower operating points are favored because the FCR revenue increase is higher than the loss in efficiency. For PSH with rated power outputs around twice the size of the indivisible FCR bid size, the operating point with the highest FCR (MFP) provision is favored.

In pump mode, the drop in efficiency is higher for lower operating points compared to the turbine mode. Hence, higher power output is generally favored, and the FCR price has less influence. However, for higher FCR prices and PSH with less power output, optimal operating points tend to decrease to the MFP at 0.86 p.u..

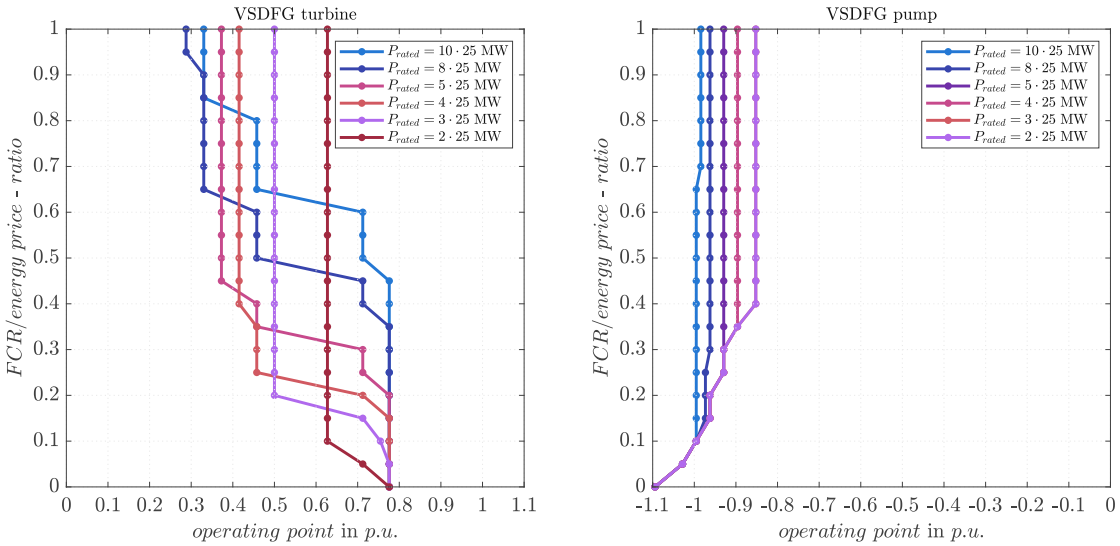

(a) VSDFG in turbine mode

(b) VSDFG in pump mode

Figure 7.7: Operating points for maximum total revenue (wholesale & FCR provision)

Results for the optimal operating points for the VSFSC can be found in figure 7.8. In turbine mode, the drop in electrical efficiency is steeper but occurs at lower operating points. Therefore, the results compared to the VSDFG in turbine mode indicate lower optimal operating points for higher FCR prices. As the rated power output of the PSH decreases, optimal operating points tend to the maximum FCR provision point at 0.62 p.u.. The drop in efficiency in pump mode is again higher for lower operating points compared to the turbine mode of the VSFSC. Therefore, higher power input is favored in general and a FCR price increase over 0.5 of the wholesale price has little effect on the results. For PSH with less power output, optimal operating points tend to decrease up to the MFP at 0.86 p.u., but only for higher FCR price scenarios.

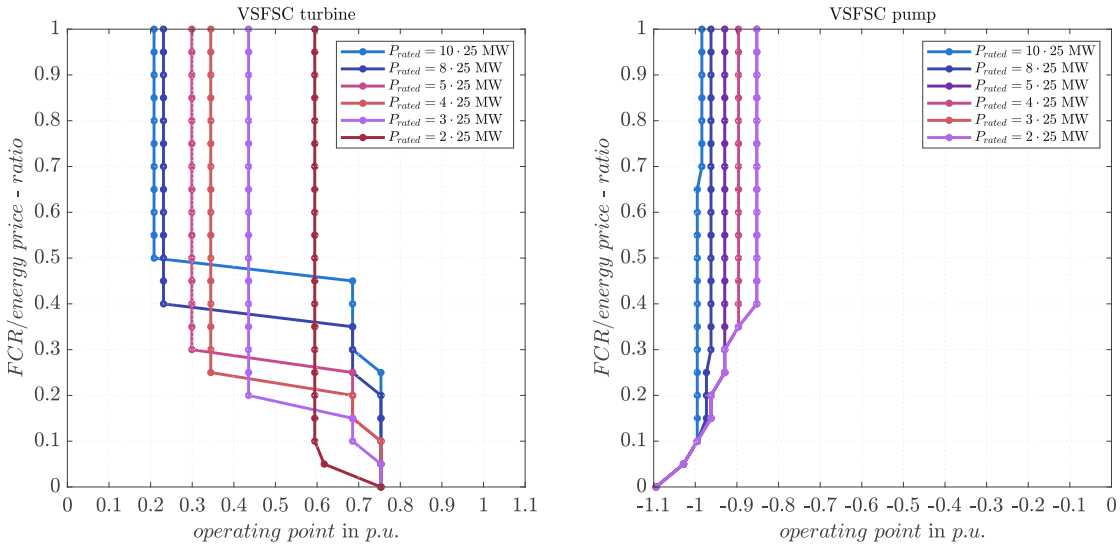

(a) VSFSC in turbine mode

(b) VSFSC in pump mode

Figure 7.8: Operating points for maximum total revenue (wholesale & FCR provision)

7.4 Additional Losses from FCR Provision

A FCR provision during a 4 h tendering period is accompanied by a constant change in the operating point. When the PSH operates at the BEP in turbine mode, every diversion from it leads to additional losses in efficiency. However, FCR provision can also lead to less energy depletion from the reservoir during operations. This happens for example during over-frequency periods when less overall power output is required from the PSH. First, this is investigated using the VSDFG in turbine mode and the 4 h frequency sample as an example. The operating point of the VSDFG is set to be the BEP of the PSH. For the maximum FCR bid, two scenarios are investigated. First, the maximum FCR provision is smaller than the indivisible FCR bid size, and therefore, the FCR bid can be $\pm (P_{PSP,max} - P_{MEP})$ at maximum. Second, the rated power output is

far greater indivisible FCR bid size. Hence, it is assumed that the FCR bid of the PSH at the BEP can only be $\leq \pm 25\,MW$.

Next, the additional losses due to deviation from the BEP in both scenarios are investigated. Therefore, the change in the "state-of-charge" of the PSH is calculated. The energy required for 4 hours in turbine mode at the BEP results in

$$E(P_{BEP}) = \int_{t=0}^{4h} \frac{P_{BEP}}{\eta_{el,BEP}} \cdot d\tau\,. \tag{7.37}$$

The energy required for the same period of operations with FCR provision is determined by

$$E(P) = \int_{t=0}^{4h} \frac{P_{BEP} + P_{FCR}}{\eta_{el}} \cdot d\tau\,. \tag{7.38}$$

The difference between both results leads to the additional losses in %

$$e_{losses} = \frac{E(P) - E(P_{BEP})}{E(P_{BEP})} \cdot 100\%\,. \tag{7.39}$$

Therefore, negative results indicate that due to FCR provision less energy from the reservoir is needed to meet contractual obligations for the tendering period. Positive results lead to a loss of energy in the reservoir compared to only operating at the BEP without FCR provision.

In pump mode, it is not possible to operate at the BEP and deliver FCR since the BEP is at the maximum of the operating range. To calculate losses in pump mode, the MFP is chosen. The pumped energy for the same 4 hour period at the MFP is

$$E(P_{MFP}) = \int_{t=0}^{4h} P_{MFP} \cdot \eta_{el,MFP} \cdot d\tau\,. \tag{7.40}$$

The absorbed energy into the reservoir is calculated by

$$E(P) = \int_{t=0}^{4h} (P_{MFP} + P_{FCR}) \cdot \eta_{el} \cdot d\tau\,. \tag{7.41}$$

The difference between both results leads to the additional losses in %

$$e_{losses} = \frac{E(P_{MFP}) - E(P)}{E(P_{MFP})} \cdot 100\%\,. \tag{7.42}$$

Again, negative results indicate a gain of energy in the reservoir due to FCR provision, whereas positive results lead to an additional loss of energy.

Table 7.2 lists the result for different PSH types at different key operating points and FCR provision bids.

Table 7.2: Additional losses due to FCR Provision

PSP type	e_{losses} in %
VSDFG turbine mode at BEP with max. FCR provision	−1.71
VSDFG turbine mode at BEP with 25 MW FCR provision	−0.36
VSDFG pump mode at MFP with max. FCR provision	−0.34
VSDFG pump mode at MFP with 25 MW FCR provision	−0.79
VSFSC turbine mode at BEP with max. FCR provision	−1.86
VSFSC turbine mode at BEP with 25 MW FCR provision	−0.40
VSFSC pump mode at MFP with max. FCR provision	−0.34
VSFSC pump mode at MFP with 25 MW FCR provision	−0.79

The mean value of the grid frequency of the investigated 4 hour tendering period is 50.0084 Hz and, therefore, close to the expected value of 50 Hz. In all cases in table 7.2, a small gain of additional energy in the reservoir is achieved due to FCR provision. Therefore, in this case, extra revenue can be generated. However, this is highly likely not the case in general. Longer under-frequency periods will lead to extra losses, whereas over-frequency periods will likely generate slightly more revenue. For a sorrow economic evaluation, deviations from the operating point due to FCR provision need to be considered for economic evaluations of FCR provision. To put the additional losses into perspective, the share of FCR provision contributing to the total revenue (at the operating points of maximum total revenue) is shown for turbine operations for VSDFG and VSFSC in figure 7.9. For low FCR/energy price ratios, possible FCR revenue is less than 5 % of the total revenue.

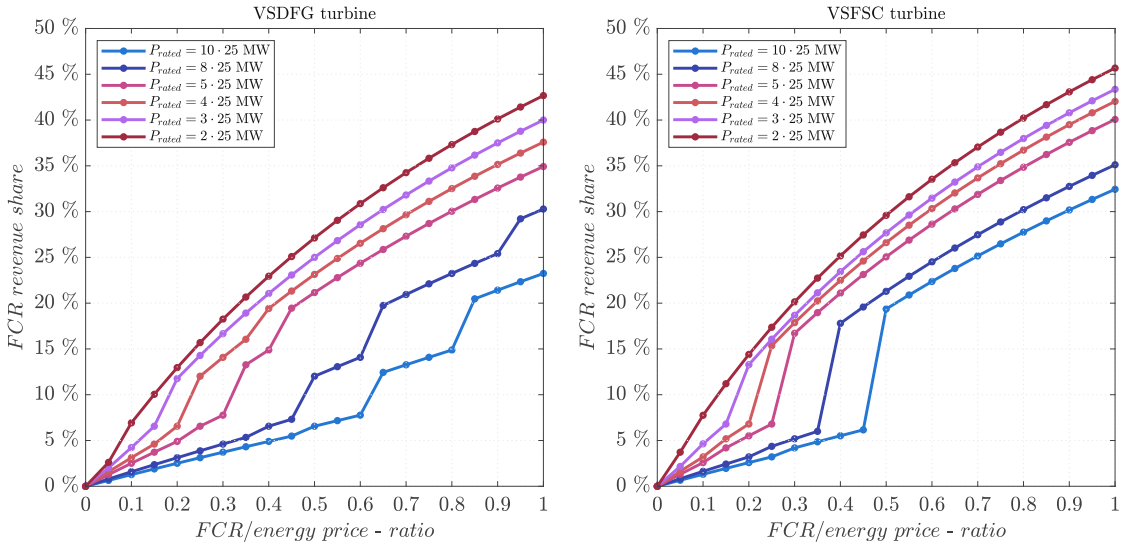

(a) VSDFG turbine mode

(b) VSFSC turbine mode

Figure 7.9: Share in revenue from FCR provision in turbine mode

8 Conclusion

The two leading technologies for variable-speed pump-turbines of recent years are the variable speed doubly-fed generator (VSDFG) and the variable-speed full-size converter (VSFSC). These technologies have the opportunity to participate in the restrictive energy balancing market in a wide operating range to generate additional revenues for new pumped-storage projects. The investigation's main focus lies in analyzing the frequency containment reserve (FCR) capability of this two schemes based on ENTSO-E Continental Europe requirements. Transient models of both concepts are developed and validated inspired by a real-life pumped hydro storage facility. These models are the bases to approach the research questions defined in section 1.2. An effort is made to answer them based on the results of this thesis in the following paragraphs.

What dynamic aspects and properties of variable speed pumped storage hydropower plants need to be considered for modeling FCR provision?

The hydraulic, electrical, and control components of the PSH variants are built with SIMSEN to establish an accurate representation. The modeling part of the thesis introduces the hydraulic efficiency hill chart of both hydraulic machines for turbine and pump mode. Best efficiency lines are presented based on unit speed and unit flow for both storage schemes. Results highlight the advantages of the VSFSC for lower power outputs in turbine mode, where higher efficiencies are possible because of lower speed settings. The outcome in pump mode is fairly similar as speed limitations do not affect the operation area of both machine types. Control strategies of the variable speed machines are compared to the fixed speed pump-turbine and indicate the additional degree of freedom in control. The start-up process for turbine and pump operations of

the VSDFG and VSFSC are compared to the conventional fixed-speed pump-turbine. The VSFSC has the ability to start delivering electrical power to the grid after 20 seconds, and therefore, 20 seconds faster than the FSPT, and 10 seconds faster than the VSDFG. In pump mode, the VSFSC can start up with rated power, whereas the VSDFG can use the existing rotor converter to start the rotating assembly when the impeller runs in air. The FSTP requires additional equipment to accelerate the pump-turbine in pump direction as it always operates at synchronous speed. This can be provided by an auxiliary motor, a start-up turbine, or a start-up converter. Therefore, the VSFSC is by far the fastest scheme in this operating mode, while the VSDFG has significant advantages compared to the FSTP. However, switch-over times between pump and turbine operations are too long for FCR requirements, especially for VSDFG and FSTP, while VSFSC, in general, could have the possibility to do so.

The dynamic behavior of the VSDFG and VSFSC during operating point changes during pump and turbine operations to determine FCR capability are done through transient simulations. The duration necessary to change from one operation point to another is presented for each scheme and a wide operating range. The operating points are further restricted by implementing minimum mechanical efficiency requirements. The effective operating ranges of the VSPT schemes are determined for a minimum mechanical efficiency of 65 % and 80 % in subsection 6.2.1. The results show that both schemes are fast enough to provide FCR in their respective operating mode.

What is the effective operating range of variable speed pumped storage hydropower plants for FCR provision?

Since FCR provision has to be done symmetrically, the effective operating range for FCR provision is slightly smaller than the overall range. At the lowest and highest power output/input points, no FCR bidding is possible. Furthermore, the scheduled set-point limits the FCR bid size. The operating point of maximum FCR provision is defined for both schemes and operating modes and depends on cavitation and stability limitations. Since these are not investigated in this thesis, minimal efficiency requirements for operating are introduced based on the literature. The current maximum FCR bid size is also taken in consideration. Indivisible bids can have a maximum bid size of 25 MW in all the participating countries in FCR. When the indivisible bid size is significantly smaller than the possible FCR power of the power plants, FCR provision can only take up a small share in the overall power delivery of the plants.

What are suitable methods for monitoring a correct FCR provision?

Accurate monitoring methods to prove a correct FCR provision from the balancing service provider are becoming more and more advanced as data transfer to the TSO intensifies. Three methodologies (correlation, channel and dynamic normalization methodology) are presented, which are still in a state of research and are more and more introduced in live operations at TSOs. The correct FCR provision of the VSDFG and VSFSC for a 4 hour long frequency signal is monitored, and all three methods determine a correct FCR provision. The correlation methodology delivers a statistical approach to calculate the linear correlation between the grid frequency and the activated FCR of the balancing service providers. This steady-state performance monitoring is helpful for compensation according to the bids successfully placed on the market platform. However, the suitability for highly dynamic frequency and power signals is poor. Two requirements (SOGL and SAFA) are considered for the channel methodology, and further practical improvements for real-life applications are implemented and tested. Results show the advantage of the channel methodology in dynamic performance monitoring. However, the effort to implement the method is considerably higher. The dynamic correlation methodology faces the same advantages and disadvantages as the channel methodology. Furthermore, small simulation time steps are needed for a practical realization of the method. Sampling steps of 1 s or 2 s, currently used for data transmission of FCR provision, are too slow for correct implementations of all functionalities of this method.

What are economically feasible operating points for FCR provision by variable speed pumped storage hydropower plants?

The analysis of the economics of FCR provided by variable speed pumped hydropower plants show that changing the operating point or operating at specific power outputs only to maximize FCR provision revenues might not be economically reasonable and depends highly on the FCR/electricity price ratio. The indivisible FCR bid cap of 25 MW plays an essential role in the economic considerations. If the PSP is scheduled to operate during a FCR tendering period, offering FCR provision (when possible) in combination with normal operations can bring additional revenues, but also additional losses need to be considered. In the worst case, the additional revenue is compensated by the additional losses. The method described in chapter 7 allows this consideration of the change in efficiency and thus the additional losses.

9 Outlook

As an outlook, the following improvement and further investigations should be considered in the future:

- The validation of the transient model is mainly based on comparing the reference signal to the power signal and its accuracy. A thorough comparison with actual plant values should be undertaken for more parameters, like head, flow, speed, and GVO. Furthermore, the minimum mechanical efficiency assumption, which limits the operating range, should be specified more accurately, focusing on vibrations, vortices, and cavitation.
- While the focus of this thesis is active power control, reactive power control is also implemented in the models. Further research in the provision of reactive power by converter-based pump-turbine power plants should be made.
- There is certainly room for optimization of the implemented start-up process of the VSDFG, VSFSC, and the FSPT, which was not the model's main focus. Especially, the blow-out process and the utilization of different auxiliary components should be modeled in detail for further investigations of variable speed pump-turbines. The synchronization process to the grid should also be compared to real plant reactions.
- An investigation of a comparable ternary set configuration is omitted and could further provide inside into the advantages and disadvantages of variable speed schemes.
- The monitoring methodologies have been implemented in great detail and with improvements for real-life application. However, further research needs to be done if technical entities of a BSP provide more than one frequency control process (e.g. FCR and aFRR) at a time. In this case, the monitoring concepts need to be expanded to distinguish which process is responsible if an incorrect provision

occurs. Therefore, a strategy for error allocation to the different frequency control processes needs to be developed.

- The tendering periods have changed over the years from weekly to daily and finally to 4 hour periods for FCR. A further reduction of the bid resolution is possible. Therefore, more flexible and dynamically accurate FCR provision could be required in the future, creating opportunities for FCR provision of variable speed pump-turbines.

- Since large-scale converters are present in VSDFG and VSFSC schemes, integrating battery storage to provide balancing power, especially during turbine and pump transitioning times, could further improve participation in the balancing markets.

10 Appendix

10.1 Hydroelectric Turbine-Governor Simulation Models

Table 10.1: Hydro Governor Models in the PSSE Software (Source: [34] Table 3-1)

Model Name	Description
HYGOV	Standard hydro turbine governor model
HYGOV2	Linearized hydro turbine governor model
HYGOVM	Hydro turbine governor model with lumped parameters
HYGOVT	Hydro turbine governor model with traveling wave
HYGOVRU	Fourth order lead-lag hydro turbine governor model
IEEEG2	General-purpose linearized turbine governor model
IEEEG3	General-purpose linearized turbine governor model
PIDGOV	Hydro turbine governor model for plants with straightforward penstock configurations and three-term electro-hydraulic governors
TURCZT	General-purpose turbine governor model
TWDM1T	Hydro turbine governor model with tail water depression
TWDM2T	Hydro turbine governor model with proportional, integral, and derivative (PID) controller and tail water depression
WEHGOV	Woodward electro-hydraulic hydro turbine governor model
WPIDHY	Woodward PID hydro turbine governor model
WSHYDD	WECC double derivative hydro turbine governor model
WSHYPG	WECC type GP hydro turbine governor model
HYGOV4	Hydro turbine governor model

Table 10.2: Hydro Governor Models in the PSLF Software (Source: [34] Table 3-2)

Model Name	Description
G2WSCC	Double derivative hydro governor and turbine
GPWSCC	PID governor and turbine
HYG3	PID governor, double derivative governor, and turbine
HYGOV4	Hydro turbine and governor model for plants with straightforward penstock configurations and traditional dashpot-type hydraulic governors
HYGOV	Hydro turbine and governor model for plants with straightforward penstock configurations and electro-hydraulic governors that mimic the permanent/temporary droop characteristics of traditional dashpot-type hydraulic governors
HYGOVR	Fourth order lead-lag governor and hydro turbine
HYPID	Hydro turbine and governor model for plants with straightforward penstock configurations and proportional-integral-derivative governor. Includes capability to represent blade angle adjustment of Kaplan and diagonal flow turbines.
HYST1	Hydro turbine with Woodward electric-hydraulic PID governor, penstock, surge tank, and inlet tunnel
IEEEG3	IEEE hydro turbine and governor model for plants with straightforward penstock configurations and hydraulic-dashpot governors with optional deadband and nonlinear gain
PIDGOV	Hydro turbine and governor model for plants with straightforward penstock configurations and three-term electro-hydraulic governors (Woodward electronic)
W2301	Woodward 2301 governor and basic turbine model

10.2 Gross Head Variations

The variation of the gross head between the minimum and the maximum limits, influences the hydraulic efficiency during operation at specific operating points. This behavior for the investigated pump-turbine is analyzed by [55] and the results are shown in figure 10.1.

In turbine mode, the behavior of the FSTP, VSDFG, and the VSFSC is similar. The FSTP achieves its highest operating efficiency at high head values. At high head levels, the unit speed n_{11} is reduced. Therefore, the operating line is moved towards higher efficiency levels. The VSFSC and the VSDFG have the ability to vary the speed setting and can compensate design trade-offs made to improve the pump operation. Hence, they achieve higher efficiencies compared to the FSTP. For high head values, the results for VSFSC and VSDFG are comparable since relatively high speed values are necessary to operate at the highest efficiencies. At declining heads, lower speed values lead to higher efficiency. Here, the VSDFG is limited to its lower speed boundary. The VSFSC has no speed restrictions in this matter and can offer higher efficiencies and operating range.

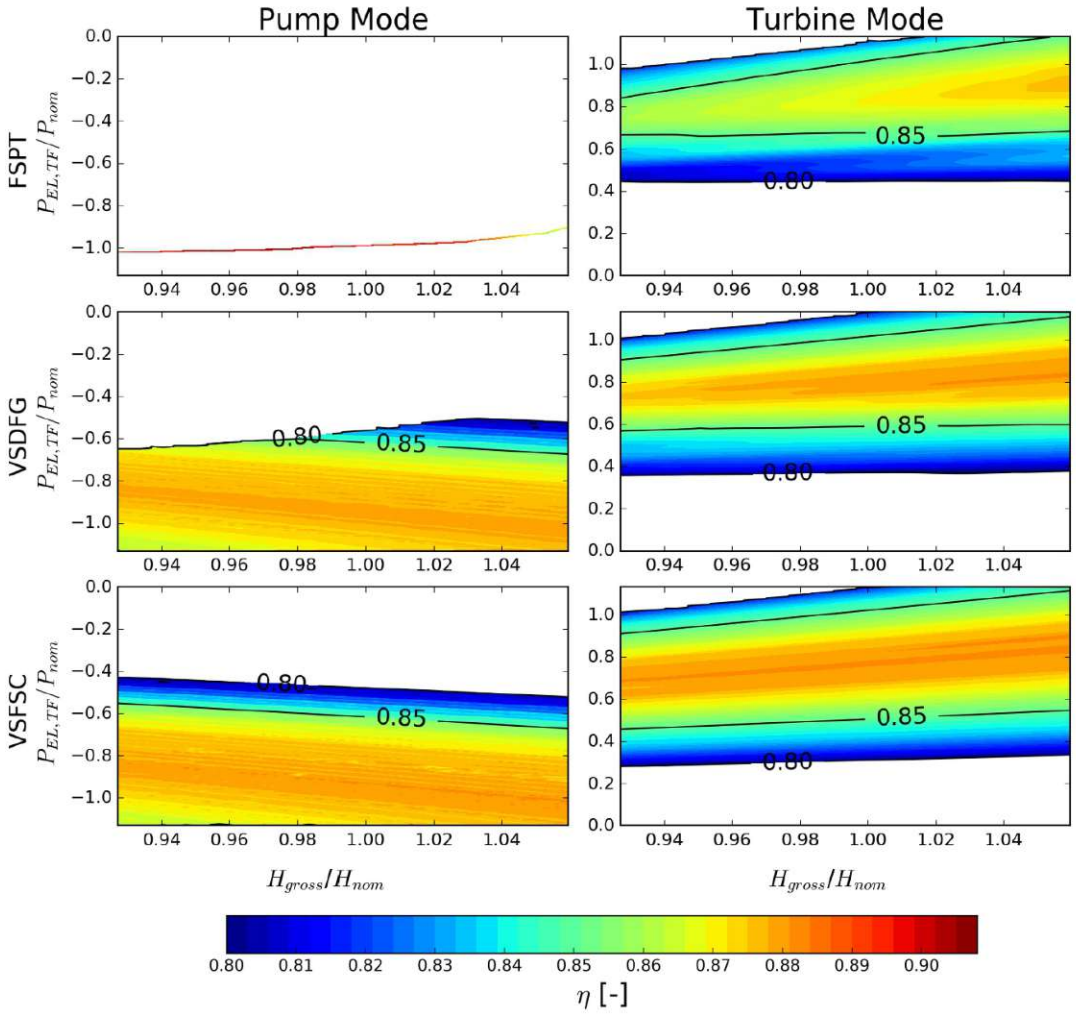

Figure 10.1: PSH plant efficiency depending on gross head and power input/output (modified, source: [55])

In pump mode, the FSPT has only one operating point per head value, whereas the VSDFG and the VSFSC offer several values. The behavior of both variable speed technologies is again similar for pump operations. The minimum pump power (considering a minimum of 80 % efficiency) is increasing with rising head values. The VSDFG reaches its speed restriction for lower head levels. Hence, its operating area is reduced at lower heads compared to the VSFSC.

List of Figures

List of Tables

Bibliography

[1] ENTSO-E. *ELECTRICITY IN EUROPE 2015: Synthetic overview of electric system consumption, generation and exchanges in the ENTSO-E Area*. 2016.

[2] Ruifeng Yan et al. "The combined effects of high penetration of wind and PV on power system frequency response". In: *Applied Energy* 145 (2015), pp. 320–330. ISSN: 0306-2619.

[3] Christoph Maier, Sabina Nemec-Begluk, and Wolfgang Gawlik. "Optimal allocation of energy storage and conversion technologies in an urban distributed energy system". In: CIRED - International Conference on Electricity Distribution, Madrid, Spain, 3 - 6. June (2019).

[4] Didier Colin, Jesus Lugaro, and Jean-Claude Pinna. "The VENTEEA 2 MW / 1.3 MWh battery system: an industrial pilot to demonstrate multi-service operation of storage in distribution grids". In: *The 23rd International Conference and Exhibition on Electricity Distribution - CIRED* (2015).

[5] Pieter Tielens and Dirk van Hertem. "The relevance of inertia in power systems". In: *Renewable and Sustainable Energy Reviews* 55 (2016), pp. 999–1009. ISSN: 1364-0321.

[6] FfE - Forschungstelle für Energiewirtschaft e.V. *Gutachten zur Rentabilität von Pumpspeicherkraftwerken*. 2014. URL: `http://www.stmwi.bayern.de/fileadmin/user_upload/stmwivt/Themen/Energie_und_Rohstoffe/Dokumente_und_Cover/2014-Pumpspeicher-Rentabilitaetsanalyse.pdf`.

[7] ENTSO-E. *Synchronous Area Framework Agreement for Regional Group Continental Europe: Annex 1: Policy on Load-Frequency Control and Reserves*. 2019.

[8] Christoph Maier. "Zukünftige Speicherbewirtschaftung bei regenerativer Stromerzeugung am Beispiel Österreichs: Future storage planning with renewable electricity generation based on the example of Austria". Diplomarbeit. TU Wien, 2012.

[9] Christoph Maier. "Speicherbewirtschaftung bei Vollversorgung Österreichs mit regenerativem Strom". In: *8. Internationale Energiewirtschaftstagung (IEWT) an der TU Wien, Wien* (2013).

[10] Christoph Maier et al. "Eigenverbrauchssteigerung in Haushalten durch Demand-Side-Management". In: *13. Symposium Energieinnovation Graz/Austria* (2014).

[11] Christoph Maier et al. "Demand-Side-Management in einer Modellsiedlung - Endergebnisse des Projekts aDSM". In: *9. Internationale Energiewirtschaftstagung (IEWT) an der TU Wien, Wien* (2015).

[12] Christoph Maier and Wolfgang Gawlik. *Modeling of flexible power plants in SIMSEN*. Vienna, 2015.

[13] Christoph Maier et al. "SYMBIOSE-4-IUG - Verschränkung der Energienetze bei Industrie- und Gewerbekunden". In: *14. Symposium Energieinnovation Graz/Austria* (2016).

[14] Christoph Maier, Markus Heimberger, and Alexander Winter. "Symbiose-4-IuG - Systemübergreifende optimale dezentrale Verschränkung der Energienetze bei Industrie & Gewerbe". In: *Smart Grids Week 2016, Graz, Austria* (2016).

[15] Christoph Maier, Wolfgang Gawlik, and Leopold Ruppert. "Combined Electrical and Hydraulic Model for Dynamic Long-Term Operation of Pumped -Storage in SIMSEN". In: *19th International Seminar on Hydropower Plants - Flexible Operation of Hydropower Plants in the Energy System, Laxenburg, Austria, 9.-11. Nov.* (2016).

[16] Markus Heimberger et al. "Energieträgerübergreifende Planung und Analyse von Energiesystemen". In: *e & i Elektrotechnik und Informationstechnik* 133.8 (2016), pp. 359–361. ISSN: 1613-7620. DOI: 10.1007/s00502-016-0446-2.

[17] Christoph Maier, Wolfgang Gawlik, and Leopold Ruppert. "Vergleich von drehzahl-variablen Pumpspeichertechnologien in einem dynamischen Modell für Langzeitbetrachtungen". In: *10. Internationale Energiewirtschaftstagung (IEWT) an der TU Wien, Wien* (2017).

[18] Manuel Bailera et al. *Energy Storage*. Cham: Springer International Publishing, 2020. DOI: 10.1007/978-3-030-46527-8.

[19] Francisco Javier Díaz González, Andreas Michael Sumper, and Oriol Gomis-Bellmunt. *Energy storage in power systems*. Chichester, West Sussex: Wiley, 2016.

[20] Edward Barbour et al. “A review of pumped hydro energy storage development in significant international electricity markets”. In: *Renewable and Sustainable Energy Reviews* 61 (2016), pp. 421–432. ISSN: 1364-0321. DOI: 10.1016/j.rser.2016.04.019.

[21] Paul A. Breeze. *Power generation technologies*. Third edition. Kidlington, Oxford, United Kingdom: Newnes an imprint of Elsevier, 2019. URL: https://www.sciencedirect.com/science/book/9780081026311.

[22] Joachim Raabe. *Hydro power: The design, use, and function of hydromechanical, hydraulic, and electrical equipment*. Düsseldorf: VDI-Verlag, 1985.

[23] Baoling Guo et al. “Reduced-Scale Models of Variable Speed Hydro-Electric Plants for Power Hardware-in-the-Loop Real-Time Simulations”. In: *Energies* 13 (2020), pp. 1–22. DOI: 10.3390/en13215764.

[24] Hans Schlunegger and Andreas Thöni. “100-MW-Vollumrichter im Pumpspeicherwerk Grimsel 2”. In: *Bulletin.ch : Fachzeitschrift und Verbandsinformationen von* 105 (2014).

[25] Richard K Fisher et al. “A Comparison of Advanced Pumped Storage Equipment Drivers in the US and Europe”. In: *Hydrovision* (2012). DOI: 10.13140/2.1.1082.4967.

[26] Christophe Nicolet et al. “Full Size Frequency Converter for Fast Francis Pump-Turbine Operating Mode Transition”. In: (2016).

[27] Jiri Koutnik. *Voith Hydro Hydro Power Plants*. Munich, 4. Nov. 2013.

[28] ABB Switzerland. *Grimsel 2, Switzerland: The world’s largest power converter for variable speed pumped hydropower*. 2014.

[29] ENTSO-E. *Electricity Balancing in Europe: An Overview of the European balancing market*. 2018.

[30] THE EUROPEAN COMMISSION. *COMMISSION REGULATION (EU) 2017/2195*. 23.11.2017.

[31] ENTSO-E. *Frequency Containment Reserves (FCR)*. URL: https://www.entsoe.eu/network_codes/eb/fcr/.

[32] Ronald Engelmair. “Analysis and benchmarking of Frequency Containment Reserve response of small control areas”. Dissertation. TU Wien, 2018.

[33] Philipp Maucher and Hendrik Lens. *Dynamic normalization methodology for the monitoring of Frequency Containment Reserve activation*. 2020.

[34] James W. Feltes et al. *Review of Existing Hydroelectric Turbine-Governor Simulation Models*. 2013.

[35] Pouyan Pourbeik et al. *Dynamic Models for Turbine-Governors in Power System Studies*. 2013.

[36] Peter Donalek et al. *Modeling Adjustable Speed Pumped Storage Hydro Units Employing Doubly Fed Induction Generators*. 2013. DOI: 10.13140/RG.2.1.2592.6481.

[37] James W. Feltes et al. *Testing Dynamic Simulation Models for Different Types of Advanced Pumped Storage Hydro Units*. 2013.

[38] Power Vision Engineering. *SIMSEN - Simulation software for the analysis of electrical power networks, adjustable speed drives and hydraulic systems*. 2013. URL: https://www.epfl.ch/research/facilities/hydraulic-machines-platform/wp-content/uploads/2019/11/02_SIMSEN_leaflet_detail.pdf.

[39] C. Nicolet et al. "A new tool for the simulation of dynamic behaviour of hydroelectric power plants". In: *Proceedings of the 10th International Meeting of the work group on the behaviour of hydraulic machinery under steady oscillatory conditions, IAHR, Norway, June 26-28* (2001).

[40] Y. Pannatier et al. "Transient Behavior of Variable Speed Pump-Turbine Units". In: *Proceedings of the 24th IAHR Symposium on Hydraulic Machinery and Systems, Foz do Iguassu, Brazil, October 27 -31* (2008).

[41] Y. Pannatier et al. "Start-up and synchronization of a variable speed pump-turbine unit in pumping mode". In: *XIX International Conference on Electrical Machines (ICEM)* (2010).

[42] Y. Pannatier et al. "Dynamic behavior of a 2 variable speed pump-turbine power plant". In: *18th International Conference 2008*, pp. 1–6. DOI: 10.1109/ICELMACH.2008.4799821.

[43] Klaus Krueger and Jiri Koutnik. "Dynamic Simulation of Pump-Storage Power Plants with different variable speed configurations using the Simsen Tool". In: *International Journal of Fluid Machinery and Systems* 2 (2009). DOI: 10.5293/IJFMS.2009.2.4.334.

[44] C. Nicolet et al. "Benefits of Variable Speed Pumped Storage Units in Mixed Islanded Power Network during Transient Operation". In: *Proceedings of HYDRO 2009, Lyon, France, October 26-28* (2009).

[45] Y. Pannatier et al. "Investigation of Control Strategies for Variable-Speed Pump-Turbine Units by Using a Simplified Model of the Converters". In: *IEEE Transactions on Industrial Electronics* 57.9 (2010), pp. 3039–3049. DOI: 10.1109/TIE.2009.2037101.

[46] Bernhard Herzmaier. "Die doppelt gespeiste Asynchronmaschine im Pumpspeicherkraftwerk". Diplomarbeit. TU Graz, 2011.

[47] C. Nicolet et al. "Variable Speed and Ternary Units to Mitigate Wind and Solar Intermittent Production". In: *Proceedings of Hydrovision Conference 2014, Nashville, TN, USA, July 22-25* (2014).

[48] Jon Suul, Kjetil Uhlen, and Tore Undeland. "Variable Speed Pumped Storage Hydropower for Integration of Wind Energy in Isolated Grids – Case Description and Control Strategies". In: *Nordic Workshop on Power and Industrial Electronics, June 9-11* (2008).

[49] R. Schürhuber, A. Lechner, and J. Hell. "Stationary behaviour of different variable speed pumped storage concepts". In: *Proceedings of the 18th International Seminar of Hydropower Plants, Vienna, Austria* (2015).

[50] J. Schmidt, W. Kemmetmüller, and A. Kugi. "Modeling and static optimization of a variable speed pumped storage power plant". In: *Renewable Energy* 111 (2017), pp. 38–51. ISSN: 09601481. DOI: 10.1016/j.renene.2017.03.055.

[51] Roman Zensch. "Simulation of variable-speed doubly-fed induction machines for hydro-power plants". Diplomarbeit. TU Wien, 2011. URL: https://permalink.catalogplus.tuwien.at/AC07810739.

[52] Matúš Trnovec. "Simulation einer Synchronmaschine mit Vollumrichter in SIMSEN". Diplomarbeit. TU Wien, 2016.

[53] P. Kundur et al. "Definition and classification of power system stability IEEE/CIGRE joint task force on stability terms and definitions". In: *IEEE Transactions on Power Systems* 19.3 (2004), pp. 1387–1401. ISSN: 1558-0679. DOI: 10.1109/TPWRS.2004.825981.

[54] Leopold Ruppert, Klaus Käfer, and Christian Bauer. "Optimizing Steady Operating Points of Several Generating Unit Systems for Transient Applications". In: *Wasserwirtschaft Extra* (2014).

[55] Leopold Ruppert. "Pumped-storage implementation in order to balance volatile renewable energy generation". Dissertation. TU Wien, 2017.

[56] J Krenn, H Keck, and M Sallaberger. "Concept of small and mid-size pump-turbines". In: *17th International Seminar on Hydropower Plants* (2012).

[57] Vlad Hasmatuchi et al. "Experimental Evidence of Rotating Stall in a Pump-Turbine at Off-Design Conditions in Generating Mode". In: *Journal of Fluids Engineering* 133.5 (2011). ISSN: 0098-2202. DOI: 10.1115/1.4004088.

[58] Ademir Husanovic. "Modellierung eines drehzahlvariablen Pumpspeicherkraftwerks in SIMSEN: Modelling of a speed variable pumped hydro power plant using SIMSEN". Diplomarbeit. TU Wien, 2014.

[59] Xin-Lan Li, Jong-Gyu Park, and Hwi-Beom Shin. "Comparison and Evaluation of Anti-Windup PI Controllers". In: *Journal of Power Electronics* 11.1 (2011), pp. 45–50. ISSN: 1598-2092. DOI: 10.6113/JPE.2011.11.1.045.

[60] Feng Gao, Daping Xu, and Yuegang Lv. "Pitch-control for large-scale wind turbines based on feed forward fuzzy-PI". In: *2008 7th World Congress on Intelligent Control and Automation* (2008), pp. 2277–2282. DOI: 10.1109/WCICA.2008.4593277.

[61] ENTSO-E. *P1 – Policy 1: Load-Frequency Control and Performance [C]*. URL: https://www.entsoe.eu/fileadmin/user_upload/_library/publications/ce/oh/Policy1_final.pdf.

[62] André Veltman, Duco W.J. Pulle, and Rik W. de Doncker. *Fundamentals of electrical drives*. Second edition. Power systems. Zürich: Springer, 2016.

[63] APG. *Balancing Statistics in APG Control Area*. 23.08.2021. URL: https://www.apg.at/de/markt/netzregelung/statistik.

[64] Regelleistung.net. *Data Center FCR*. URL: https://www.regelleistung.net/apps/datacenter/tendering-files/.

[65] European Commission. *Dashboard for energy prices in the EU and main trading partners*. URL: https://ec.europa.eu/energy/data-analysis/energy-prices-and-costs/energy-prices-eu-member-states-and-main-trading-partners_en.

[66] European Commission et al. *Study on energy prices, costs and their impact on industry and households : final report*. Publications Office, 2020. DOI: 10.2833/49063.